Molecular assignment of light-induced structural changes using site-directed mutant reaction centers

Sasmit S. Deshmukh

A Thesis

In the Department

Of

Chemistry and Biochemistry

Presented in Partial Fulfillment of the Requirements

For the Degree of

Doctor of Philosophy (Chemistry) at

Concordia University

Montreal, Quebec, Canada

March 2013

CONCORDIA UNIVERSITY
SCHOOL OF GRADUATE STUDIES

This is to certify that the thesis prepared

By: **Sasmit S. Deshmukh**

Entitled: **Molecular assignment of light-induced structural changes using site-directed mutant reaction centers**

and submitted in partial fulfillment of the requirements for the degree of

DOCTOR OF PHILOSOPHY (Chemistry)

complies with the regulations of the University and meets the accepted standards with respect to originality and quality.

Signed by the final examining committee:

_____ Chair
Dr. J. Kornblatt

_____ External Examiner
Dr. V. Barzda

_____ External to Program
Dr. A. Johnson

_____ Examiner
Dr. C. Dewolf

_____ Examiner
Dr. J. Turnbull

_____ Thesis Supervisor
Dr. L. Kalman

Approved by _____
Dr. H. Muchall, Graduate Program Director

March 28, 2013

_____
Dr. B. Lewis, Dean
Faculty of Arts and Science

Abstract

Molecular assignment of light-induced structural changes using site-directed mutant reaction centers

Sasmit S. Deshmukh, Ph.D.
Concordia University, 2013

The photosynthetic reaction center from purple photosynthetic bacteria is a membrane-bound protein-pigment complex that serves as an excellent model for studying biological energy conversion. This energy conversion takes place by electron transfer reactions, which occur within the protein and are often coupled to conformational changes that influence the lifetime of the charge-separated state. In order to identify these light-induced conformational changes, near the bacteriochlorophyll dimer, wild type and 11 different mutants of reaction centers from *Rhodobacter sphaeroides* were studied. Upon 1 min illumination the recovery of the charge-separated states, characterized by steady-state and transient optical spectroscopy, was nearly an order of magnitude slower in one group of mutants (including the wild type) than in mutants carrying the Leu to His mutation at the L131 position. The slower recovery, unlike in the mutants carrying His at the L131 position, was accompanied by a substantial decrease of the electrochromic absorption changes associated with the Q_Y bands of the nearby bacteriochlorophyll monomers, plus a large proton release at pH 6, and a decrease up to 79 mV of the oxidation potential of the dimer during the illumination. The results in the mutants carrying His at the L131 position are modeled as arising from the loss of a proton conducting pathway from the dimer to the solvent, which inhibits the formation of the

long-lived charge-separated state. On the other hand, combination of the light-induced conformational changes and lipid binding near accessory bacteriochorophyll pigment under optimized conditions resulted in unprecedented 5 orders of magnitude increase in lifetime of the charge-separated state, which sheds light on a new potential application of the reaction center in energy storage as a light-driven biocapacitor. Moreover, these conformational changes near the dimer can also be blocked by Mn^{2+} binding. The metal ion binding induced a significant ~ 100 mV increase in the oxidation potential of the dimer and inhibition of formation of the long-lived charge-separated state similar to mutants carrying Leu to His mutation at L131 position. The elevation of oxidation potential of the dimer upon Mn^{2+} binding can make reaction center protein gain some specific functional features of much more complicated photosystem II.

Acknowledgements

First, I would like to thank my supervisor, Dr. László Kálmán, for all your valuable help and support throughout the project. I learned many things from you. You taught me to become better researcher. Thank you for keeping faith in me and giving me an opportunity to work with you.

I am thankful to my committee members, Drs. Joanne Turnbull and Christine DeWolf, for all helpful discussions. I would like to thank you for evaluating my progress during the project and giving valuable advices.

Our collaborators, Drs. J. C. Williams and J. P. Allen, are thanked for constructing and providing all mutant reaction centers.

I would also like to thank and dedicate my work to my wonderful family (Aai, Baba, Saurabh, and Shikha). Thank you for your continuous support and faith in me.

My past and present lab colleagues, Kai Tang, Hassan Akhavein, and M-Alexandru Ivanescu, are thanked for all valuable lab discussions.

Finally, I would also like to acknowledge technical staff, Richard Allix, Aldo Dissegna, Gheorghe Dan Duru, Chris Kowalewski, and Robert Pisarsky for all technical support and making the spectroelectrochemical cell.

Thank you all for being there for me. Without you this work wouldn't have accomplished.

Table of Contents

Abbreviations

Ala	Alanine
Arg	Arginine
Asp	Aspartic acid
B	Bacteriochlorophyll monomer
BChl	Bacteriochlorophyll
Bis-tris propane	1, 3-bis(tris(hydroxymethyl)methylamino)propane
B_L	Bacteriochlorophyll monomer L (active)
B_M	Bacteriochlorophyll monomer M (inactive)
Bpheo	Bacteriopheophytin
BRC	Bacterial reaction center
BWHM	Band width at half maxima
CAPS	*N*-cyclohexyl-3-aminopropanesulfonic acid
CHES	*N*-cyclohexyl-2-aminoethanesulfonic acid
C.M.C.	Critical micelle concentration
CTAB	Cetyltrimethylammonium bromide
Cyt c_2	Cytochrome c_2
Da	Dalton
DAD	Diaminodurene
DEAE	Diethylaminoethyl
DLPC	1, 2-dilauroyl-*sn*-glycero-3-phosphocholine
DLPS	1, 2-dilauroyl-*sn*-glycero-3-phospho-L-serine

DMPC	1, 2-dimyristoyl-*sn*-glycero-3-phosphocholine
DOC	Sodium deoxycholate
DOPC	1, 2-dioleoyl-*sn*-glycero-3-phosphocholine
DOPS	1, 2-dioleoyl-*sn*-glycero-3-phospho-L-serine (sodium salt)
DOTAP	1, 2-dioleoyl-3-trimethylammonium- propane (chloride salt)
EDTA	Ethylenediaminetetraacetic acid
E_M	Midpoint potential
EPR	Electron paramagnetic resonance
Glu	Glutamine
Gly	Glycine
H	Bacteriopheophytin
H_L	Bacteriopheophytin L (active)
H_M	Bacteriopheophytin M (inactive)
His	Histidine
LDAO	Lauryldimethylamine-oxide
Leu	Leucine
LFP	Laser flash photolysis
Lys	Lysine
Met	Methionine
MES	2-(*N*-morpholino)ethanesulfonic acid
MOPS	3-(*N*-morpholino)propanesulfonic acid
MWCO	Molecular weight cut off
NIR	Near-infrared

NMWL	Nominal molecular weight limit
P	Bacteriochlorophyll dimer, primary electron donor of BRC
PDB	Protein data bank
P_L	Bacteriochlorophyll dimer L-half
P_M	Bacteriochlorophyll dimer M-half
Phe	Phenylalanine
Q_A	Ubiquinone A, primary electron acceptor of BRC
Q_B	Ubiquinone B, secondary electron acceptor of BRC
Rb.	*Rhodobacter*
RC	Reaction center
Rps.	*Rhodospirillum*
Ser	Serine
TEN	Tris-HCl, EDTA, NaCl
TLE	Tris-HCl, LDAO, EDTA
Tris	Tris(hydroxymethyl)aminomethane
Trp	Tryptophan
TX-100	Triton X-100
Tyr	Tyrosine
UV	Ultraviolet
VIS	Visible
WT	Wild type

List of figures

List of tables

List of Schemes

Chapter 1

Introduction

1.1 Basic principles of photosynthesis

Photosynthesis is the primary process of biological energy conversion, where light energy is converted into chemical energy. This process exploits solar energy to provide the energy for complex physico-chemical reactions of living organisms therefore sunlight is the ultimate energy source for all biological processes on Earth. Life began very early in Earth's history in photosynthetic organisms (Figure 1.1) and even today's life on Earth derives all its energy from this process.

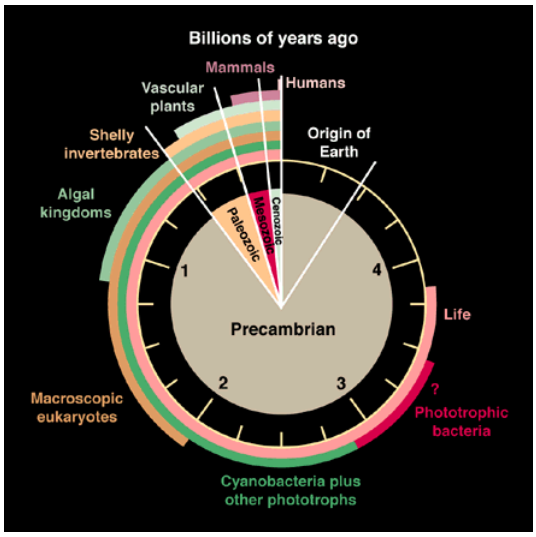

Figure 1.1 Earth's biogeologic clock. The entire 4.6 billion year old history of Earth is represented in a circular clock. Life began ~3.8 billion years ago and there are records of the existence for primitive anoxygenic phototrophic bacteria as old as 3.6 billion years. Major development occurred in the abundance of life at ~2 billion years ago, when the oxygenic atmosphere was established by oxygen producing cyanobacteria. The geological and molecular biological records of microorganisms indicate that photosynthetic organisms arose much earlier in Earth's history.[1]

Essentially, all of our food are related to photosynthesis and all of our current fossil fuels are the products of ancient photosynthetic activities. Photosynthesis therefore serves as a vital link between the light energy of the sun and all living creatures. There are two types of photosynthesis: oxygenic and anoxygenic. Both oxygenic and anoxygenic organisms contain membrane bound protein-pigment complexes, photosystem II (PS II) and bacterial reaction center (BRC), respectively. As evidence indicates that oxygen producing photosynthesis made life possible for aerobic organisms (Figure 1.1).

The first step of the conversion of light energy into chemical energy occurs in reaction centers (RC). In green plants and cyanobacteria water is used as the electron donor and carbon dioxide is the carbon source in the conversion of light energy into chemical energy, while sugars are synthesized and oxygen as a byproduct is released (Figure 1.2).

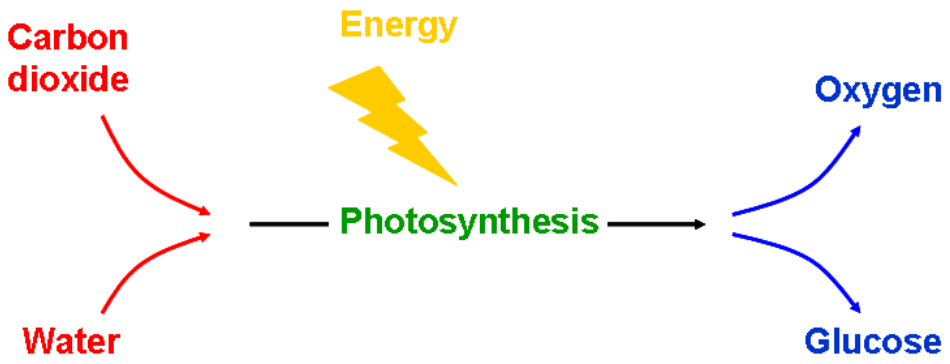

Figure 1.2 Photosynthesis. The process of oxygenic photosynthesis, where carbon dioxide and water are converted into oxygen and glucose using the energy of light.

In algae, cyanobacteria and chloroplasts of green plants, PS II reaction center is responsible for splitting the water into molecular oxygen, electrons, and protons while bacterial photosynthesis does not produce oxygen therefore it is termed as anoxygenic photosynthesis.

The structural and functional similarities between the evolutionarily related (Figure 1.1) but much more complex PS II and the simpler BRC make the latter an excellent model for studying biological energy conversion.

1.2 Structure of the photosynthetic bacterial reaction center (BRC)

The BRC, from purple photosynthetic bacterium *Rhodobacter (Rb.) sphaeroides*, has been for a long time the primary testing ground for our understanding of electron and proton transfer processes followed by conformational changes that occur in biological energy conversion.[2] The three dimensional protein structure of the BRC has been identified by X-ray diffraction method at a resolution of 2.8 Å, which has helped to illustrate structure-function relationship.[3,4] It is an integral membrane protein that contains three protein subunits namely L, M, and H, and 9 cofactors (Figure 1.3A). The BRC from *Rhodobacter sphaeroides* has around ~ 800 amino acid residues that includes five membrane spanning helices each for L and M subunit and several helices that do not span the membrane whereas H subunit has only one membrane spanning helix and a globular domain on the cytoplasmic side, that contains one helix and several β-sheets, with a total molar mass of ~100 kDa (1 Da = 1 g/mol). Cofactors are associated with the L and M subunits forming a two fold symmetry axis, including one bacteriochlorophyll dimer (P) composed of two bacteriochlorophylls, two bacteriochlorophyll monomers (B_L and B_M), two bacteriopheophytins (H_L and H_M), two ubiquinones (Q_A: Primary quinone and Q_B: secondary quinone), and a non-heme iron (Figure 1.3B).

The H-subunit does not contain any cofactor but it is believed to be facilitating the electron transfer between Q_A and Q_B and transfer of protons to Q_B from the cytoplasm.[5]

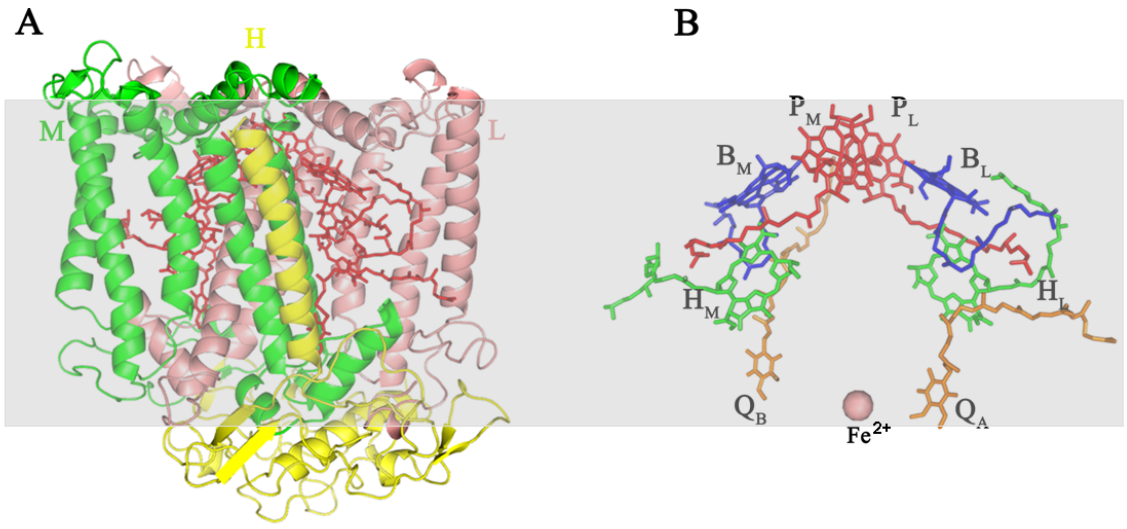

Figure 1.3 Structure of the bacterial reaction center (BRC) from *Rhodobacter sphaeroides* A. Cartoon representation of the isolated BRC structure showing the arrangement of protein subunits: L (salmon), M (green), and H (yellow). The molecules shown in red are the cofactors bound to the protein by non-covalent interactions. **B.** Details of the 9 cofactors of the BRC, which are aligned across the 2-fold symmetry axis that passes through vertically from the dimer (P) to non-heme iron (Fe^{2+}). The membrane is represented by a gray shaded area. The periplasmic side of the membrane is near the top and cytoplasmic side is near the bottom of the structure.[3] Figure was modified by using Pymol software from PDB file 1PCR.[6]

1.3 Electron transfer process in the BRC

The primary process of bacterial photosynthesis is a stepwise, light-induced, transmembrane electron transfer, which creates charge-separated states. Based on extensive spectroscopic studies since the middle of 1970s, it was established that the primary electron donor is the P,[7-9] Q_A and Q_B are electron acceptors,[10, 11] and B_L and H_L are intermediate acceptors.[12]

Absorption of photon excites the bacteriochlorophyll dimer to its electronic excited state and the electron is subsequently shuttled through series of intermediate steps creating $P^+Q_B^-$ charge-separated state (Figure 1.4A). This electron transfer process takes place with the quantum yield of nearly unity, making it most efficient biological energy conversion process. Oxidized dimer (P^+) can be re-reduced by exogenous electron donor cytochrome c_2 (cyt c_2) then after second light excitation a transfer of a second electron takes place and the secondary quinone can be reduced twice. During this process Q_B (accepts two protons from the cytoplasmic side to become quinol (Q_BH_2). Despite apparent two-fold symmetry, Q_A and Q_B have differences in their environment which lowers the energy of Q_B relative to Q_A, which results electron transfer from Q_A^- to Q_B. The Q_A is tightly bound, shielded from the external solvent, and functions as a one-electron acceptor whereas Q_B is weakly bound, surrounded by polar residues, and can accept two electrons and two protons. Then quinol (Q_BH_2) dissociates and is oxidized by cytochrome bc_1 complex, releasing protons and electrons across the membrane.[13] The first proton transfer to Q_B^- from the cytoplasmic side is coupled with the second electron transfer from Q_A^- to Q_B^-. Proton transfer pathway to Q_B is well established elsewhere by carrying out mutagenesis experiments.[14-19]

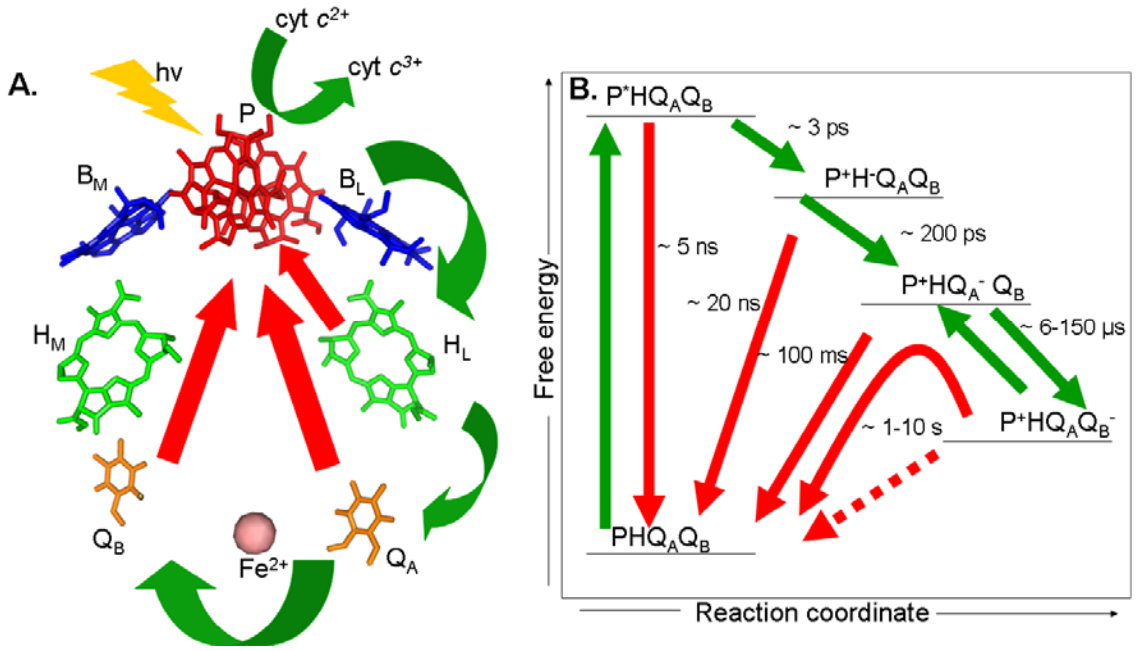

Figure 1.4 Light-induced electron transfer process in photosynthetic BRC. A. Light-induced electron transfer pathway. Phytyl chains are truncated for clarity purpose. **B.** The energy levels of various redox states formed during the electron transfer process. Indicated times represent the lifetime of the different redox states. Green arrows show the forward electron transfer while red arrows show the charge-recombination processes.

Free energy levels suggest that forward electron transfer is favorable to the charge-recombination from intermediate state because it is orders of magnitude faster (Figure 1.4B). Several explanation for this phenomenon have been proposed, such as well-positioned cofactors and surrounding amino acid residues making forward electron transfer energetically more favorable, and conformational changes accompany the formation of charge-pair making the charge-recombination less favorable.[20] Although as mentioned above the cofactors are arranged in quasi-symmetric manner across two-fold axis joining P and iron, electron transfer only occurs through L branch to Q_B (Figure 1.4A).

This is due to partly the interaction between three natural lipids (glycolipid, phospholipid, and cardiolipin) and cofactors.[21] These integral lipids alter the energy levels of the charge-separated state making $P^+B_M^-$ at higher energy level than $P^+B_L^-$ (Figure 1.5). The electron transfer from Q_A^- to Q_B is attributed by a conformational gating step, which causes the movement of Q_B from it's distal to a proximal position[22] and it is facilitated also by the different amino acid surroundings of the two quinones.

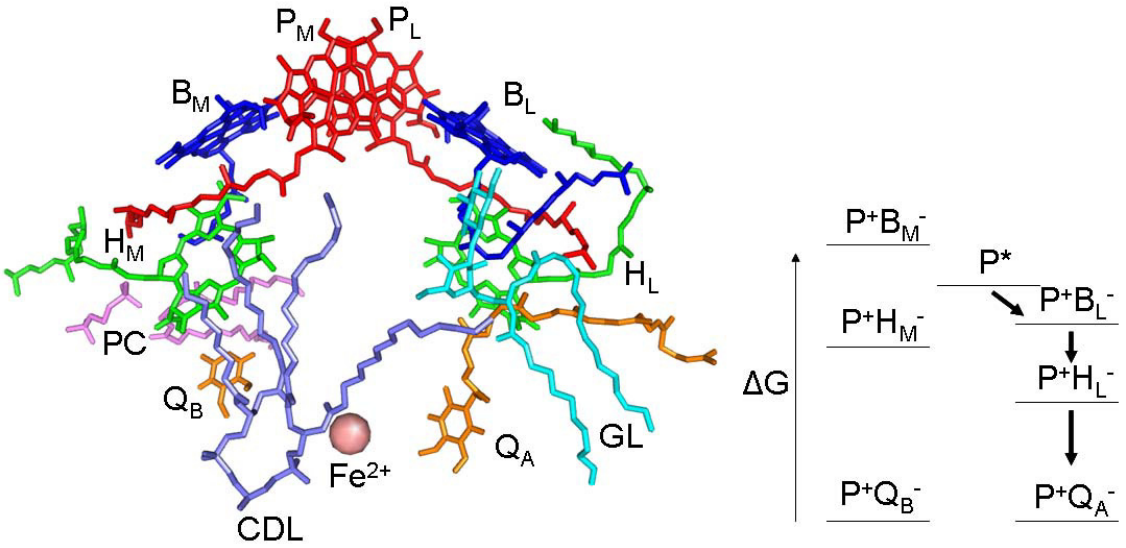

Figure 1.5 Arrangement of natural integrated lipids along with the cofactors and their influence on the energetics of the unidirectional electron transfer. Glycolipid (GL, cyan molecule) binds near B_L. The phospholipid phosphatidylcholine (PC, violet molecule) binds near the H_M. The cardiolipin (CDL, slate molecule) binds near the M subunit without directly interacting with any cofactor. Due to the interactions of these integral lipids with cofactors, the energy levels of the different redox states are altered and therefore the electron transfer proceeds along "L-branch" only. Figure was prepared by using Pymol from PDB code 1M3X.[21]

1.4 Photosynthetic electron transfer cycle and generation of proton electrochemical gradient in the natural membrane of *Rb. sphaeroides*

In a natural membrane environment, the transmembrane electron transfer takes place upon light excitation, which creates the charge-separated state $P^+Q_B^-$. Water soluble cyt c_2 then reduces the oxidized dimer (P^+), a second light excitation transfers a second electron from the dimer to Q_A forming the $P^+Q_A^-Q_B^-$ state. After accepting a proton from the cytoplasmic side Q_BH accepts a second electron from Q_A^- and finally a second proton transfers to form Q_BH_2. Then this quinol will be replaced by a new quinone from the quinone pool and the quinol becomes oxidized by cytochrome bc_1 complex.[20,23,24] During this whole process protons are released at the periplasmic side, generating proton electrochemical gradient to drive ATP synthase[24] and electrons can be transferred from cyt bc_1 complex to mobile electron carrier cyt c_2 to complete the whole cycle (Figure 1.6).

In order to study BRC in detail, it needs to be isolated from the natural membrane environment because the studies of BRCs in membrane fragments (chromatophores) using optical techniques are hampered by the presence of light harvesting complex pigments (LH1 and LH2). After isolation, BRCs are dispersed in mild detergent micelles.[25]

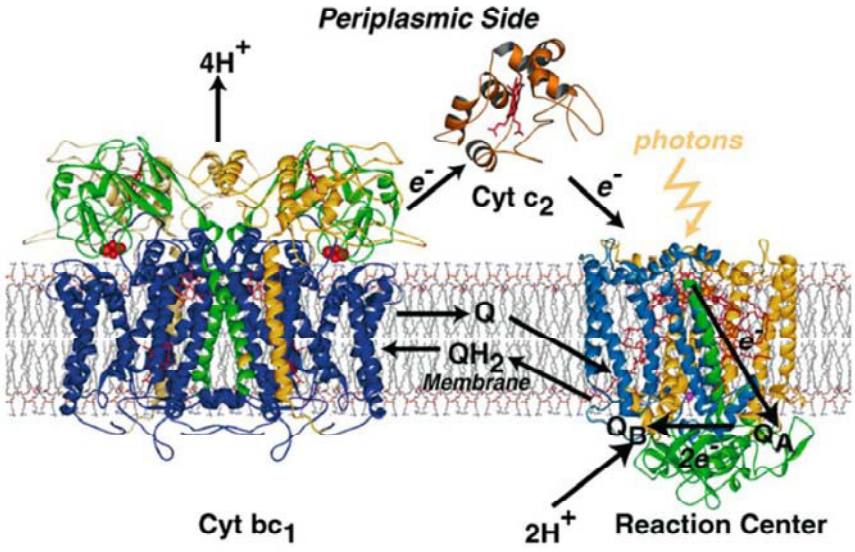

Figure 1.6 The photosynthetic electron transfer cycle in the membrane of the photosynthetic bacterium *Rb. sphaeroides*. Electron transfer from the dimer of the BRC to the acceptor quinone (Q_B) via series of intermediate steps takes place upon light excitation. Reduced secondary quinone is then released and replaced by the new quinone from the quinone pool. Protons are pumped across the membrane and electrons released during oxidation of reduced quinone by cytochrome bc_1. The mobile electron carrier cyt c_2 transfers electron from cytochrome bc_1 complex to the oxidized dimer to re-reduce it.[24, 26]

1.4.1 Substitution of the natural membrane environment of the BRC with detergent micelles and artificial lipid bilayers

Since the BRC is a membrane protein, it is surrounded by a large hydrophobic region of transmembrane helices and therefore it has to be in an amphiphilic environment to survive. In Nature, the membrane has different combination of phospholipids, phosphatidylcholine, phosphatidylethanolamine, and other lipids.[27]

These naturally occurring lipids vary depending on growth conditions of bacteria such as temperature or aerobic/semi-aerobic growth.[27] After extraction of BRCs from natural membrane (chromatophores), it has to be incorporated in detergent micelles, which are substitutes for the membrane (Figure 1.7).

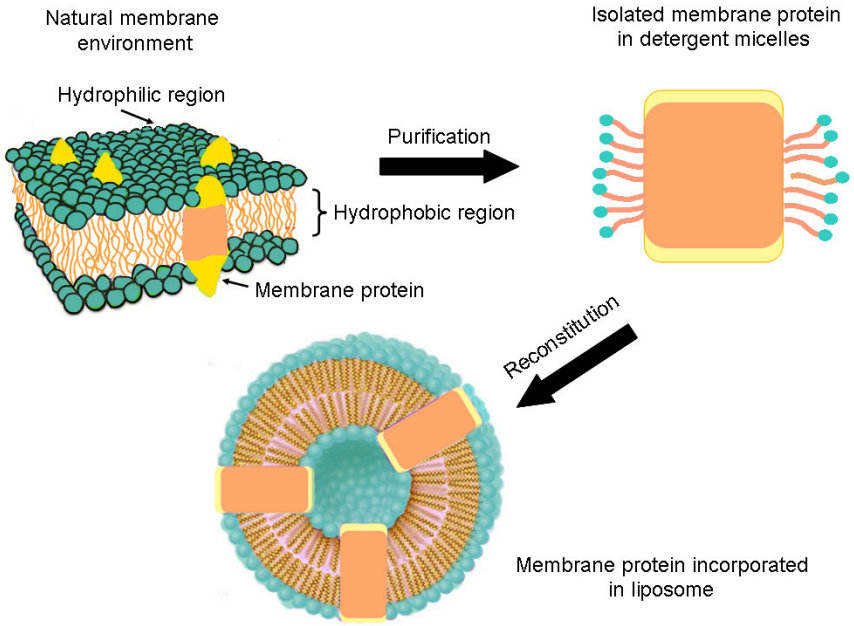

Figure 1.7 Schematic representation of BRC protein in the natural membrane environment, in detergent micelles, and in liposomes. After isolation of BRCs from natural membrane environment into membrane substituent detergent micelles, latter will form belt-like structure around the hydrophobic region of the BRC. The BRC's hydrophilic and hydrophobic regions are represented as yellow and pale orange colors, respectively. These BRCs can further be incorporated into liposomes by removing detergent micelles, which can mimic and to some extent restore the hydrophobic environment of the natural membrane.

These detergent micelles encompass BRC's hydrophobic region by forming belt like structure.[28] Moreover, the lipid environment is known to have a significant influence on membrane morphology, but it is questionable whether it can affect the photosynthetic energy transfer process.[29]

A promising approach is to reconstitute the BRCs into liposomes with different lengths of fatty acid chains that results in different hydrophobic thickness of the lipid bilayers. These artificial liposomes can also mimic natural membrane environment.

In BRCs isolated and crystallized from detergent micelles the hydrophobic thickness of the detergent belt was reported to be ~ 23 Å.[28] This thickness is about 5 Å shorter than the length of the hydrophobic transmembrane helices of the BRC. The detergent molecules orient with their alkyl chains towards hydrophobic regions of BRC, while the hydrophilic head-groups are facing towards the external solvent (Figure 1.7).

The structure of the detergent belt that surrounds the BRC was determined by low-resolution neutron diffraction experiments[28] (Figure 1.8A). For proper solubilization of BRCs, the detergent concentration has to be higher than the critical micelle concentration (c.m.c.) of the detergent. The c.m.c. is the minimum concentration of detergent required to form micelles spontaneously. Initially as detergent is added to water then hydrophobic tails point away from the water by concentrating at the surface to minimize the free energy of the solution. Once c.m.c. is reached then this can be done by forming micelles by orienting hydrophobic tails inward and hydrophilic head-groups outward. These detergent micelles then cover the hydrophobic region of the protein and help to disperse it in aqueous environment. Now the question becomes how good these membrane substituent detergent micelles are as compared to the natural membrane (Figure 1.8B and C). Indeed there are indications that thermodynamics and kinetics of electron transfer reactions in the BRCs have different features in chromatophores than in the membrane substituents. For instance the lifetime of the charge recombination from Q_B (i.e. $P^+Q_B^- \rightarrow PQ_B$) is ~1 s in detergent micelles while it was measured as ~10 s in chromatophores.[30]

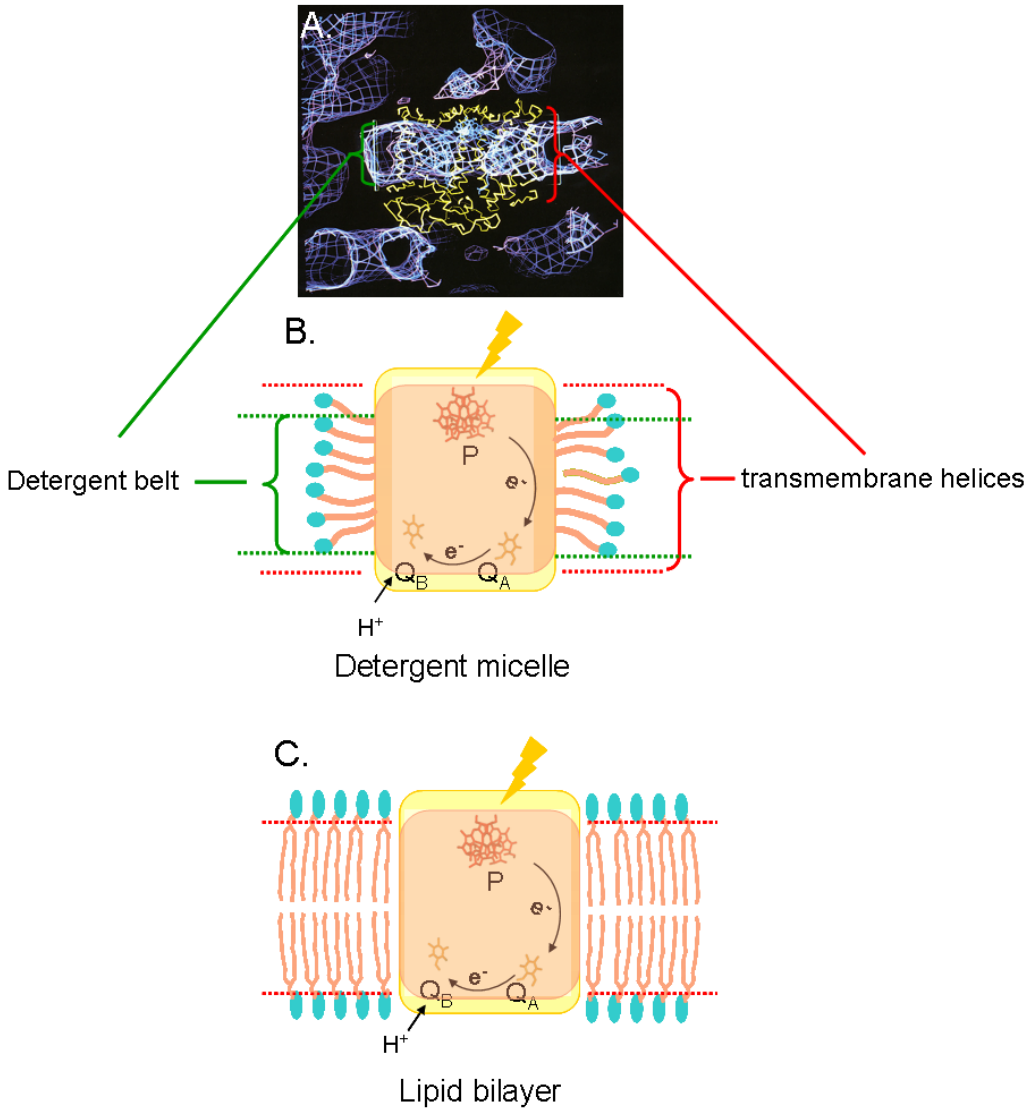

Figure 1.8 Protein interactions with its hydrophobic environment in BRC from *Rb. sphaeroides*. A. Belt-like structure of detergent micelles (blue) around BRC (yellow) where thickness of the detergent belt (green bracket and dotted line) is 5 Å smaller than the hydrophobic thickness of the BRC (red bracket and dotted line).[28] Schematic representation of BRC dispersed in **(B)** detergent micelles and **(C)** lipid bilayer. The BRC's hydrophilic and hydrophobic regions are represented as yellow and pale orange colors, respectively. In the BRC, dimer (P) and quinones (Q_A and Q_B) are shown with the light-induced electron transfer pathway along with proton transfer from cytoplasmic side to Q_B. Thickness of the hydrophobic region of the BRC (pale orange color and red dotted line) can match the hydrophobic thickness of the lipid bilayer.

Various different detergent molecules are used as membrane substituents, such us lauryldimethylamine-oxide (LDAO, zwitterionic at pH 7 and above with pK_a ~ 6.6), [31,32] Triton X-100 (non-ionic), cetyltrimethylammonium bromide (cationic), and deoxycholate (anionic) detergents have been used to disperse the BRC protein having c.m.c. of 0.023%, 0.033%, 0.036%, and 0.2% in the dispersion at 25 °C respectively.

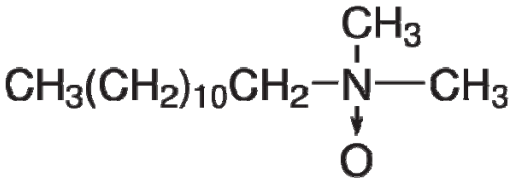

lauryldimethylamine-oxide (LDAO) (zwitterionic detergent)

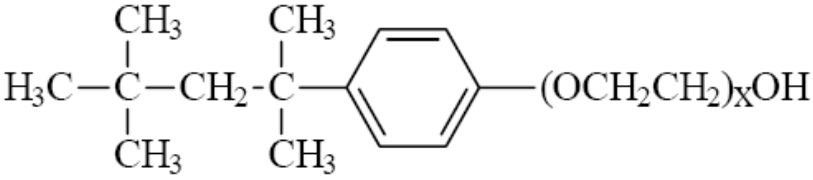

X = 9-10

Triton X-100 (non-ionic detergent)

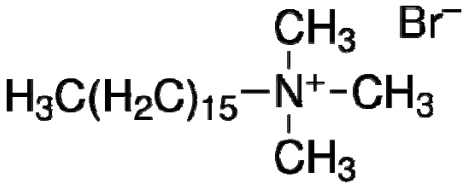

Cetyltrimethylammonium bromide (CTAB) (cationic detergent)

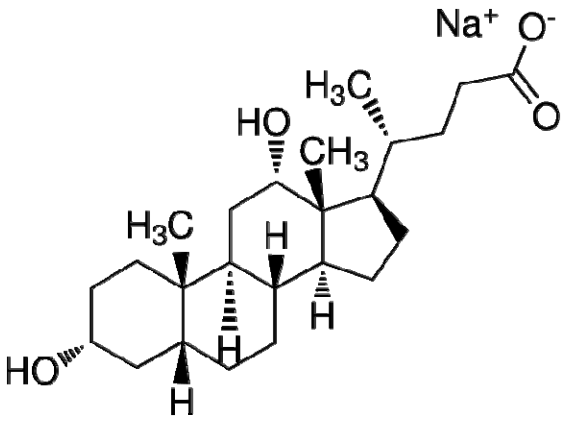

Sodium deoxycholate (DOC) (anionic detergent)

The properties of the detergents also play important role in protein structure-function relationship. For example, changes in temperature, detergent concentration, and functional group in the detergent may all cause change in the size, shape, and aggregation number of the micelle. For ionic detergents the aggregation number (the number of molecules present in a micelle) is less than 100 in aqueous solution with low ionic strength. It is due to the presence of a net head-group charge on detergent molecule that repel one another and hence destabilizing the micelle. On the other hand, at high ionic strength due to screening of the charges, this aggregation number increases substantially with formation of cylindrical micelles. Aggregation numbers of LDAO, Triton X-100, CTAB, and DOC detergents are 70, 140, 61, and 5 respectively in solutions without salt.[33]

Moreover, an increase in the temperature causes small decrease in the aggregation number in aqueous solutions because thermal agitation increases the head-group area.[33]

Functional groups of the detergent or the general structure itself can affect the c.m.c. in aqueous solutions. If the number of carbon atoms in the hydrophobic group in the structure increases then c.m.c. decreases. This decrease in the c.m.c. is slightly larger in case of non-ionic and zwitterionic detergents; an increase by two methyl groups reduces the c.m.c. by an order of magnitude. Similarly, presence of phenyl group in hydrophobic chain is equivalent to three and one-half methyl groups. When the number of carbon atoms in the straight-chain increases beyond 18 then c.m.c. remains unchanged due to the coiling of these long chains in aqueous media.[33]

Similar to detergent micelles different lipids such as cationic 1,2-dioleoyl-3-trimethylammonium- propane (chloride salt) (DOTAP), anionic 1,2-dioleoyl-*sn*-glycero-3-phospho-L-serine (sodium salt) (DOPS), zwitterionic 1,2-dioleoyl-*sn*-glycero-3-phosphocholine (DOPC), zwitterionic 1,2-dilauroyl-*sn*-glycero-3-phosphocholine (DLPC), and 1,2-dimyristoyl-*sn*-glycero-3-phosphocholine (DMPC) can be used. These lipids contain fatty acid chains with carbon length of 18 with a one double bond at 9^{th} carbon from the head-group except DLPC and DMPC, which have 12 and 14 carbon atoms in their acyl chain with no double bond, respectively. Lipids containing 18 carbon atoms with mono-unsaturation can naturally form bilayer structures with different curvatures and have several other properties in common with biological membranes. The thickness of the hydrophobic part of these lipid bilayers is in agreement with the natural membrane thickness of the BRCs.[34]

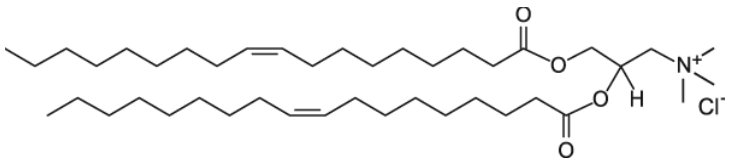

18:1 DOTAP (cationic)

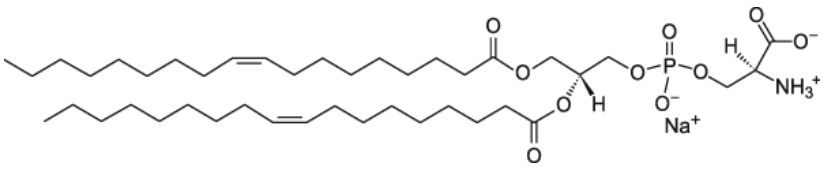

18:1 DOPS (anionic)

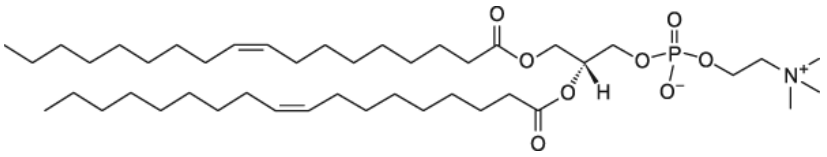

18:1 DOPC (zwitterionic)

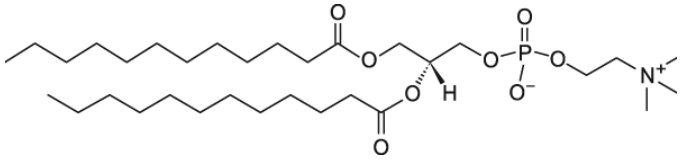

12:0 DLPC (zwitterionic)

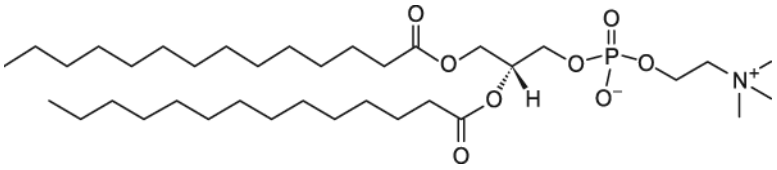

14:0 DMPC (zwitterionic)

Due to wide variety of lipids with different fatty acid chain lengths there will be different lipid-protein hydrophobic interactions. These interactions are discussed in detail in the following section.

1.5 Hydrophobic interaction between the BRC and surrounding environment

During and after isolation and purification, BRC's can be incorporated into different detergent micelles or different liposomes (Figure 1.8B and C). Detergent micelles form belt-like structure around the BRC covering its hydrophobic region by orienting alkyl chains inward whereas liposomes form bilayer of lipid molecules to minimize solvent accessibility to the hydrophobic region (Figure 1.8B and C). The surrounding hydrophobic environment of the BRCs can alter the electron transfer significantly. For instance, the charge recombination from Q_B in detergent micelles (i.e. $P^+Q_B^-$) takes place in ~ 1 s while in liposome it takes ~ 10 s upon flash excitation.[35] For optimal conditions it is necessary that the hydrophobic thickness of the protein should be equal to the hydrophobic thickness of the surrounding environment. These hydrophobic interactions play major role in stabilizing the membrane proteins and can significantly alter the functional parameters. When the hydrophobic region of the BRC is thinner or thicker than the surrounding hydrophobic region of the lipid bilayer or detergent micelles then tension is created to minimize the solvent accessible surface. This hydrophobic mismatch can be minimized by two ways[36]:

1. Deformation of lipid bilayer or detergent micelles, and/or
2. Deformation of α-helices of the BRC protein.

1.5.1 Deformation of lipid bilayer or detergent micelles

In order to minimize the hydrophobic mismatch at the interface of hydrophobic environment and the BRC, the lipid or detergent molecules near the BRC undergo deformation. If there is no hydrophobic mismatch at the interface of the BRC and its hydrophobic environment then there is no need of deformation (Figure 1.9A). If the hydrophobic tail length of the lipid or detergent is shorter or longer than the hydrophobic thickness of the protein then the lipid or detergent has to extend or compress so that the hydrophobic mismatch can be minimized (Figure 1.9B and C). Due to less curvature elasticity in detergent micelles this compensation from the detergent molecule is generally less than the lipid molecule.[36] During this compensating mechanism several lipid molecules near the BRC will be affected and this perturbation in the bilayer extends over few molecules and recovers back to normal thickness in exponential function.[37, 38]

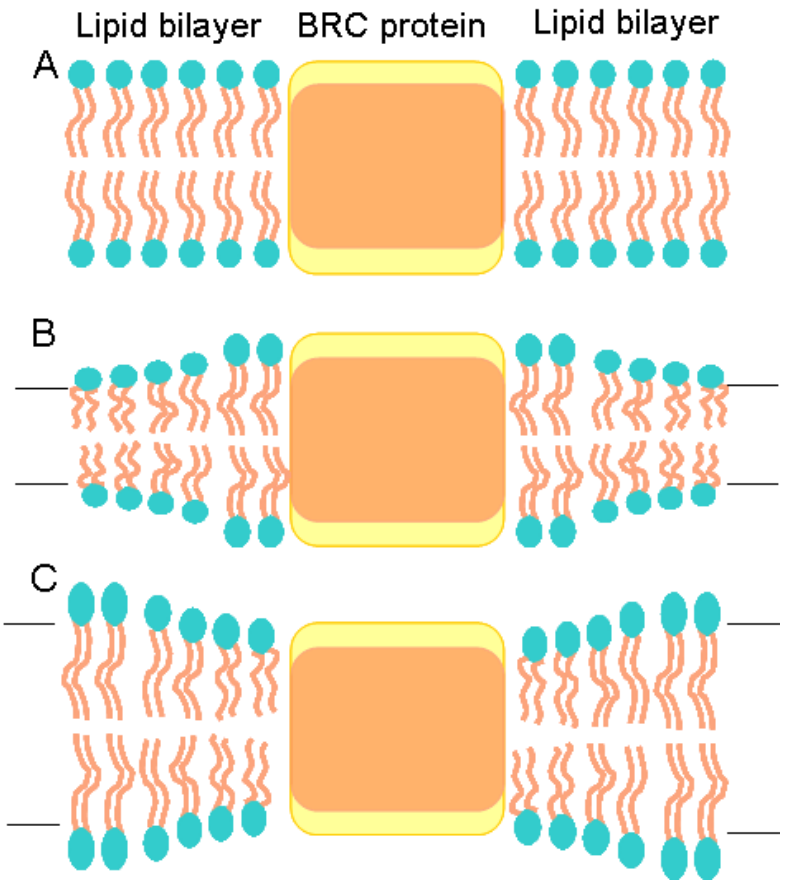

Figure 1.9 Compensation for hydrophobic mismatch from the lipids. A. Hydrophobic thickness of the protein matches exactly the hydrophobic chain length of the lipid. **B.** Hydrophobic thickness of the protein is greater than hydrophobic acyl chain length of the lipid hence, compensation occurs by extending the acyl chain length. **C.** Hydrophobic thickness of the protein is smaller than that of the acyl chain length of the lipid hence, compensation occurs by compressing the acyl chain length.

This lipid response to the hydrophobic mismatch leads to the alteration in the phase transition temperature of the lipid. Lipids can either be in gel or liquid crystalline phase depending on what temperature they are at. In the gel phase the acyl chains are quite rigid and fully extended whereas in the liquid crystalline phase these acyl chains remain fluidic and randomly oriented.

At the phase transition temperature the lipid actually undergoes physical change from one phase to another.[39] The interaction between the lipids and the BRC at the interface will determine the nature of upward or downward shift in the transition temperature of the lipid.

1.5.2 Deformation of α-helices of the BRC protein

Similar to the deformation of lipid or detergent molecules, α-helices of the protein can also tilt or stretch to compensate the hydrophobic mismatch (Figure 1.10). These structural rearrangements in the protein can also be found in the X-ray structure of the BRC where α-helices were slightly tilted (Figure 1.3A).[20,40,41] Aggregation of the proteins in response to the hydrophobic mismatch is also possible but it leads to the loss of function of the proteins. Tilting of the α-helices is limited and therefore the hydrophobic mismatch that cannot be compensated by tilting alone, can be compensated by aggregation.

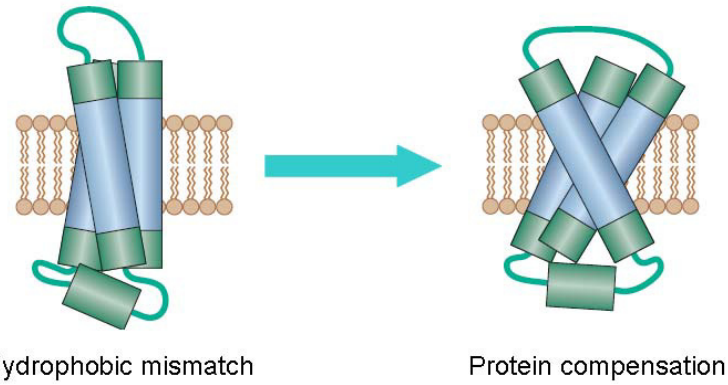

Figure 1.10 Compensation for the hydrophobic mismatch from the protein. If there is hydrophobic mismatch between lipid bilayer and the protein then latter can also tilt its α-helices to compensate for the hydrophobic mismatch. This can occur only up to certain extent and protein adjustment cannot compensate solely for hydrophobic mismatch. Figure was modified from ref.[36]

There are some conformational changes that occur in the BRC protein in the presence of different hydrophobic environment even if the deformation primarily occurs in the surrounding membrane. These structural changes can eventually alter the electron transfer and charge-recombination processes in different liposomes as compared to different detergents. Under physiological conditions, the primary charge recombination ($P^+Q_A^- \rightarrow PQ_A$) occurs in 100 ms while from secondary quinone ($P^+Q_B^- \rightarrow PQ_B$) occurs in 1 s upon flash excitation.[42]

The light-induced electron transfer takes place from P to Q_A and then finally to Q_B depending on the occupancy of the secondary quinone binding site. This Q_B has two binding sites. As electron transfer between Q_A and Q_B takes place then Q_B moves in its binding pocket. This electron transfer step is facilitated by a conformational gating mechanism.[22] During this process Q_B moves from its distal position to its proximal position by 5 Å along with the isoprenoid chain.[22] These binding sites of Q_B were determined by freezing the BRC crystal to cryogenic temperature in the dark and under illumination.[43,44] These structural differences occur as Q_B moves in to the proximity of the non-heme iron upon illumination (Figure 1.11).

As conformational changes occur near the cytoplasmic side, two distinct structural changes were also reported on the periplasmic side near P^+ depending on the type of detergent micelles in which the BRCs were dispersed.[25,45]

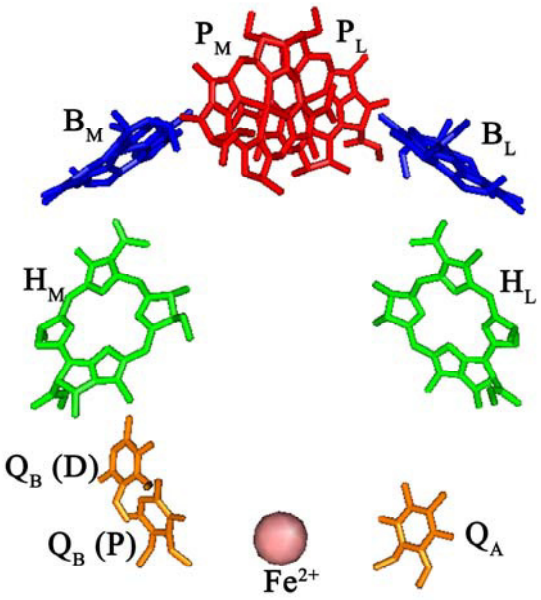

Figure 1.11 Structure of the BRC cofactors with two binding sites of secondary quinone demonstrating approximate symmetry between Q_A and Q_B (P) position. Q_B is bound at distal (D) position, which moves to proximal (P) position to facilitate electron transfer between Q_A and Q_B. The figure was prepared by using Pymol from PDB file 2UXK.[44]

Continuous illumination can increase the lifetime of this charge recombination due to the formation of altered light-adapted conformations. The formation of these altered long-lived conformational changes is independent of the presence of secondary quinone (Q_B). Spectroscopically, these long-lived conformational changes have similar features as that of flash induced $P^+Q_A^-$ or $P^+Q_B^-$.[35,46] The nature of the hydrophobic environment plays crucial role in light-induced conformational changes. While detailed information concerning the conformational changes near the quinone (cytoplasmic side) have been identified, light-induced structural changes near the periplasmic side were still unclear at the time of the design of our research.

1.6 The significance of the structural changes

In membrane proteins proton translocation across the membrane can be facilitated by two types of proton pumps: redox-driven and conformational proton pumps.[47] In a redox-driven proton pump the linear sequence of redox carriers should be localized in the membrane in a way that produces the observed proton translocation. In Nature, the BRC represents the first half of the transmembrane proton pumping and the redox loop is completed by the ubiquinol:cytochrome oxido-reductase enzyme (see Figure 1.6). Within this process the secondary quinone (Q_B) acts essentially as proton and electron carrier in two loops that leads proton translocation across the membrane by cyt bc_1 complex.

In case of conformational pump, such as bacteriorhodopsin from *Halobacterium halobium*, due to a light-induced conformational change the dielectric properties of the protein change rapidly that in turn causes the protonational states of the amino acid residues to be altered, which results the translocation of the protons. Unlike in the redox-driven proton pump, there is no need of proton and electron to bind the same component.[48,49]

Regardless of the classification even in the isolated BRC, which is a redox-driven proton pump, the solvation of newly created charges by individual electron transfer steps is often facilitated by secondary compensating charge motions, which are coupled to conformational changes in the BRC protein. A large variety of conformational changes associated with the electron and proton transfer in BRCs in the vicinity of all cofactors have been reported: two distinct conformations of P^+ were identified that depended on the polarity of detergent and the temperature.[25]

Illumination time and temperature dependent conformational change of the photoactive bacteriopheophytin L (H_L) was determined by the freeze-trapping technique.[50] On the microsecond to submillisecond time scale, protein relaxation before the $Q_A^- \rightarrow Q_B$ electron transfer was identified.[51-54] As mentioned before a slow conformational rearrangement of the Q_B binding pocket has been reported to take place in minutes.[55,56] Even several tens of minutes have been reported as the relaxation time of the protein from a light-induced conformation to a dark-adapted one using photoacoustic[55] or optical spectroscopic and protonational[57] studies.

Thus, descriptions of a functioning BRC call attention to the important role of protein motion and conformational reorganization in the electron transfer process over a wide range of time scales from nanoseconds to minutes.[35,55-66] The study of slow conformational rearrangements upon illumination was inspired by the pioneering work of Kleinfeld and coworkers.[46] Many groups have followed their path in the past quarter of a century and provided new insights to the details of these changes.[35,56,57,65,67,68] Despite these extensive efforts, the exact molecular mechanism of such structural changes was not clear at the time of our project was designed. Therefore the molecular origin of the conformational changes can be of great importance in the quest of identifying the structural mechanism responsible for the altered lifetime of various charge-separated states, observed in earlier studies.

1.7 Electronic transitions of the pigment molecules in BRC

As the BRC is a pigment-protein complex, the properties of the imbedded pigment molecules (bacteriochlorophylls and bacteriopheophytins, and quinones) are heavily dependent upon the immediate protein environment of the individual pigments. Given the unique protein environment of each pigment, the electronic absorption spectrum of the BRC (Figure 1.12A) shows distinct features for each pigments. Due to a great degree of conjugation in these molecules, the $\pi \rightarrow \pi^*$ electronic transitions no longer fall into the ultraviolet (UV) spectral region but rather into the visible (VIS) or occasionally even into the near infrared (NIR) regime. Due to the complex planar structure of the molecules, each pigment possesses two dipole moments (Q_X and Q_Y) along which electronic excitation can take place. The Q_X transition requires higher energy than that of the Q_Y providing two absorption bands for each pigments. The Q_X transition has a dipole moment in the plane of ring 4 to ring 2 while the Q_Y has a dipole moment in the plane of ring 3 to ring 1 (Figure 1.12B). The absorption spectrum of the BRC shows that the bacteriochlorophyll dimer absorbs around 865 nm, bacteriochlorophyll monomers (B_L and B_M) absorb around 800 nm, bacteriopheophytins (H_L and H_M) absorb around 760 nm and in the Q_X region, bacteriochlorophylls and bacteriopheophytins absorb around 600 and 540 nm, respectively. The intense absorption band below 400 nm represents porphyrin macrocycle (Soret band) whereas 260 nm absorption band is characteristic to aromatic amino acids.[69]

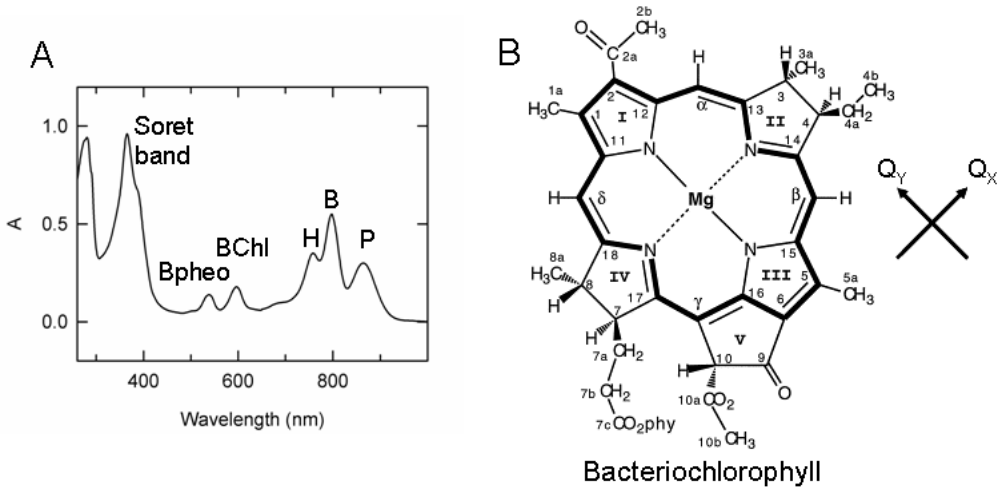

Figure 1.12 UV-VIS-NIR electronic absorption spectrum of the BRC (A) and the structure of the bacteriochlorophyll molecule (B). In the optical spectrum of the BRC, the dimer (P), two monomers (B_L and B_M), and two bacteriopheophytins (H_L and H_M) absorb around 865, 800, and 760 nm in the Q_Y transition region, respectively. In the Q_X region bacteriochlorophylls (BChl) and bacteriopheophytins (Bpheo) absorb around 600 and 540 nm, respectively. The bacteriochlorophyll molecule, which is a tetrapyrrole macromolecule with central magnesium. Ring 1 has 2-acetyl and ring 5 has 9-keto carbonyl group. Dipole moments of Q_X and Q_Y are in ring 4-2 and ring 3-1 plane, respectively. Phy is a phytyl chain.

The conjugation level of the macrocycle in the Q_Y transition is more than the Q_X transition therefore the absorption bands are shifted to the longer wavelengths. The dimer has two halves of bacteriochlorophylls that are electronically coupled, which results even a higher wavelength for the absorption band at 865 nm. Since the absorption bands of the electronic transitions of the individual chromophores are sensitive to changes of their nearby protein environment, optical spectroscopy can be used to probe changes in the local electrostatics upon light excitation.

The internal electric field generated by the light-induced charge separation is always oriented in each BRC, and the electrochromic absorption changes are pronounced in the light-minus-dark optical difference spectrum even at room temperature. To investigate the changes in the local electric field due to the conformational changes, the band shifts of the tetrapyrroles at physiologically relevant temperatures can be monitored using optical spectroscopy.

The absorption bands in the electronic absorption spectrum are induced by the absorption of the photon and subsequent electron transfer. The absorption bands of chromophores can be bleached, shifted, or broadened upon light excitation of the BRC. The former is due to the formation of new species whereas the latter two are due to the changes in the polarizability and dipole moment of the chromophores, respectively. These changes can happen due to the structural changes in the vicinity of these cofactors or by introducing charges on the dimer and quinones by light-induced electron transfer process.

The NIR spectrum of the BRC is very informative because the dimer has strong absorption at ~ 865 nm in the dark-adapted state (Figure 1.13A). Light excitation causes transmembrane electron transfer from dimer to the quinone that creates the charge-separated state ($P^+Q_X^-$; X: A or B), this results in bleaching of the dimer absorption band in the light-adapted state due to oxidized dimer (P^+) (Figure 1.13A). The formation of the charge-separated state causes the hypsochromic shift in the bacteriochlorophyll monomer band and a bathochromic shift in the bacteriopheophytin absorption band due to electrochromic effects.

To identify the small changes in the spectrum as a result of illumination, light-minus-dark difference spectrum can be generated by subtracting dark-adapted spectrum from light-adapted spectrum (red trace in Figure 1.13B).[69] This light-minus-dark spectrum can be decomposed further into the band of the oxidized dimer (P^+) and electrochromic shifts in the bacteriochlorophyll monomer and bacteriopheophytin bands (blue, pink, and green traces in Figure 1.13B). The presence of these spectral signatures is characteristic to the presence of the charge-separated state ($P^+Q_X^-$; X:A or B).

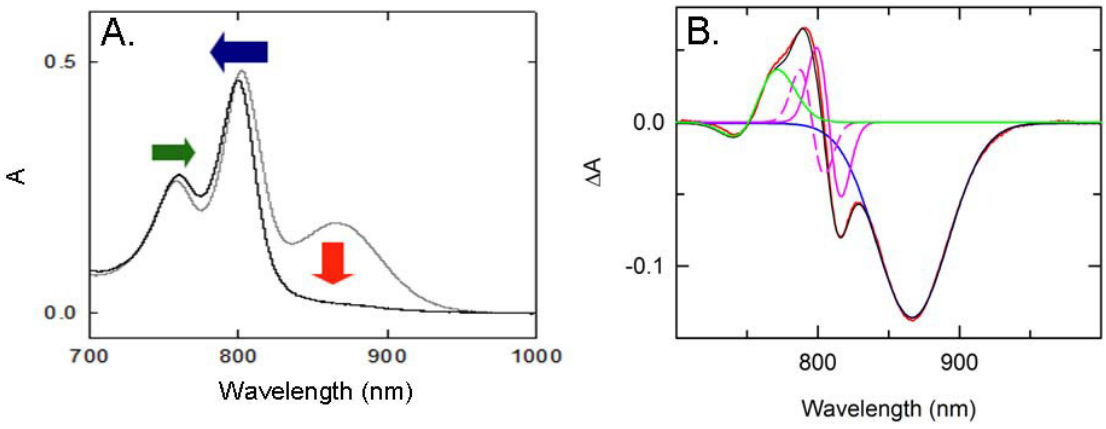

Figure 1.13 Near-infrared (NIR) absolute and light-minus-dark difference spectrum of the BRC. A. The NIR dark-adapted spectrum of the BRC is shown in gray. The spectrum recorded under illumination is shown in black. Upon illumination, transmembrane electron transfer takes place from the dimer to the quinone resulting in bleached dimer band (red arrow), a hypsochromic shift in monomer (B) band (blue arrow), and a bathochromic shift in the bacteriopheophytin (H) band (dark green arrow) due to electrochromic effect. **B.** Light-minus-dark difference spectrum (red trace) can be fitted by summation of Gaussians for the bleached dimer band (blue trace), shifts in the both monomer bands (B_M in dashed pink and B_L in solid pink traces), and bacteriopheophytin band (green trace) to determine shifts in the band positions from dark- to light-adapted states. Total fit is represented by black trace. The values of the fit are listed in the text.

The ground state spectrum has absorption bands centered around 760, 800, and 865 nm due to absorption of the bacteriopheophytins, bacteriochlorophyll monomers, and bacteriochlorophyll dimer, respectively (Figure 1.12A).[69] The widths of the absorption bands can be determined by Gaussian fits of the individual bands of the optical spectrum, yielding band widths at half-maxima (BWHM) of 28 nm centered at 865 nm for the P band, 8 nm each centered at 790 and 810 nm for B_L and B_M, respectively contributing to the 800 nm band, and 14 nm centered at 760 nm for both bacteriopheophytins (H_L and H_M). The overall shift in the bacteriopheophytin band is much smaller and it is due to the formation of Q_A^-, therefore this band was not decomposed into two individual contributions of H_L and H_M for simplicity.

Once the spectra were recorded for dark-adapted and light-adapted state of the BRCs then absorption changes at the dimer band position (865 nm) can be monitored for kinetic analysis (Figure 1.14).[70] Before turning the light on there is no change in the kinetic trace but after turning on the external illumination a transmembrane electron transfer takes place creating the $P^+Q_B^-$ charge-pair. Due to the instantaneous oxidation of the dimer there is sudden change in the kinetic trace (red portion of the kinetic trace in Figure 1.14). Upon further illumination this charge-separated state slowly converted to a different conformational state (light-adapted state) and this can be seen as a slow rise in the signal of the kinetic trace (blue portion of the kinetic trace in Figure 1.14). One must realize that this slow increase of the signal can only be observed if subsaturating illumination is used, namely only a fraction of the BRCs are in the charge-separated state at any given moment during the illumination.

Once the external illumination is turned off then the fraction of the BRC which is still in the dark-adapted state recovers rapidly whereas the fraction of the BRC, which underwent conformational changes recovers on longer time-scale (green and pink portions of the kinetic traces in Figure 1.14).

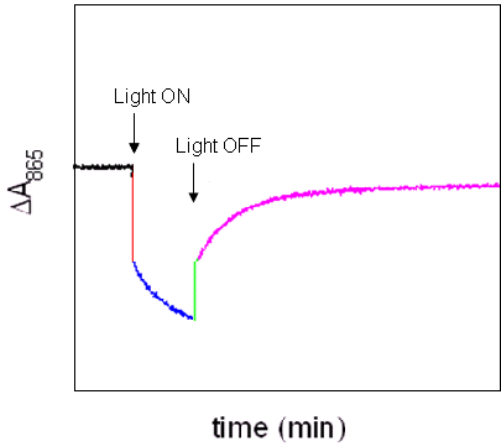

Figure 1.14 Schematic representation of identification of different conformational states formed after the illumination by kinetic analysis. Multiple components were identified in the kinetic traces. Red component represents sudden change in the absorption upon illumination due to the formation of charge-separated state in the dark-adapted conformation. Prolonged non-saturating illumination causes light-induced structural changes which can be attributed to the blue part of the kinetic trace that increases gradually. After turning off the illumination, charge recombination from the dark-adapted conformation takes place very rapidly (~ 100 ms from Q_A and ~ 1 s from Q_B), which is represented by unresolved green part of the trace. The fraction of P^+ that is recovering from altered light-adapted state recovers on longer time-scale (pink part of the trace). Charge-recombination kinetics can have multiple components depending on light-adapted conformational sub-states but only one component was shown for simplicity (pink trace).

1.8 Site-directed mutants for altering the immediate vicinity of the primary electron donor

The two halves of P contain two π-conjugated groups: the 2-acetyl and the 9-keto carbonyl that are possible proton acceptors for hydrogen bonds (H-bonds) (Figure 1.12B). Structural and spectroscopic data demonstrated that in the wild type (WT) *Rb. sphaeroides* reaction center only one H-bond exists between His L168 and the 2-acetyl group of the L half of the dimer (P_L) in addition to the Mg-coordinating His residues at L173 and M202.[3,71,72] A series of mutants have been constructed to modify the H-bonding pattern on the conjugated carbonyl groups of P by introducing histidine residues into each H-bonding position or replacing His L168 (Figure 1.15).[73] In the mutants, Leu to His at L131, Leu to His at M160, Phe to His at M197, and His to Phe at L168, the formation and removal of H-bonds were confirmed by Raman, infrared, and special triple spectroscopies.[74-76]

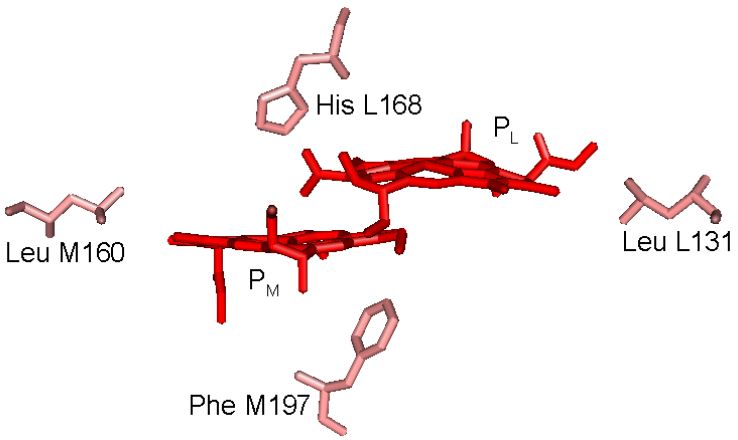

Figure 1.15 Top view of the two halves of the bacteriochlorophyll dimer (P_L and P_M in red) with nearby amino acid residues (salmon sticks). The four residues, Leu L131, Leu M160, His L168, and Phe M197, were modified to introduce or remove H-bonds. Coordinates were taken from Protein Data Bank entry 1PCR.[6]

Even though the spectroscopic properties of these mutants, including the shifts of the Q_Y band of P caused by the mutations, have been extensively studied in the past, the shifts of the absorption bands of the surrounding cofactors upon extended illumination have not yet been scrutinized.[77,78]

In WT reaction centers the carotenoid pigment was located near B_M surrounded by mostly aromatic side chains that could place steric constraints on its conformation (Figure 1.16B). Carotenoids are key elements necessary for the photosynthetic complexes. They transfer the energy to the dimer by harvesting the light energy where bacteriochlorophylls have weak absorbance. Under intense light condition they can prevent photo-degradation of pigments and can regulate light energy.[79,80] If the carotenoid is removed from the BRC then the mutant is referred as R-26 (Figure 1.16A). Apart from the presence or absence of the carotenoid there are no other structural differences between these two strains, but due to absence of carotenoid pigment in R-26 mutant B_M has access to external solvent.[11]

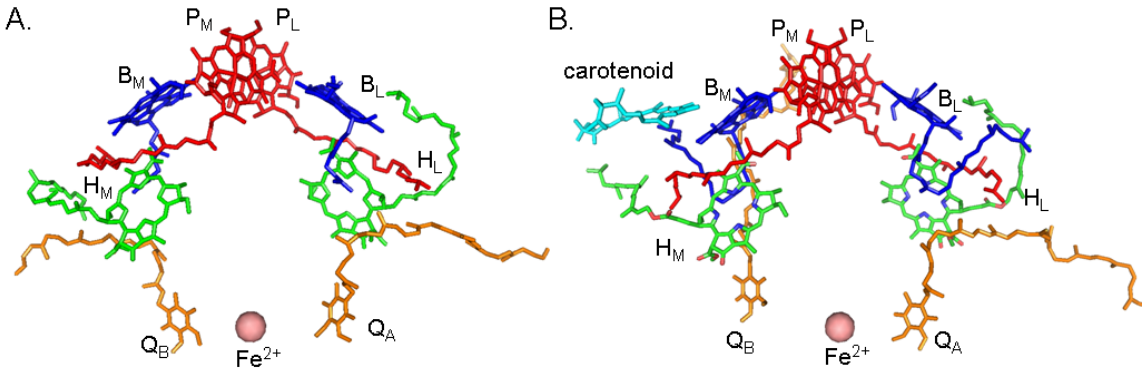

Figure 1.16 Details of 9 cofactors of the BRC in (A) carotenoidless R-26 mutant and in (B) WT. The carotenoid molecule (cyan) binds near inactive B_M. Other notations are similar to figure 1.3. Coordinates were taken from PDB entries 4RCR[81] and 2GMR[82].

1.9 Research perspective

During photosynthesis solar energy can be harnessed and this process has provided much of the world's energy requirements for more than three billion years ever since life began on Earth.[83] Additionally, photosynthesis is the source of carbohydrates in our food and the carbon that we burn in current fossil fuels, which are the products of ancient photosynthetic activities. Photosynthesis can offer an environmentally friendly way to convert the solar energy with the least amount of cost.[84] Nature has created life on Earth in the form of photosynthetic bacteria, which has been present over billions of years, and represents the most efficient biological energy conversion system. Since the BRC has functional similarities to that of PS II but it is much simpler than the latter, it can be an excellent model for studying biological energy conversion and understand the structure-function relationship. Light-induced transmembrane electron transfer is followed by the protein motion and conformational reorganization to solvate newly created charges. Nature's photosynthetic apparatus offers at least three different model examples for solar energy conversion that can inspire humanity to develop artificial light-driven energy converters for future energy production and storage: (i) creation of long lived, energetic charge-separated states in many photosynthetic enzymes, (ii) generation of proton-electrochemical gradient in both oxygenic and anoxygenic systems, and (iii) catalytic splitting of water in oxygenic photosynthetic organisms. Although these model examples are heavily dependent on charge stabilization via conformational changes, very little is known about the role of the conformational flexibility of the enzymes carrying out the reactions.

In a cell membrane, the BRCs along with the redox loop ubiquinol:cytochrome oxido-reductase complete the electron and proton transfer processes, where oxidized dimer (P^+) is reduced by cytochrome and quinol is replaced by new quinone from the quinone pool to complete the cycle (Figure 1.6). In the absence of secondary electron donor to the dimer and upon exhaustion of quinone pool in isolated BRCs, subsaturating continuous illumination causes structural changes to stabilize charge-pair. Extent of these structural changes depends on various factors such as pH, illumination time, nature of hydrophobic environment etc. to name a few.

Many groups have studied the slow conformational rearrangements upon illumination and provided new insights to the details of these changes[35,56,57,65,67,68] and much of this work has centered on the quinones *i.e.* cytoplasmic side (Figure 1.17)[43,85].

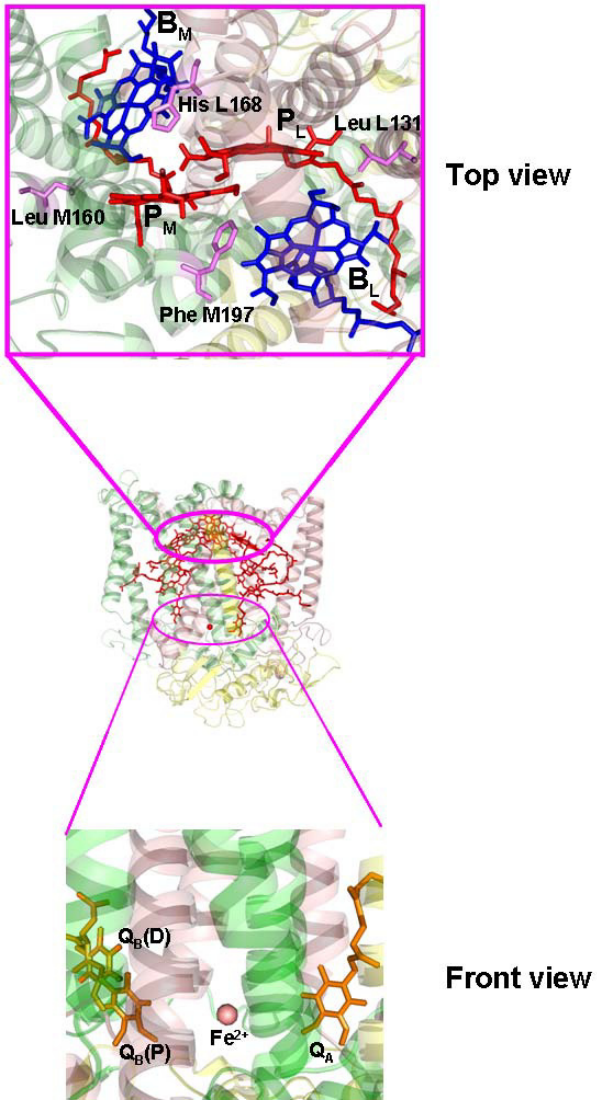

Figure 1.17 Structure of the BRC (at the center) and highlighted periplasmic (at the top) and cytoplasmic (at the bottom) side of the reaction center cofactors. Top panel shows the top view of two halves of the bacteriochlorophyll dimer (P_L and P_M in red) and monomers (B_L and B_M in blue) along with nearby amino acid residues (Leu L131, His L168, Leu M160, and Phe M197 in violet). The L, M, and H subunits are also shown in the background with salmon, green, and yellow colors, respectively. Since light-induced structural changes in the vicinity of the dimer (periplasmic side) are identified in this dissertation, it is highlighted by the pink box. Bottom panel shows primary and secondary quinone (Q_A and Q_B in orange) with non-heme Fe^{2+}. This represents conformational gating mechanism for Q_B (distal (D) to proximal (P) movement) as part of the light-induced structural changes at the cytoplasmic side. The protein subunits are shown in the background.

In contrast to the detailed information concerning the conformational changes near the quinones, no specific light-induced structural changes involving tetrapyrrole macro cycles or specific amino acid residues near the periplasmic side have been identified. Therefore within this research project we used site-directed mutants to identify conformational changes near the dimer induced by continuous illumination (Figure 1.17). Preliminary results showed that the prolonged lifetime of the light-induced charge-separated state is primarily observed due to the structural changes that are occurring in the vicinity of the dimer. To identify these structural changes in the BRC systematically, it is inevitable to study the effects of alterations in amino acid side chains near the P on the light-induced conformations of the BRCs in all site-directed mutant reaction centers.

These studies by using site-directed mutants from *Rb. sphaeroides* were then extended to reaction centers from another strain, *Rb. capsulatus*, which has homologous structure to *Rb. sphaeroides*.

The studied structural changes can be physiologically significant if environmental conditions, such as excess light or redox competitions limit the sizes of quinone and cytochrome pools and the normal function of the BRCs are suppressed. Our goal was also to systematically tune the conformational changes by controlling the environment and utilize the BRC as an artificial light induced charge-storage device. Within this research project alteration of the local environment of the BRC was done by binding different transition metal ions, detergent, or lipid molecules with different head-group charges. The nature and net head-group charge of these molecules was seen to influence the stability of charges by altering the local dielectric constant.

Under physiological conditions the light-induced transmembrane electron transfer creates positive and negative charges that are separated by a low dielectric medium *i.e.* hydrophobic core of the protein. The ability of the BRC protein to form light-induced charge-pair with an extended lifetime as compared to 100 ms (In Nature) can provide new opportunities to utilize BRC as a light-driven biocapacitor for energy storage.

First, we have identified the molecular information behind the conformational changes that occur in the BRC, which leads to the extended lifetime of the charge-separated state. Further evidence was provided to support these structural changes by studying the reaction center from another strain *Rb. capsulatus*. Then we have demonstrated how to control these conformational changes by systematically changing various parameters like illumination time, binding of lipid or detergent molecules with different head-group charge, temperature, pH, binding of different metal ions etc. With these changes, the lifetime of the charge-separated state has been increased by an unprecedented 5 orders of magnitude.

Chapter 2

Materials and methods

2.1 Growth of *Rb. sphaeroides* bacterium

Reaction centers from carotenoid-less mutant R-26 and WT of *Rb. sphaeroides* were grown and purified for all experiments according to Feher and coworkers.[86] This process involves preparation of media, sterilization of media, inoculation, and finally growing bacteria photosynthetically.

Growth media were prepared by using 4 g of casamino acid, 4 ml of growth factor (vitamin solution), 80 ml of concentrated base, 40 ml of potassium succinate, 80 ml of phosphate buffer (1M), and 25 ml of ammonium sulfate. Finally the volume was adjusted to 4 L. Then the media solution was autoclaved in a SV-120 scientific pre-vacuum sterilizer (using Pyrex glass bottles) for an hour and cooled to room temperature before doing inoculation.

The solutions for the growth media are prepared as follows:

The growth factor or vitamin solution was prepared by combining 2 mg of biotin, 50 mg of sodium bicarbonate, 100 mg of nicotinic acid, 50 mg of thiamine-hydrochloride, and 100 mg of p-amino benzoic acid. The solution was boiled to dissolve all the ingredients and the final volume was adjusted to 100 ml. Once it is dissolved, the solution was autoclaved for an hour and cooled to room temperature.

Concentrated base was prepared by using 12 g of potassium hydroxide and 20 g of nitrilotriacetic acid. The solution was stirred for 20 minutes and only the supernatant was used. Then 58 g of magnesium sulfate heptahydrate, 6.8 g of calcium chloride dehydrate, 200 mg of ferrous sulfate heptahydrate, and 4 ml of ammonium molibdenate solution in the portion of 1 ml were added slowly. All contents were dissolved before adding the next. Finally the 'metals 44' solution was added, pH adjusted to ~ 6.7 and volume brought to 2 L.

'Metals 44' solution contains 200 mg of ethylenediaminetetraacetic acid (EDTA), 1.1 g of zinc sulfate heptahydrate, 500 mg of ferrous iron sulfate heptahydrate, 150 mg of manganous sulfate monohydrate, 40 mg of cupric sulfate pentahydrate, 20 mg cobalt chloride, 12 mg of boric acid, and 150 µl of 6 N sulfuric acid. The volume was adjusted to 100 ml. The color was greenish at the beginning but becomes amber later.

The potassium succinate solution with 20% concentration was prepared by pouring 200 g of succinic acid in a beaker with 250 ml water and stirring, it did not dissolve completely. In another beaker, 200 g of potassium hydroxide was dissolved and cooled. Using an ice bath, the potassium hydroxide was added slowly to the beaker containing succinic acid. The final volume was adjusted to 1 L and pH was brought to 7.0 by adding HCl.

The 1 M phosphate buffer was prepared by adding 274 g of dibasic potassium phosphate trihydrate to 1200 ml of distilled water and dissolving 136 g of monobasic potassium phosphate in 800 ml of distilled water then slowly combining the solutions. Final volume was made to 2 L at a pH of 7.0.

The ammonium sulfate solution with 10% concentration was prepared by dissolving 50 g of ammonium sulfate in 500 ml of water and pH was adjusted to 7.0.

All solutions were prepared in distilled water and final solutions were stored at 4 °C. Inoculation with bacteria was done near the Bunsen burner to avoid any external contamination. The inoculated media were put in the dark for a maximum of 6 hours in order to consume the oxygen. *Rb. sphaeroides* was grown under anaerobic conditions in the presence of light (60 W power) for two days. Once the cells were completely grown, they were centrifuged using a Beckman J2-HS centrifuge at 4 °C by generating force of 7,000 g for 20 minutes with a JA-10 rotor. The supernatant was discarded and all cells were collected and stored at −20 °C.[86]

2.2 BRC purification

The BRCs were purified and dispersed in LDAO detergent micelles according to previously described standard procedure.[87-89] Briefly, 100 g of collected cells were allowed to stir in 200 ml of distilled water and 2 ml of 1 M Tris buffer for 1 hour. At the end of stirring, a homogenized solution was obtained. Then 2 ml of EDTA, 1.25 g of sodium chloride (NaCl) salt for ionic strength and 1.7 ml of LDAO detergent was added. The cells were lysed with 40 minutes of pulsed sonication in 10 s intervals in an ice bath using a Mandel Scientific company's ultrasound processor (Model XL2020, Farmingdale, New York, USA) to avoid excessive temperature.

The final volume of the solution was adjusted to 210 ml, which was filled in 8 tubes and centrifuged by generating force of 200,000 g at 4 °C for 2 hours in Beckman Optima XL-100K ultracentrifuge (Fullerton, California, USA) with Ti-70 fixed angle rotor. After the first centrifugation, pellets were re-suspended in 205 ml of TEN buffer. TEN buffer contains 15 mM **T**ris-HCl, 1 mM **E**DTA, and 0.1 M **N**aCl. Then 4.66 ml of LDAO was added in the dark and allowed to stir for 10 minutes at room temperature. Centrifugation of this solution was done with same parameters as the above-mentioned ultracentrifuge procedure to solubilize BRCs in detergent micelles. Crude BRCs dispersed in detergent were collected from the supernatant discarding the pellets containing cell membranes. For 220 ml of supernatant 72 g of ammonium sulfate and 7.3 ml of 30% LDAO were used for the isolation of crude BRCs. The mixture was allowed to stir for 15 minutes at room temperature. These crude BRCs were centrifuged by generating force of 10,000 g at 4 °C for 15 minutes in Beckman J2-HS centrifuge machine with a rotor type of JA-17 and re-suspended in TEN buffer. Re-suspended BRCs were dialysed overnight, to remove ammonium sulfate, in $TL^{0.1}E$ which contains 15 mM **T**ris-HCl, 0.1% **L**DAO, and 1 mM **E**DTA.

For further purification of the BRCs, diethylaminoethyl (DEAE) ion exchange column chromatography was used. The Toyopearl 650 M column was equilibrated with excess of $TL^{0.1}E$ buffer then protein was loaded onto the column, which binds to the column material. Then column material was washed with bound protein by using $TL^{0.1}E$ buffer until no more free pigment was coming out. To verify whether the free pigment was coming, optical spectrum of eluate was recorded every 10 minutes in 260 to 1000 nm range.

By creating a linear salt gradient from 0.03 to 0.25 M NaCl in $TL^{0.1}E$ buffer purified protein and other free pigments were separated. Afterwards the column material was cleaned with 1M NaCl. The purity of the BRC protein was checked by taking the ratio of the absorbances at 280 nm and 800 nm (A_{280}/A_{800}). This ratio was kept below 1.6 but for the purest protein this ratio has to be 1.2. Aromatic amino acids have absorbance at 280 nm, which is 1.2 times that of bacteriochlorophyll monomer at 800 nm. For pure BRC, the ratio of amplitude of absorption bands of bacteriochlorophyll dimer, bacteriochlorophyll monomer and bacteriopheophytin has to be 1:2:1. After the column chromatography, excess salt from the BRC protein was removed by dialysis against salt free $TL^{0.1}E$ buffer. All dialysis were done at 4 °C in the dark using dialysis membranes with a molecular weight cut off (MWCO) of 12-14 kDa. The BRC protein dispersed in detergent micelles were further concentrated by ultra filtration using Millipore membranes having a nominal molecular weight limit (NMWL) of 30 kDa under nitrogen pressure. The concentration of BRC protein was checked by optical spectroscopy by determining absorption of bacteriochlorophyll monomer at ~ 800 nm where it has extinction coefficient of 288 mM^{-1} cm^{-1}.[90] In order to block the electron transfer from Q_A to Q_B, terbutryn, a potential inhibitor was routinely added at a 100 μM concentration.[32] Purified protein was stored at −80 °C in the dark. The purified BRC can be dispersed into different detergent micelles by running same column chromatography technique explained before for the purification with $TX^{0.1}E$ (15 mM **T**ris-HCl, **X**: TX-100, DOC, or CTAB and 1 mM **E**DTA) buffer that has appropriate concentration of the detergent (above c.m.c.) and buffer with high salt concentration was applied to elute the protein. All used chemicals were ordered from Sigma-Aldrich.

2.3 Proteoliposome preparation

Reconstitution of the BRCs from detergent micelles into the liposomes was done by the standard procedure.[30] The proteoliposomes prepared in this work were from phosphatidylcholines and phosphoserine with different fatty acid chains and different head-group charge manufactured by Avanti Polar Lipids (Alabaster, Alabama, USA). These lipids were used without further purification (>99%). Briefly, 4 mg of phospholipids were dissolved in 200 μL chloroform in a conical tube and chloroform was evaporated with continuous nitrogen stream to form a thin uniform film of phospholipids on a surface of the tube. The film can be stored at −20 °C for a month. This lipid film was dissolved in 0.5 mL of 4% sodium cholate solution prepared in respective buffer that has 15 mM potassium chloride (KCl) and sonicated for 45-60 minutes with 10 s pulse interval using the same ultrasonic processor that was used to break the cells, to form lipid-detergent mixed micelles. After the addition of the BRC in ~ 2 μM final concentration the mixture was agitated with a vortex mixer to allow the phospholipid/protein/detergent mixed micelle formation. This dispersion of BRCs with mixed micelles was then loaded into 15 cm long Sephadex G-50 superfine gel filtration column. The column was pre-equilibrated and packed with a respective buffer. Appropriate buffer was used to set desired pH of the experiment. During the elution, the mixed micelles containing BRCs were derived from detergents while phospholipids and protein could rearrange to form proteoliposome. The formation of these proteoliposomes was verified by light-scattering measurement superpositioned by active BRC absorption spectrum.[91]

The following lipids were used in this thesis.

Zwitterionic 1,2-dilauroyl-*sn*-Glycero-3-Phosphocholine (DLPC), zwitterionic 1,2-dimyristoyl-*sn*-Glycero-3-Phosphocholine (DMPC), zwitterionic 1,2-dioleoyl-*sn*-glycero-3-phosphocholine (DOPC), cationic 1,2-dioleoyl-3-trimethylammonium-propane (DOTAP), anionic 1,2-dioleoyl-*sn*-glycero-3-phospho-L-serine (DOPS). Since lipids containing 18 carbon atoms with mono-unsaturation (dioleoyl family) form lipid bilayers that have hydrophobic thickness similar to the cell membranes of *Rb. sphaeroides*, the effect of head-group charge on light-induced conformational changes can be studied in proteoliposomes. Using shorter acyl chain length of lipids with same head-group the role of hydrophobic mismatch on stability of light-induced charge-pair can be identified.

2.4 Construction of mutants

A series of reaction center mutants have been constructed by our collaborators, J. C. Williams and J. P. Allen (Arizona State University, Tempe, Arizona, USA) in the 1990s, to modify the hydrogen bonding pattern on the conjugated carbonyl groups of P by introducing histidine residues in the hydrogen bonding position or replacing His L168. In the mutants, Leu to His at L131, LH(L131), Leu to His at M160, LH(M160), Phe to His at M197, FH(M197), and His to Phe at L168, HF(L168), the formation and removal of hydrogen bonds were confirmed both by Raman and infrared spectroscopies.[75,77,89,92,93,]

Comparison of reaction centers with different combinations of hydrogen bonds in terms of the light-minus-dark optical difference spectra and the kinetics of the absorbance changes after long continuous illumination allowed us to identify the contribution of hydrogen bonds to possible structural changes involving P.

The construction of the mutant strains of *Rb. sphaeroides* by oligonucleotide-directed mutagenesis has been described before[78,89,92] and construction was done by our collaborators. For shorter abbreviations, the mutants will be identified in the text by only the position of the mutation. The term wild type used in this study refers to those isolated from the deletion strain complemented with a plasmid bearing the wild-type reaction center genes. Reaction centers were kept in 15mM Tris-HCl, pH 8.0, 0.025% LDAO and 1 mM EDTA.

2.5 pH buffer preparation

Different buffers were used to alter the pH of the assay suspension. Buffer solutions were prepared from distilled water by using 15 mM of respective buffer, 1mM EDTA, and different detergents above their c.m.c. Following buffers were used to prepare assay suspensions at different pH values.

pH 5.5: MES (2-(*N*-morpholino)ethanesulfonic acid)

pH 6: MES (2-(*N*-morpholino)ethanesulfonic acid)

pH 7: BIS-TRIS Propane (1,3-bis(tris(hydroxymethyl)methylamino)propane)

pH 7: Phosphate buffer

pH 7: MOPS (3-(*N*-morpholino)propanesulfonic acid)

pH 8: BIS-TRIS Propane (1,3-bis(tris(hydroxymethyl)methylamino)propane)

pH 8: TRIS (tris(hydroxymethyl)aminomethane)

pH 9: CHES (*N*-cyclohexyl-2-aminoethanesulfonic acid)

pH 10: CAPS (*N*-cyclohexyl-3-aminopropanesulfonic acid)

2.6 Biophysical techniques used in the characterization

2.6.1 Laser flash photolysis (LFP)

The kinetics of the charge recombination reactions upon flash excitation were recorded using a miniaturized LFP-112 laser flash photolysis (Luzchem Research Inc. Ottawa, Ontario, Canada) equipped with a pulsed Nd-YAG laser (Model MINILITE II from Continuum, Santa Clara, California, USA, 532 nm output wavelength) as a photo excitation source that generates 5 ns saturating laser pulse directed perpendicular to the direction of the monitoring beam. Data were collected by monitoring at the center of absorption band of the dimer (~ 865 nm) on a digital oscilloscope (Tektronix TDS-2012, Beaverton, Oregon, USA) in a DC-coupled mode, which was used as an analog to digital converter. The digitized signal was then processed using the software supplied with the LFP unit. The monitoring light was generated by an "Ozone-free" Xe lamp and was guided to the sample with fiber optics. To improve the signal to noise ratio, 25 traces were collected and averaged manually.

In these measurements 4 μM BRCs along with 100 μM terbutryn were used. The recorded traces were analyzed using Sigma-Plot software by decomposing the signals to exponentials using linear Marquardt algorithm.

2.6.2 Steady-state absorption spectroscopy

Measurements of light-induced charge recombination and structural changes were performed on a Cary 5000 UV-VIS-NIR spectrophotometer from Agilent (formerly Varian, Mulgrave, Victoria, Australia). The formation of light-induced states can be achieved by external, continuous wave excitation using 250 W tungsten lamp source (Oriel 6129, Stamford, Connecticut, USA) and delivering it through fiber optics (Newport Corp., Irvine, California, USA). Different light intensities (from 40 to 250 W) can be controlled using the power supply (AMETEK, Sorensen, DCS33-33E, San Diego, California, USA). The light intensity was set to ~ 30% of the saturating value for wild type at a 2 μM reaction center concentration. The samples were prepared under very weak green light and were adapted to the dark in the spectrometers for ~ 30 min before being exposed to any illumination. Terbutryn was used at a concentration of 100 μM to eliminate the secondary quinone activity. All measurements were performed in 3 ml quartz cuvette with the following parameters.

Scanning wavelength: 700-1000 nm or 500-700 nm

Average time to scan: 0.033 s

Data interval: 0.5 nm

Scan rate: 909.091 nm/min

Spectral bandwidth: 2 nm

Baseline was corrected before measuring the spectra. For light-minus-dark difference spectra the baseline was taken with the BRC sample in the dark-adapted state. Then series of spectra were recorded during and after the prolonged non-saturating illumination with 1 minute intervals up to 5 minutes and with 5 minutes intervals until the signal recovered completely. During illumination, the spectra were recorded every minute. For the temperature measurements, a dual Peltier-cell accessory was used and the temperature was varied using external temperature controlling unit with 0.1 °C accuracy. To cool Peltier-cell water was continuously circulated using small aquarium pump. A small magnetic stirrer was used as needed to mix the solution in the cuvette which was controlled by Peltier-cell assembly.

Kinetic analysis was done in the Kinetic mode of the spectrophotometer by monitoring the absorption changes at a single wavelength. The kinetic traces were analyzed by decomposing them into exponentials using a Marquardt algorithm.

For different binding studies of metal ions, detergents or lipids, the titrations were carried out in the cuvette and kinetic traces were recorded with external illumination. To remove EDTA the BRCs were dialysed extensively for 48 hours at 4 °C against EDTA-free buffer that has detergent. The dialysing baths were changed every 12 hours.

2.6.3. Spectroelectrochemical redox titrations

The oxidation-reduction midpoint potential of the P/P^+ couple was determined by spectroelectrochemical oxidation-reduction titration both in the dark and under a weak continuous, external illumination. For these measurements the ionic detergent, LDAO, was replaced with a non-ionic detergent, Triton X-100 (TX-100) by ion exchange chromatography.[93] The intensity of the illumination was selected to achieve the bleaching of 3-7% of the dimer only depending on the mutants. This very weak illumination prevented the samples from suffering photo damage during the long experiments and also ensured that the vast majority of the dimer is in its reduced state at any given time without an applied potential. The angle of the illumination was ~ 45° with respect to the propagation of the monitoring beam to avoid stray light entering the detector chamber. The degree of the electrochemical oxidation of P was determined by monitoring the absorption at the maximum of the Q_Y band centered at 865 nm in WT from the near-infrared (700-1000 nm) spectra recorded at different ambient redox potentials with a Cary 5000 spectrophotometer as described earlier.[93,94] The ambient redox potential was adjusted with a CV-27 potentiostat from Bioanalytical Systems (West Lafayette, Indiana, USA), and the reaction centers were placed into a thin-layer spectroelectrochemical cell of local design containing a 333 lines/in. gold mesh (Precision Eforming, Cortland, New York, USA), similar to a system described earlier.[94] A miniature calomel electrode (Cole Palmer, Vernon Hills, Illinois, USA) was used as the reference electrode. The calibration of the calomel electrode potential was done according to O'Reilly.[95]

Potassium hexacyanoferrate-(II) and potassium tetracyanomono(1,10-phenanthroline)ferrate-(II) were added in 300 μM concentration as redox mediators. The BRCs for the electrochemical titrations were concentrated to ~ 300 μM and were kept in 0.05% TX-100, 1mM EDTA, 15 mM MES, Tris-HCl, or MOPS depending on the pH. All measurements were performed at room temperature.

2.6.4 Proton uptake/release measurements

For these measurements the ionic detergent LDAO was replaced by 0.05% TX-100 by using ion-exchange column chromatography to eliminate the buffering capacity caused by the protonatable groups of LDAO. Then the buffer (15 mM Tris-HCl) and the EDTA were removed by a long (24-48 h) dialysis, with frequent changing of the dialysing medium (0.05% TX-100, 100 mM NaCl, pH 8.0). The ionic strength of the assay solution was kept constant by 100 mM NaCl to ensure a stable reading. Light-induced pH changes were measured by an Orion Ross semimicro combination pH electrode connected to an Orion 920A precision pH meter (Thermo Scientific). The net proton uptake or release was the difference of the electrode responses between the unbuffered (~ 1 μM) and buffered (15 mM) samples. To determine the buffering capacity of the entire system, a known amount of strong acid (HCl) was added during extensive stirring of the sample solution. All measurements were performed at room temperature. All chemicals were stored under nitrogen pressure after preparation to avoid the absorption of carbon dioxide, which can act as a weak buffer in the carbonic acid and bicarbonate equilibrium.

2.7 Data analysis

2.7.1 Analysis of the kinetic traces

Kinetic traces, measured by LFP or absorption spectroscopy depending on the time-scales, are characteristic to the various conformational sub-states. Decomposition of the kinetic traces was done into exponentials assuming three kinetic components according to the following equation:

$$A(t) = Be^{-k_1 t} + Ce^{-k_2 t} + De^{-k_3 t} \quad (1)$$

Where,

A(t): total signal amplitude at any time t

B, C, and D: amplitudes of the decaying kinetic components

t: time

k_1, k_2, and k_3: rate constants of the decaying kinetic components

Lifetime of the charge-separated state was determined by,

$$\text{Time constant } (\tau) = \frac{1}{k} \quad (2)$$

Where, k is the rate constant of the kinetic component.

2.7.2 Analysis of metal binding

The dissociation constant for metal binding study was determined based on a model that explained earlier.[96] This model was later modified for the manganese binding site near the dimer[97] and also used in similar context before.[98] Kinetic traces in the presence of different concentrations of metal ion were analyzed according to equation (1) and dissociation constant of metal binding was determined by using following equation:

$$R_M = \frac{[M^{2+}] + [RC] + K_D - \sqrt{([M^{2+}] + [RC] + K_D)^2 - 4[RC][M^{2+}]}}{2[RC]} \quad (3)$$

Where,

R_M: fraction of the slow kinetic component

$[M^{2+}]$: added metal ion concentration

[RC]: BRC protein concentration

K_D: dissociation constant

The BRC concentration for these measurements was 1 μM, which sets the lower limit for determining the value for K_D to ~ 1 μM.[98]

During some measurements value of R_M does not reach to unity even at the highest applied metal ion concentration.[99] Therefore it is necessary to add an offset for these fitting models. With the addition of this offset the fraction of P^+ can be given as follows:

$$f(P^+) = 1 - R_M + \frac{\Delta A_\infty}{\Delta A_0} \quad (4)$$

Where,

ΔA_∞: absorbance change at 865 nm at the highest applied metal concentration

ΔA_0: absorbance change at 865 nm without any metal ion

2.7.3 Decomposition of absorption spectrum into individual components

Ground state spectrum of the BRC was fitted by Gaussians or sum of Gaussians for bacteriochlorophyll dimer, bacteriochlorophyll monomers (B_L and B_M), and bacteriopheophytin as follows:

$$A = C + a(e)^{-0.5\left(\frac{W-W_0}{L}\right)^2} \quad (5)$$

Where,

A: absorbance at any given wavelength

C: offset, applied if traces did not recover to zero

a: peak absorbance

W: wavelength

W_0: peak position in the wavelength scale

L: bandwidth at half maxima (BWHM)

2.7.4 Determination of P/P^+ midpoint potential

The Nernst equation was used to fit the data of fraction of P reduced as a function of applied potential to get the midpoint potential value of the P/P^+ couple. The data were fitted with a one-electron Nernst equation as described earlier.[93]

During the measurements conducted under and within a certain time interval after weak illumination two/three populations of P had been observed with two/three different midpoint potentials and two/three components were used instead of one. This equation is given as follows:

$$E_i = E_m + \frac{RT}{nF} \ln \frac{O_i}{R_i} \quad (6)$$

Where,

E_i: applied potential

R_i: fraction reduced at applied potential

O_i: fraction oxidized at applied potential

E_m: midpoint potential

R: universal gas constant; R=8.314 $JK^{-1}mol^{-1}$

T: absolute temperature

n: number of electrons

F: Faraday constant; F: 9.648×10^4 C mol^{-1}

2.7.5 Determination of proton dissociation constant

The Henderson-Hasselbalch curve was used to explain *pK* shifts of the amino acid residues, which is expressed by the following equation:

$$f(H) = \frac{1}{1+10^{(pH-pK)}} \quad (7)$$

Where,

f(H): fraction protonated

pK: negative logarithm of the proton dissociation coefficient

2.7.6 Determination of redox properties of the dimer as a function of metal ion concentration

The change in P/P^+ potential as a function of pM (pM=–log[M], [M]:metal ion concentration) is described by the following relation taken from previously used model[100]:

$$E_{1/2} = E_{1/2}(P/P^+) + 0.059 \log \frac{10^{-pM} + 10^{-pM_0}}{10^{-pM} + 10^{-pM_M}} \quad (8)$$

Where,

$E_{1/2}$ = applied potential

$E_{1/2}$ (P/P^+) = midpoint potential

pM=-log[M], [M]:metal ion concentration in moles

$[M_0]$ = maximum applied metal ion concentration without binding

$[M_M]$ = maximum applied metal ion concentration after binding

This model was used to estimate the maximum P/P^+ midpoint potential value in the presence of manganese metal ion by extrapolating the fitted data.

Chapter 3

Identification of molecular mechanism behind the light-induced conformational changes using site-directed mutant reaction centers from *Rhodobacter sphaeroides*

The results in this chapter are based on the following published papers:

1. **Deshmukh, S. S.**, Williams, J. C., Allen, J. P., and Kálmán, L. (2011) Light-induced conformational changes in photosynthetic reaction centers: Dielectric relaxation in the vicinity of the dimer. *Biochemistry*, *50*, 340-348.
2. **Deshmukh, S. S.**, Williams, J. C., Allen, J. P., and Kálmán, L. (2011) Light-induced conformational changes in photosynthetic reaction centers: Redox-regulated proton pathway near the dimer. *Biochemistry*, *50*, 3321-3331.

Author contributions:

S. S. Deshmukh performed the experiments, analyzed the data, and contributed to writing the papers. L. Kálmán designed the research, guided the data analysis, and wrote the papers. J. C. Williams and J. P. Allen designed, constructed, and supplied the mutants and contributed to writing the papers.

In this chapter, we report the effects of alterations in amino acid side chains near P on the light-induced conformation of BRCs, as evidenced by the correlation between the electrochromic absorption changes of the light-minus-dark difference optical spectra and kinetics of the charge recombination after prolonged illumination. The combination of light-induced optical spectroscopy, electrochemical redox, and protonational measurements are used here to identify the characteristics of the conformational states such as energetics and protonational states.

3.1 Characterization of mutant reaction centers by optical spectroscopy

3.1.1 Light-minus-dark difference optical spectra

In the presence of terbutryn, the light-induced changes in the optical spectra of WT and the 11 mutants exhibited characteristic features associated with both P^+ and Q_A^-. These changes include an absorption decrease of the Q_Y band of P centered at 865 nm in WT but varied in the mutants, an electrochromic blue shift on the bacteriochlorophyll monomer (B) region around 800 nm and an electrochromic red shift on the bacteriopheophytin (H) band around 760 nm. Figure 3.1 shows these absorption changes recorded 1 min after the illumination had begun. The observed variations in the light-minus-dark spectra of the mutants involved differences in the position of the Q_Y band of P, and in the extent of the electrochromic changes around the B bands (vertical lines in Figure 3.1).

Some characteristic differences were also found in the spectra of the individual mutants recorded at different times during and after the illumination as discussed later. The position of the Q_Y band of the dimer showed some correlation with the introduced H-bonds. Generally, the formation of an H-bond with P_M resulted in a blue shift in the position of the P-band, and the introduction of the H-bonds with P_L caused red shifts in this parameter. Table 3.1 and Figure A1a of the Appendix A summarize the observed peak positions of the P band after 1 min illumination upon addition of each H-bond at the L168, M197, L131, and M160 positions. For example, the presence of the H-bond between the 2-acetyl group of the P_L and the His L168 in the WT reaction center resulted in a 16 nm red shift relative to the position of the P band in the L168 mutant, which lacks any of the H-bonds. Interestingly, comparison of mutants with the symmetrical H-bond between the 2-acetyl group of P_M with the His substitution at the M197 position shows almost the same value of 17 nm upon comparison of mutants with and without the His L168 change, namely, the M197 and M197+L168 double mutant. Formation of H-bonds with the 9-keto groups on both sides of P showed smaller quasi-symmetrical shifts of 9 nm to the blue and 7 nm to the red in the M160+L168 and L168+L131 double mutants, respectively, compared to the L168 mutant. The differences in the position of the P band were smaller in mutants with more than one H-bond. For example, the hypsochromic shifts resulting from the H-bond at P_M in the M160 and M197 mutants are only 1-3 nm relative to the WT, which has one H-bond. A bit larger bathochromic shift of 5 nm was observed in the presence of the H-bond at P_L in the L131 mutant.

With the increase in the number of H-bonds from two to three and from three to four, the observed shifts of the dimer band from 865 nm became negligible (structure Figure 1.15 and Figure A1a of the Appendix A).

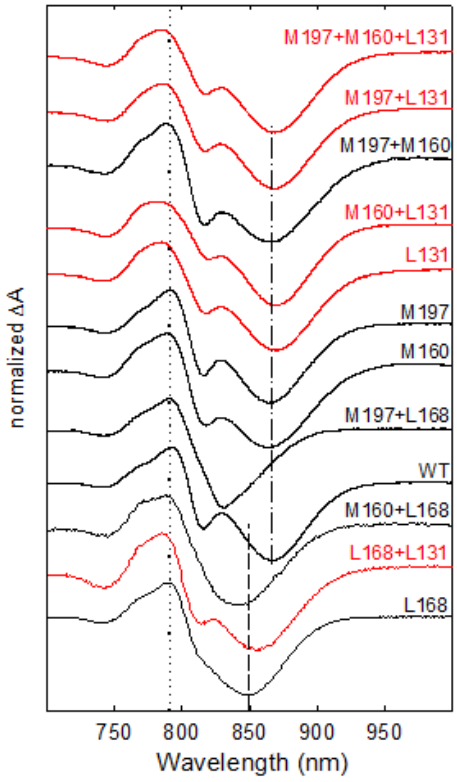

Figure 3.1 NIR light-minus-dark optical difference spectra of BRCs isolated from WT and 11 hydrogen bonding mutant. The spectra were recorded after continuous illumination for 1 min and were normalized to the center of the Q_Y band of the dimer (832- 870 nm depending on the mutant). The position of the dimer (dotted-dashed line), the position of the positive band of the electrochromic absorption change of the monomers in the WT (dotted line), and the position of the dimer in the L168 mutant (short dashed line) are indicated by vertical lines for reference. The spectra of mutants that have L131 mutation are shown in red. The spectra are approximately arranged in increasing order of oxidation potential of the dimer.[73] Conditions were as follows: 2 µM BRC in 15 mM Tris (pH 8), 0.1% LDAO detergent, 1 mM EDTA, 100 mM NaCl, and 100 µM terbutryn. The illumination time was 1 min (through a 870 nm interference filter using a water bath as a heat filter). The scanning rate was 800 nm/min.

Differences were also found in the electrochromic absorption changes involving the bands of B_L and B_M near 800 nm. The basis of the comparison was the position of the positive peak centered at 790 nm in the WT spectrum (Figure 3.1, vertical dotted line). The BRCs that have H-bonds at the L131 position exhibited a 6-9 nm blue shift in the position of this peak relative to the WT (red traces in Figure 3.1), while the other mutations resulted in only 0-2 nm changes. This trend is clearly visible in Figure A1b of the Appendix A, where the change in the position of the positive band near 790 nm is plotted as a function of the number of H-bonds upon introduction of any new H-bond into a particular mutant.

3.1.2 Kinetics of formation and recovery of light-induced states

After recording the light-minus-dark difference spectra, the kinetics of the absorption changes caused by non-saturating illumination were measured at the center of the Q_Y band of the dimer observed in the BRCs from each mutant (Figure 3.2). In the presence of terbutryn, the $P^+Q_A^-$ state was formed immediately after the light was turned on, resulting in a rapid absorption change. In addition, a further slower bleaching was also observed in all BRCs. Because the excitation was sub-saturating, with only ~ 30% of WT reaction centers excited at the beginning of the illumination, this slow increase can be interpreted as arising from another light-induced state being formed with a longer lifetime. Once the light is turned off, complex recovery kinetics that depended on the duration of the illumination and the mutation are observed (Table 3.1).

For most measurements, the BRCs were poised at pH 8.0 and illuminated for 1 min for comparison of the recovery kinetics of the oxidized dimer in the mutants after prolonged illumination.

Table 3.1 Kinetic and steady-state optical spectroscopic parameters of the WT and 11 H-bond mutants measured in BRCs of *Rb. sphaeroides*.

mutant[a]	P position[b] (nm)	position 790[c] (nm)	k_{slow} decay[d] ($\times 10^2$ s^{-1})	no. of H-bonds[e]
L168	849	790	1.63	0
M160+L168	840	788	1.72	1
M197+L168	832	790	1.69	1
WT	865	790	1.96	1
M160	862	788	2.56	2
M197	863	790	3.33	2
M197+M160	864	788	7.14	3
L168+L131	856	784	9.58	1
L131	870	784	14.28	2
M160+L131	868	781	12.50	3
M197+L131	865	782	12.51	3
M197+M160+L131	865	784	14.28	4

[a] Only the positions where the mutations were made are shown. The exact substitutions are listed in section 1.8.

[b] Position of the Q_Y band of the dimer in the light-minus-dark difference spectra of the mutants in Q_A active BRCs (data taken from Figure 3.1).

[c] Position of the lower wavelength band of the electrochromic shift on bacteriochlorophyll observed at ~ 790 nm in the light-minus-dark difference spectrum of the WT (data determined from Figure 3.1).

[d] Rate constants of the slowly decaying component of P^+ after illumination for 1min (determined from Figure 3.2).

[e] Number of H-bonds to P in the mutants.

During this 1 min illumination, the optical absorbance changes reached their saturating values in all mutants and were fully reversible even in the mutants with high dimer potentials. After the illumination was turned off, a fraction of the reaction centers followed the fast $P^+Q_A^- \rightarrow PQ_A$ charge recombination while the rest of P^+ recovered on a much longer time scale. In the BRCs containing the Leu to His mutation at the L131 position, the slower component of the P^+ decay had a lifetime of 7-8 s, corresponding to rate constants of 1.2-1.4 $\times$ 10^{-1} s^{-1}. Contrarily, in BRCs without this mutation, this kinetic parameter was much longer, with lifetimes of 30-63 s, corresponding to rate constants of 1.6-3.3 $\times$ 10^{-2} s^{-1}. The L168+L131 and M160+M197 mutants exhibited intermediate values with 11 and 14 s lifetimes, or k_{slow} values of 9.58 $\times$ 10^{-2} and 7.1 $\times$ 10^{-2} s^{-1}, for that slow phase, respectively. The relative amplitude of the slow phase in the formation (during the illumination) and recovery (in dark) was much smaller in the case of the L131 family of mutants and the M160+M197 double mutant compared to the rest of the mutants (Figure 3.2).

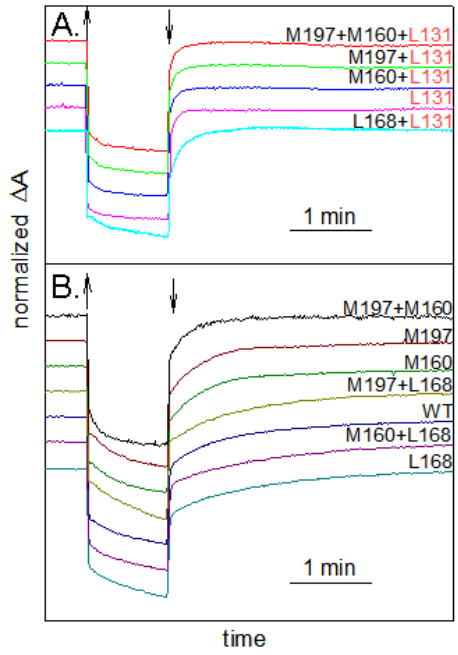

Figure 3.2 Formation and disappearance of the continuous light-induced $P^+Q_A^-$ redox states in the WT and 11 hydrogen bond mutants measured at the position of the P band (832-870 nm depending on the mutant) at pH 8. A. Mutants containing the Leu to His mutation at the L131 position. **B.** All other mutants and WT. The illumination time is 1 min. The traces were normalized and vertically shifted for better comparison. The vertical up and down arrows indicate when the illumination was turned on and off, respectively. Conditions as described in the legend of Figure 3.1.

3.1.3 Correlation between the slow kinetic components and the light-induced spectra

Comparison of the results shown in Figures 3.1 and 3.2 and also Figure A1a, b of the Appendix A suggests that there is no obvious correlation between the position of the Q_Y band of the P and the kinetics of the recovery of the charge-pair after continuous illumination. Because the BRCs contain only Q_A and not Q_B due to the addition of the terbutryn, no significant differences are expected among the mutants in the spectra or

kinetics due to Q_A^-. On the other hand, the 6-9 nm blue shift from 790 nm in the light-minus-dark spectra (red traces in Figure 3.1 and Figure A1b of the Appendix A) in the mutants carrying the Leu to His mutation at the L131 position was coupled to faster recovery kinetics of the $P^+Q_A^-$ charge-pair after the continuous illumination was turned off. On the basis of this correlation, we decided to investigate the electrochromic absorption changes in the accessory B region around 800 nm thoroughly. These spectral changes are sensitive to the alteration of the local electric field near the B molecules because of both the charge separation and the conformational changes proposed in this work. Even though the resolution and the assignments of the spectral features would be more accurate in low-temperature spectra, we decided to perform the analysis at room temperature. Cooling the samples to cryogenic temperatures introduces additional changes in the spectra such as shift on the Q_Y absorption band of P from 865 nm measured at room temperature to 890 nm at 77 K due to structural changes,[77] and it would be difficult to separate these changes from those that were caused exclusively by the prolonged illumination. In the room-temperature, light-minus-dark spectra presented in Figure 3.1, the electrochromic changes near 800 nm are partially overlapped with contributions associated with the formation of Q_A^- and bleaching of the P band. These overlapping contributions were removed by subtraction of the light-induced Q_A^-/Q_A difference spectrum and the photo-bleached P band from the light-minus-dark difference spectrum for each mutant and the WT. The resulting spectra contain spectral signatures that are exclusively characteristic of the accessory B monomers. The light-induced Q_A^-/Q_A difference spectra were recorded in each mutant and the wild type in the presence of a secondary electron donor, ferrocene (data shown for only the WT).

The treatment of the light-minus-dark difference spectra is presented for the WT as an example in Figure 3.3A. In the analysis, each monomer B is modeled as giving rise to an absorption band near 800 nm (794 and 810 nm for B_L and B_M, respectively) with three parameters, namely amplitude, width at half-maximum, and position. The spectra were fitted assuming that the 800 nm band is due to the two B monomers with each absorption band shifting and broadening in response to illumination. The resulting spectra featuring only the electrochromic absorption changes of the B monomers are shown for two representative BRCs: the WT and the L131 mutant in panels B and C of Figure 3.3, respectively. For the entire set of studied BRCs, these spectra can be reviewed in Figure A2 of the Appendix A. The light-induced electrochromic absorption changes of the accessory B monomers were analyzed by assuming shifts and broadenings of the bands of B (B_L and B_M) upon illumination for 1 min. The parameters of the fits for all mutants and the wild-type are listed in Table A1 of the Appendix A.

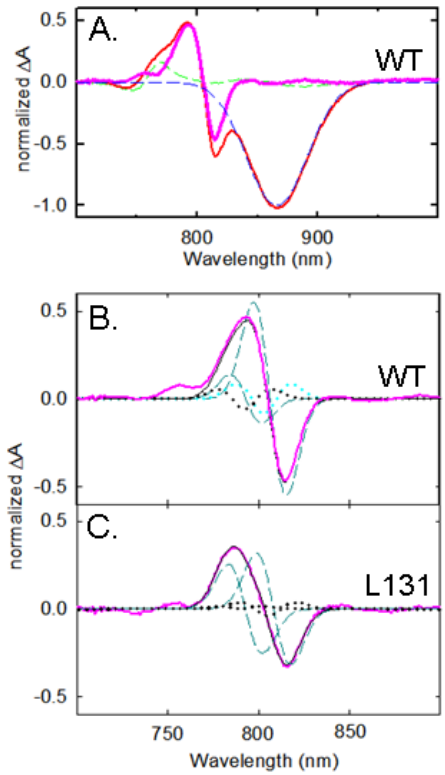

Figure 3.3 Analysis of the NIR light-minus-dark difference optical spectra. Panel A shows the treatment for the WT reaction center. The contribution of the dimer band (blue dotted line) and the Q_A^-/Q_A difference spectrum (green dotted line) were subtracted from the spectrum measured after illumination for 1 min (red trace). The resulting trace (thick pink solid line) represents the electrochromic absorption changes of B_L and B_M. **Panels B** and **C** show the electrochromic absorption changes of B_L and B_M after the subtractions performed in the spectra of WT and the L131 mutant, respectively. The electrochromic absorption changes were analyzed in terms of shifts (dashed dark cyan) and broadenings (dotted lines) of the Q_Y absorption bands of B_L and B_M. The conditions and the parameters of the fit are described in the text and listed for all mutants in Table A1 of the Appendix A.

Shifts in the absorption band of a chromophore are generally due to the change in the polarizability, while band broadenings are associated with the change in the dipole moment of the chromophore.[101]

The positions and the widths at half-maximum of the bacteriochlorophyll monomer bands were determined by Gaussian fits from the absolute absorption spectra of each BRC, assuming equal bands for each of the B monomers as introduced previously.[102] The observed position of the B band at 803 nm is remarkably conserved in the room-temperature absolute optical spectra of the mutants in this study and even in mutants that contain five or six amino acid substitutions near the dimer.[97] The contributions of the two B monomers, however, to the light-induced spectra were found to be significantly different in the two groups of mutants. In the mutants containing the Leu to His mutation at the L131 position, the hypsochromic shift of the B_M band from 810 nm was only 4.1-5.3 nm, while in the rest of the mutants including the WT, this shift was approximately twice as large (6.9-11.3 nm). Contrarily, the blue shift of the B_L band from 794 nm was found to be slightly larger in the group of the L131 family with values of 2.5-3.8 nm compared to the 0.3-2.7 nm shift in the family that lacks this mutation. It should be noted that the mutants that have no H-bonds with P_L at all (L168, L168+M160, and L168+M197) exhibited negligible shifts in the B_L band and the largest shifts in the B_M band with values of 0.3-2.0 and 9.6-11.3 nm, respectively. In summary, the light-induced electrochromic shifts were almost balanced between the bands associated with B_L and B_M in the L131 family, whereas in the group whose members lack this mutation, the shift of the B_M band outweighed the small to negligible shift of the B_L band. Small broadenings with decreased peak absorbances had to be considered in most cases, indicating that not only the polarizability but also the dipole moment of the B molecules is changing upon illumination. These broadenings, however, were much less prominent than the shifts and mostly were below 1 nm (Figure A2 and Table A1 of the Appendix A).

3.1.4 Electron transfer rates in different conformational states

All 12 studied BRCs exhibited complex recovery kinetics for the $P^+Q_A^-$ charge-pair after illumination for 1 min with rate constants for the slow kinetic component ranging from 1.63×10^{-2} to 1.42×10^{-1} s^{-1} (Figure 3.2). The flash-induced $P^+Q_A^- \rightarrow PQ_A$ charge recombination is expected to be a single-exponential decay in the WT and the mutants used in this work with rate constants ranging between 4.5 and 25 s^{-1}.[93] Even if the Q_B activity of the BRCs is retained, there must be two components in the charge recombination kinetics in WT reaction centers with rate constants of ~ 10 and ~ 1 s^{-1} at pH 8.[103] It has been shown previously by several groups that continuous illumination generates a heterogeneous population of detergent-isolated BRCs that have significantly longer lifetimes for the $P^+Q_A^-$ or $P^+Q_B^-$ charge-pairs in the WT and in the R-26 strain compared to those obtained after single-flash excitation.[35,46,56,57,65,67,68] The longer lifetimes determined using prolonged illumination were attributed to the recombination of the charge-pairs in BRCs that adopt different conformations induced by the illumination. The quantum yields of the proposed conformational changes were found to be low, and the light-adapted conformations could not be detected in the kinetic traces using single-flash excitation. During continuous illumination or trains of flashes, however, these altered conformations can be built up because of the long lifetimes of the charge-separated states in these different conformers. Although earlier studies used various different conditions (temperature, pH, detergent environment, illumination time and intensity, Q_B occupancy, etc.) that influence the recovery kinetics, the lifetimes determined in this study for the WT are in good agreement with those previously reported for the WT and R-26.[57,65,68]

The lifetime and the number of the kinetic components are variable and dependent on the illumination time, indicating that the conformational changes are strongly linked and some involve consecutive reactions.[57,68] After the sample had reached equilibrium, two major components can be distinguished at pH 8 that are characteristic of the dark-adapted and one kind of light-adapted conformation, depending upon the conditions, such as pH and detergent environment as described elsewhere.[57] The individual conformational changes that give rise to different lifetimes have not been identified yet at the molecular level, although most of the studies so far proposed conformational changes near the quinones,[35,56,65,67] as supported by X-ray crystallographic analysis of the BRCs that had been illuminated.[43,85,104] These studies, however, were either conducted at cryogenic temperatures or used very short, sub-second illuminations because it was found that the detergent-grown crystals do not diffract when exposed to prolonged illumination.[104] The formation of the long-lived charge-separated states investigated in this work and many previous kinetic studies certainly requires an illumination time of much longer than 1 s at room temperature (Figure 3.2).[35,56,57,65,68] Crystallographic and FTIR spectroscopic studies provided opposing models with regard to the movement of Q_B itself.[43,105,106] Thus, while there is no doubt regarding the conformational changes near the cytoplasmic site of the BRC, it is questionable whether the low-temperature, light-induced X-ray crystallographic studies are fully applicable to the conformational changes observed at room temperature during illuminations that are orders of magnitude longer than sub-seconds. In this study, we attempt to localize the conformational changes that give rise to the longest-lived kinetic component in the recovery kinetics after illumination for 1 min.

In Figure 3.4, we plotted the relative rate constants of the slowest kinetic component found in each mutant with respect to those measured for the WT (k_{slow} ^{mutant}/k_{slow} ^{WT}) as a function of the number of H-bonds. We grouped the mutants on the basis of the location of the H-bonds found in the L131, L168, M160, and M197 positions. The rate constants of the slowest kinetic component that represent the recovery of the $P^+Q_A^-$ state in the one kind of light-adapted conformation in four mutants with the H-bond of P_L at the L131 position (L131, M160+L131, M197+L131, and M160+M197+L131) showed no dependence on the number of H-bonds and were ~ 7 times higher than that measured in the WT. Similarly, the rate constants in the mutants that lack any H-bond with P_L (L168, L168+M160, and L168+M197) exhibited quasi independence from the number of H-bonds, while they were even slightly smaller than that in the WT. The L168+L131 double mutant that lacks the H-bond at the L168 position but has the one at the L131 position has been excluded from both groups, although it showed more similarity to members of the L131 family of mutants (Figure 3.4). It appears that the presence of the H-bond between P_L and the L131 His is not allowing the formation of the longest-lived charge-separated state regardless of whether the H-bond at the M160 or M197 position is established with P_M if a 1 min illumination is used. On the other hand, the lack of any H-bond with P_L favors formation of the long-lived charge-separated state despite the presence of the H-bonds with P_M. Furthermore, the rate constants in the mutants having H-bonds introduced into P_M either at the M160 or at the M197 position exhibited a very pronounced and similar dependence on the number of H-bonds, provided the H-bond at L168 with P_L was established (Figure 3.4).

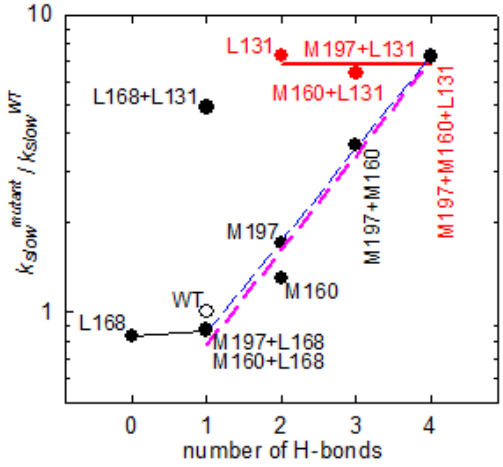

Figure 3.4 Dependence of the relative rate constant ($k_{slow}^{mutant}/ k_{slow}^{WT}$) of slow recovery of the oxidized dimer on the number of H-bonds. The mutants are numbered according to Table 3.1. Regression lines were generated through the data points associated with the mutants having H-bonds created with the dimer at positions L131 (thick solid red line), M160 (thick pink dashed line), and M197 (thin blue dashed line) or the existing H-bond removed at L168 (thin black solid line). The rate constants were determined from Figure 3.2 and were taken from Table 3.1.

It is not obvious whether the H-bonds at the M160 and M197 positions have the same influence because two of the mutants (M197+M160 and M197+M160+L131) have both H-bonds. More evidence points toward the importance of the M197 position as the orientation of the 2-acetyl group of P_M can be different when free or H-bonded.[76] Nonetheless, the lifetime of the long-lived charge-separated state is clearly sensitive to the number of H-bonds with P_M, provided the H-bond with P_L at the L168 position is present, but it becomes independent of it if either the H-bond with P_L at L131 is present or that at L168 is removed.

3.2 Illumination time dependence of the light-induced spectral changes

To identify the changes that occur in the spectral signatures in the dark- and light-adapted states during the illumination, near-infrared light-induced spectra were recorded at different times during and after the illumination for the studied BRCs with a 1800 nm/min scanning rate. Figure 3.5A shows traces for WT and for the L131 mutant representing the two groups of reaction centers. For each sample, four spectra were measured: immediately after the onset of the illumination (red trace), after illumination for 1 min (black trace), 1 min after the illumination ceased (blue trace), and 6 min after the illumination ceased (pink trace) as labeled A-D, respectively, in Figure 3.5A. The spectra were normalized to the bleaching of the P band because it had been demonstrated previously using a very high (1 W/cm^2), saturating illumination intensity that the oscillator strength of this band does not change during the illumination.[57] It is clearly visible in the spectra that the absorption changes associated with the B monomers around 800 nm are the largest immediately after the onset of illumination both in the WT and in the L131 mutant (red traces in Figure 3.5A).

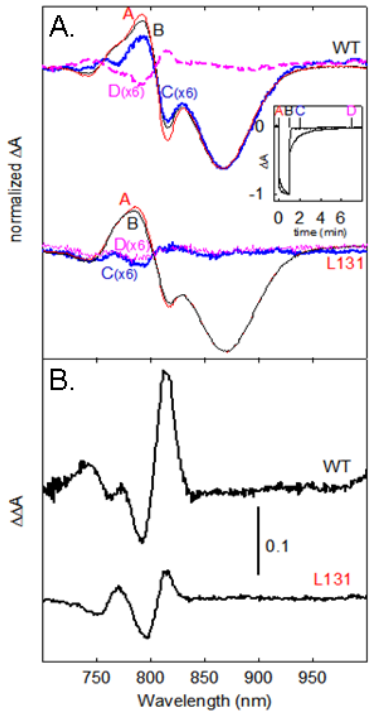

Figure 3.5 A. Normalized light-minus-dark optical difference spectra of WT and the L131 mutant recorded immediately after the light had been turned on (traces A in red), after illumination for 1 min (traces B in black), and 1 and 6 min after the illumination had been turned off (traces C in blue and D in pink, respectively). Traces C and D were magnified by 6-fold to match the absorption change at 865 nm with traces A and B in WT and also to emphasize the residual absorption changes around 800 nm. The inset shows the time dependence of the absorption changes and indicates the times at which the spectral traces were recorded. **B.** Double difference spectra (traces B-minus-A from panel A) for the WT and for the L131 mutant. Conditions as in Figure 3.1 except the traces were recorded at a scanning rate of 1800 nm/min.

With increasing illumination time, these changes decreased with respect to the extent of P^+. After illumination for 1 min, the decreases in the electrochromic absorption changes of the B bands were approximately twice as large in the WT versus the L131 mutant as evidenced by the double difference spectra (traces A and B in Figure 3.5A, and the difference spectrum, namely trace B-minus-trace A in Figure 3.5B).

In Figure 3.5A, we also show the spectra recorded 1 min after the illumination was turned off (traces C). For the WT, this spectrum represents the population of the BRCs still in the $P^+Q_A^-$ state but exclusively in the light-adapted conformation, while for the L131 mutant, the spectrum reflects the light-adapted PQ_A ground state (see the inset in Figure 3.5A). It should be noted that spectra recorded 6 min after the light was turned off still contained absorption changes around 800 nm in all samples even after the $P^+Q_A^-$ charge-pair recovered completely (traces D of Figure 3.5A). All of these spectra recovered to the ground state ~ 1 h after it had been exposed to illumination for 1 min. Similar long-lasting absorption changes around 800 nm were observed but not discussed earlier both in the low-temperature spectra and in the room-temperature spectra for BRCs dispersed either in LDAO or in n-dodecyl β-D-maltoside after prolonged continuous illumination or trains of flashes.[35,65,67] Analysis of the spectra for WT (traces A and C of Figure 3.5A) as described in section 3.1 and shown in Figure 3.3 confirmed that the B_M band that has been blue-shifted from 810 to 801 nm as a result of the onset of the illumination moved back to 804 nm during the 1 min illumination in those fractions of the BRCs that exhibited long recovery kinetics of the $P^+Q_A^-$ charge-pair. No such relaxation of the B_L band could be observed. Because of the much shorter lifetime of the $P^+Q_A^-$ state in the L131 mutant, only the spectra recorded under illumination could be analyzed with the same emphasis (traces A and B). Only ~ 1 nm differences in the positions of the B_L and B_M bands could be determined as the illumination time increased from 0 to 1 min with values of 790-791 and 805-806 nm, respectively.

From the illumination time dependence of the electrochromic absorption changes, we conclude that prolonged illumination causes dielectric relaxations in the BRCs near P^+ resulting in the smaller electrochromic absorption changes in the nearby B bands. In the WT, this relaxation was approximately twice as large as that found for the L131 mutant and predominantly involved B_M, whereas in the L131 mutant, they affected both monomers. The absorption changes around 800 nm remained detectable for up to 1 h in the spectra under the conditions used. It must also be noted that in the spectra recorded 1 min after the illumination had been turned off the electrochromic absorption changes near 760 nm have also decreased in all of the mutants of the WT family, where the long lived charge-separated states could still be detected. This is indicative of a similar dielectric relaxation near the H molecules, most likely due to the stabilization of Q_A^- and/or the weakening of the long-range electrostatic interactions between P and H molecules due to the structural changes near P.

3.3 Effects of mutations and internal water molecules on light-induced structural changes

3.3.1 Alterations in the local electric field by the H-bonds

The addition of the H-bonds may alter the local electric field by at least three mechanisms: (i) modifying the local dielectric constant by substituting more hydrophilic residues, (ii) changing the spin density distribution between the two halves of P, and (iii) displacing structural water molecules.

The H-bonds were created by substituting His residues for the highly hydrophobic residues, such as Leu or Phe, or the existing H-bond was removed by substituting the His with a highly hydrophobic Phe residue. These substitutions in the immediate vicinity of the dimer should modify the local dielectric constant and therefore the electrochromic absorption changes of the nearby B_L and B_M molecules. In the mutants that contained the H-bond between the P_L and the L131 His residue, the contribution of the B_M band to the electrochromic absorption changes was only approximately half of what was found for the other family of mutants including WT (Figure 3.3 and Figure A2 and Table A1 of the Appendix A). The smaller contribution of the B_M band even without a detailed analysis can be observed as the shift of the positive absorption peak near 790 nm by 6-9 nm toward the blue spectral range of the light-minus-dark difference spectra in the mutants with the Leu to His substitution at the L131 position (Figure 3.1 and Figure A1b of the Appendix A). In the rest of the mutants and the WT, this shift was only 0-2 nm. It has been suggested that the local dielectric constant in the active, L branch near P is significantly larger than in the inactive, M branch.[107] Because the interaction energies causing the electrochromic absorption changes are inversely proportional to the dielectric constant, the large difference in the electrochromic shifts of the B_M and B_L bands reported here for WT is in agreement with the assumption of a lower dielectric constant in the M branch (Figure 3.5). Substitution of a hydrophilic His residue near P increases not only the local dielectric constant but also the alteration of the sharing of the unpaired electron between the two halves of P upon formation of P^+.

Special Triple ENDOR spectroscopy showed that in WT the unpaired electron is residing on P_L and P_M with a ~ 2:1 ratio favoring P_L, whereas in the L131 mutant, it is distributed almost equally between the two halves of P.[76] This trend is visible for all mutants that contain the Leu to His substitution at the L131 position. The addition of the H-bond at the L131 position in all mutants lowered the spin density ratio on P_L by ~ 0.1 - 0.3, and with any given number of H-bonds, the mutants that possess the H-bond at the L131 position have the smallest spin densities on P_L compared to those that lack the Leu to His substitution at the L131 position (Figure A1c of the Appendix A). The increase in the spin density on P_M at the expense of that on P_L in the L131 mutant should decrease the magnitude of the electrochromic absorption changes of B_M because the axis of the Q_Y transition (along the 3 and 1 rings) of B_M is closer to the plane of P_L than P_M (Figure 1.15). Moreover, B_M is ~ 2 Å closer to P_L than to P_M.[6] This is in agreement with the observed decrease in the contribution of B_M to the electrochromic absorption changes in the L131 mutant compared to the WT (Figure 3.3B, C). The variation in spin density, however, does not fully account for the observed trend in the electrochromic absorption changes and the kinetics in the 11 mutants, not to mention the dielectric relaxation during the illumination shown in Figure 3.5. For example, both in the M160+L168 and in the M160+L131 mutants, the spin density distribution is very similar to that in the WT (~ 2:1 favoring P_L), but the kinetics of the absorption changes were ~ 7 times faster in the M160+L131 mutant than in the M160+L168 mutant and WT (Figure 3.2 and Table 3.1). Similarly, the electrochromic absorption changes were found to be quite different in these three reaction centers (Figure A2 of the Appendix A).

3.3.2 Internal water molecules

The X-ray crystal structure of the WT BRC identified five water molecules near the immediate vicinity of the four bacteriochlorophylls (Figure 3.6)[6]. All five water molecules are in key positions in terms of their potential to influence the electrochromic absorption changes. Two of the water molecules, namely, W728 and W729, appear to play clear structural roles as they bridge the B monomers, being within H-bond distance of the 9-keto carbonyl groups of B_L and B_M with distances of 2.7 and 2.8 Å , respectively, and also H-bonded to His M202 and L173 that coordinate the central Mg^{2+} of P_M and P_L. In these bridging positions, the two water molecules, W728 and W729, are 3.8 Å from Phe M197 and His L168, respectively. The other three water molecules, W723, W736, and W737, are also close to the amino acid residues that were replaced to establish H-bonds with P. The W723 is 5.5 Å from Leu L131 and 7.2 Å from the 9-keto carbonyl group of P_L. The W736 is 4.3 Å from Phe M197 and 5.1 Å from ring II of P_M. The W737 is 7.3 Å from His L168 and 4.1 Å from ring IV of P_L.

In each case, these water molecules are aligned with the Q_X or Q_Y transition of P or one of the B monomers. Previous studies have led to the proposal that W728 when H-bonded to the 9-keto carbonyl of B_L facilitates the ultrafast charge separation.[109] It was demonstrated that introducing a positively charged Arg at the L181 position causes the displacement of W729 by ~ 5 Å that allowed this water molecule to serve as the sixth ligand to the central Mg^{2+} of B_M.[110]

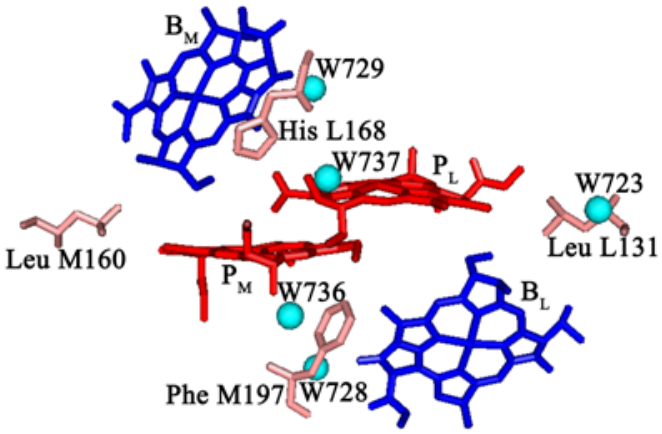

Figure 3.6 Top view of the four bacteriochlorophylls containing the dimer (P_L and P_M in red) and the monomers (B_L and B_M in blue) with nearby amino acid residues (salmon sticks) and internal water molecules (cyan spheres). The four residues, Leu L131, Leu M160, His L168, and Phe M197, were modified to introduce or remove H-bonds. Five water molecules, W723, W728, W729, W736, and W737 (cyan spheres), were identified in the immediate vicinity of the bacteriochlorophylls. This figure is color reproduction from ref. (108) and coordinates were taken from Protein Data Bank entry 1PCR[6].

One might speculate that the introduction of a positively charged His residue placed at L131 or M197 or, correspondingly, the replacement of His L168 with Phe may cause similar displacements of W723, W728, and W729 in the mutants with these substitutions. In the crystal structure of the mutant containing all three mutations at L131, M160, and M197, changes in the location of the water molecules were not modeled because of the limited resolution of the diffraction data.[97] As demonstrated in Figure 3.1, the formation or removal of H-bonds with protons donated by histidine shifts the positions of the Q_Y bands of the dimer substantially. Similarly, the formation of the H-bonds increased the potential of the dimer in all cases.[93]

The putative H-bonds between the 9-keto carbonyls of B_L and B_M with W728 and W729 should also influence these bands and are probably altered by the replacement of Phe M197 and His L168, respectively. These observations are all consistent with the stabilization of the positive charge on P by dielectric relaxation upon illumination in WT and in those mutants where the conformational changes leading to the long-lived charge-separated states are favored. Because W737 and W736 are along the Q_X transitions of P_L and P_M, any movement would be expected to cause a shift in the Q_X band of the bacteriochlorophylls around 600 nm.

3.4 Effects of different pH values on kinetics of formation and recovery of light-induced states

Since it is clear from these experimental evidences that the extent of the change of the dielectric constant was found to be strongly dependent on the identity of the residue occupying the L131 position, further experiments are performed to understand the characteristics of the light-induced long-lived charge-separated and conformational states and the nature of the involvement of L131. The kinetics of the absorption changes caused by 1 min illumination with sub-saturating light intensity was measured at the center of the Q_Y band of the P in each mutant and the WT at pH 6 and 8 (Figure 3.7).

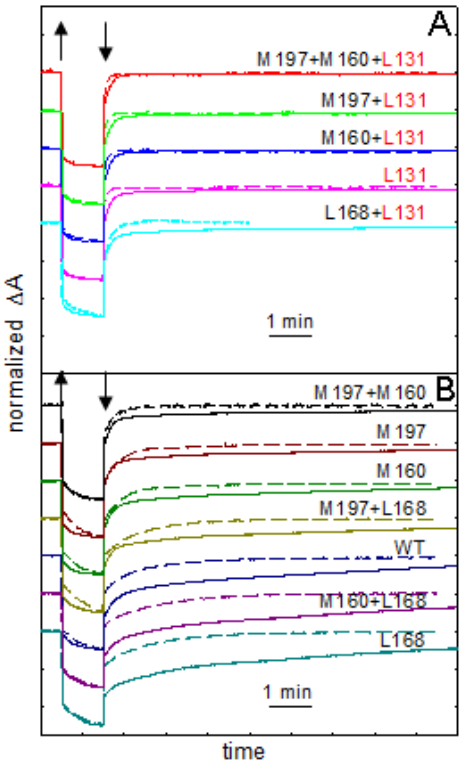

Figure 3.7 Formation and disappearance of the light-induced redox states in the wild type and 11 hydrogen bonding mutants measured at the position of the dimer band at pH 6 (solid lines) and at pH 8 (dashed lines) using 1 min illumination. Panel A. Mutants containing the Leu to His substitution at L131. **Panel B.** All other mutants and WT. The traces were normalized and vertically shifted for better comparison. The vertical up and down arrows indicate when the illumination was turned on and off, respectively.

Under the applied conditions, in the presence of terbutryn, the $P^{+}Q_{A}^{-}$ state was formed immediately. In addition to the unresolved, rapid absorption change, a further slower increase of the signal was also observed in all reaction centers at both pH values. As discussed earlier the slow increase of the signal was interpreted to be arising from altered populations of the BRCs generated by the continuous illumination.

After the illumination was turned off complex recoveries were detected with two or three components that had much different lifetimes than those observed after single flash excitation. The number of components, their relative amplitudes, and their lifetimes were strongly dependent on the pH at the given illumination time. As the illumination was turned off in a fraction of the BRCs a rapid, unresolved recovery was observed due to $P^+Q_A^- \rightarrow PQ_A$ charge recombination from the dark-adapted conformation. The additional slower components were assigned to the recoveries from different light-induced conformations. As seen in Figure 3.7, the overall recovery kinetics were much longer at pH 6 than at pH 8 in WT and one set of the mutants, whereas in another set of mutants, all of which contain the Leu to His substitution at the L131 position, the kinetics appeared only slightly longer than at pH 8. All reaction centers exhibited reversible signals with the applied 1 min illumination. Longer illumination times (>3 min) resulted in a slight degree of photo-damage at pH 6 in the mutants with a highly oxidizing P such as the M197+M160+L131 and the M197+L131 mutants. The recovery kinetics with the applied illumination conditions at pH 8 were predominantly biphasic, while at pH 6 in all mutants except in the M197+M160+L131 mutant a third, very slow component was also detected. The rate constants of the slow and very slow components for pH 6 and 8 are plotted in Figure 3.8A as a function of the midpoint potential of the P/P^+ couple that has been determined earlier for dark-adapted samples.[93] From laser flash photolysis the rate constants of the flash-induced charge recombination are also plotted for reference for all mutants at pH 8 and for a few representatives for pH 6. The values measured at pH 8 are in agreement with those reported earlier.[93]

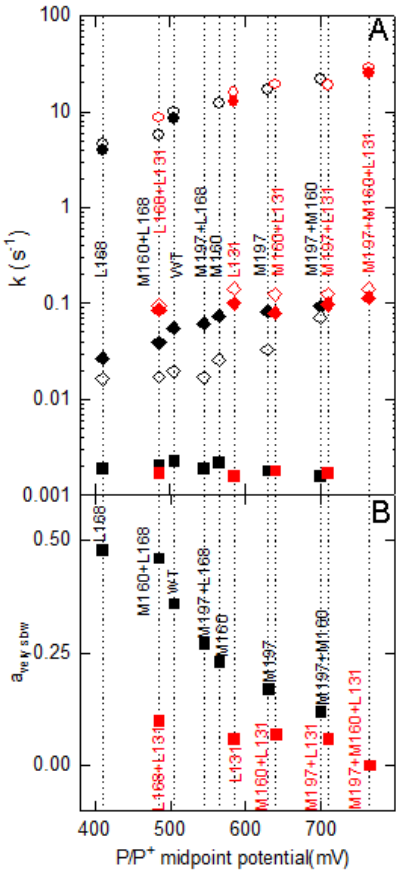

Figure 3.8 Dependence of the kinetic parameters obtained from the recovery kinetics of the oxidized dimer on the P/P$^+$ potential. Panel A. Rate constants of the flash induced charge recombination (circles) and the slow (diamonds) and very slow (squares) components in the 1 min illumination induced recovery kinetics. Open and closed symbols refer to the data obtained from the exponential fitting of the kinetic traces recorded at pH 8 and 6, respectively. **Panel B.** Amplitude of the very slow component at pH 6. The kinetic parameters of mutants that have L131 mutation are shown in red color.

The rate constants of the flash-induced charge recombination from Q_A^- to P^+ were found to be very weakly dependent on pH in the mutants. This agrees with the conclusions of former studies conducted in WT and R-26.[111]

The rate constants of the slow component at pH 8 both in the mutants with H-bonds at the L131 position and in those that lack the H-bond at the L168 position were found to be independent of the P/P^+ midpoint potential (see also Figure 3.4). The values of the rate constants for these two families of mutants, however, were about 7-8 times larger in the L131 family than in the L168 family with the most extreme values of 1.4×10^{-1} and 1.6×10^{-2} s^{-1}, respectively. At pH 6 the rate constants for the slow component were found to be faster than at pH 8 in the mutants that lack the H-bond at L131. For example in the WT this increase is almost 3-fold from 2.0×10^{-2} s^{-1} at pH 8 to 5.5×10^{-2} s^{-1} at pH 6. The rate constants of the very slow component at pH 6, which was not detectable at pH 8, after 1 min illumination, was found also to be independent of the P/P^+ potential in all mutants with a small variation between 1.6×10^{-3} and 2.3×10^{-3} s^{-1} in the 11 studied reaction centers. This component was not populated to detectable level in the M197+M160+L131 triple mutant. These observations suggest that most likely the conformational state represented by the very slow component is formed in a consecutive reaction from the state characterized with the slow component. In general, the total amplitudes of the slower phases were larger at pH 6 than at pH 8, especially in the family of mutants that lack the L131 His substitution. The relative amplitude of the very slow component, however, is only 6-7% in most of the mutants in the L131 family and only 10% in the L168+L131 mutant that, although having the H-bond at the L131 position, lacks the one at the L168 position (Figure 3.8B). Contrarily, in the mutants that lack the H-bond at the L131 position the relative amplitude of this very slow component varied from as high as 48% in the L168 mutant that lacks any H-bond to 12% in the M197+M160 mutant with three H-bonds.

3.4.1 Recovery rates

In the mutants the rate constants of the $P^+Q_A^- \rightarrow PQ_A$ charge recombination after flash excitation followed the dependence on the midpoint potential as expected from the Marcus theory.[93,112] The pH dependence of the P/P^+ potential was reported to be very weak with only about ~ 5mV/pH slope between pH 6 and 10.[113] Thus, the differences in the Marcus behavior should not be significant at different pH values (see Figure 3.7 for few representative mutants). In this work the use of prolonged continuous illumination, however, generated redox states in fractions of the reaction centers whose recovery kinetics no longer followed the classical Marcus dependence for the rate constants. In the two groups of mutants the rate constants for the slower phases were mostly independent of the midpoint potential of the dimer, indicating that the observed rate must be limited by another factor, e.g., the rate of protonation or a conformational change. Because some of these mutants have larger rate constants than other mutants with similar midpoint potentials, the presence of the Leu to His mutation at L131 is consistent with an increase in the electron transfer rate, so that the electron transfer rate is significantly faster than the observed rate. Several groups reported the multiphasic recovery kinetics associated with light-induced conformational changes in the minutes time scale, but very few of them studied their pH dependencies.[35,46,56,57,65,67,68] The observed rate constants for the slower components at pH 8 agree well with those reported in these earlier studies for similar illumination times. As the illumination time increases new, longer-lived states were identified in the kinetic traces, resulting in some changes in the rate constants of the recovery kinetics.[68] This indicates that some later conformational states are formed from the earlier ones as a result of consecutive reactions.

For example, the observation of the very slow component with the rate constant of ~ 10^{-3} s^{-1} at pH 6 also resulted in the nearly 3-fold increase of the rate constant of the slow component from 2.0×10^{-2} at pH 8 to 5.5×10^{-2} s^{-1} at pH 6.

3.5 Potential of the P/P^+ couple in the light-induced states

To identify the P/P^+ midpoint potential in the altered light-induced conformation spectroelectrochemical titrations were performed at pH 8 and 6. The results of the spectroelectrochemical redox titrations at pH 8 for the WT and for the L168 and L131 mutants in the dark and in the presence of a weak external illumination are presented in Figure 3.9. Without any external illumination the data could be fitted well with a single Nernst equation assuming only one population of P with midpoint potentials of 505, 415, and 585 mV for the WT and for the L168 and the L131 mutants, respectively. The error was estimated as ±7 mV based on the results obtained from different titrations in the dark. These values determined here are in a good agreement with those reported earlier for the P/P^+ potentials in WT and in these mutant reaction centers.[93]

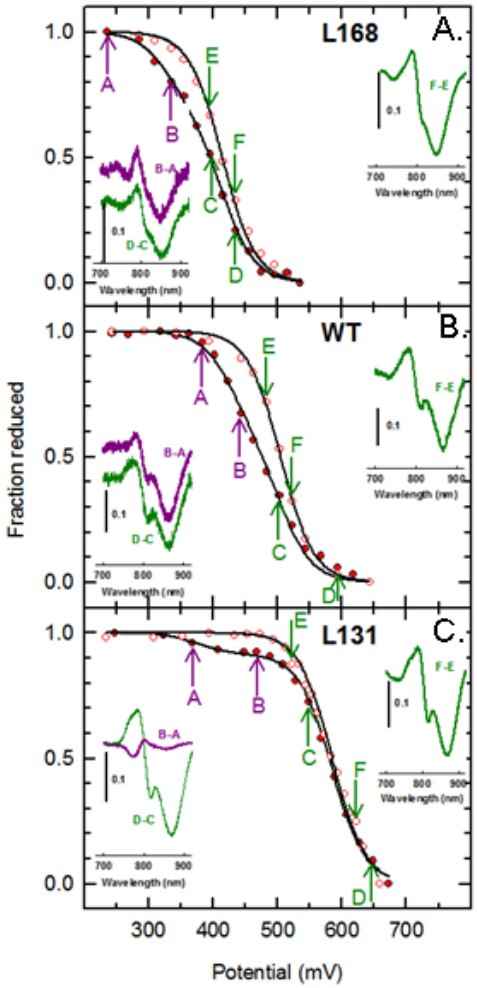

Figure 3.9 Spectroelectrochemical oxidation-reduction titrations of BRCs from WT, the L168, and the L131 mutant at pH 8. Open symbols represent the data obtained in dark-adapted samples, and the closed symbols represent the data determined in the presence of weak illumination. The continuous lines are the best fits to the Nernst equation with one (open symbols) or two (closed symbols) components with different potentials. The insets show difference spectra between two absolute spectra recorded at two different applied potential values indicated by the arrows, letters from A to F, and respective color codes (green for the dark-adapted state and maroon for the light-adapted state). Conditions, errors, and the results of the fit are described in the text and in Figure 3.10.

Normally, the P/P^+ midpoint potential is determined under dark conditions using dark-adapted samples as described above, with the potential being adjusted either chemically or electrochemically while optically monitoring the amount of P and P^+ present at each potential. Each measurement intrinsically takes few minutes in order for the protein to equilibrate with the applied potential, usually with the inclusion of mediators. The kinetics of this equilibration both in the dark and in the presence of a weak illumination is shown in Figure B1 of the Appendix B as the bleaching of the P-band at 865 nm in response to the onset and offset of +600 mV applied potential. Since the mediators are applied at nearly equimolar concentrations with the BRCs, they are not expected to serve as electron donors/acceptors in a second-order process to P^+ or P, but their absence results in much longer equilibration times in both directions. The same kinetics for the equilibration in the presence and in the absence of the weak illumination verifies that neither the BRCs nor the mediators respond differently to the potential change and that the response does not depend on the conformational state of the protein. The titrations in the dark reveal the midpoint potential of the P^+ state relative to the ground state exclusively in the dark-adapted conformation of the BRC. When the experiments were performed in the presence of weak illumination, it resulted in only a few percent of the BRCs being present in the charge-separated state, but the BRCs in the ground state were preferentially enriched in the light-adapted conformation rather than being only in the dark-adapted conformation. Thus, the measurements shown in Figure 3.9 resulted in two apparent midpoint potentials, corresponding to the two populations of P in BRCs with two different conformations.

While in the larger fraction of the BRCs the midpoint potential of the P/P^+ couple did not change in the presence of the weak illumination, in the smaller fraction significantly lower values were determined in all reaction centers. In the WT upon illumination the potential of the dimer was shifted to 430 mV in 42% of the BRCs representing a 75 mV drop in the potential (Figure 3.9B). Similarly, a 79mV difference was obtained in the L168 mutant for the P/P^+ potentials with values of 415 and 336 mV for the dark-adapted and light-adapted populations, respectively (Figure 3.9A). The fraction of the component with lower dimer potential slightly varied 27-31% and 41-45% in different measurements for the L168 mutant and WT, respectively, most probably due to the different positioning of the samples within the spectroelectrochemical cell resulting in slightly altered illumination conditions for the individual measurements. Contrarily, in the L131 mutant only 8% of P exhibited altered potentials with a value of 375 mV in the presence of the illumination. We would like to stress that even though it is obvious from Figure 3.9C that a two-component Nernst fit is required to describe the measured data well even in the L131 mutant due to the very small amplitude for this component the error of the potential is ± 32 mV as opposed to the error of ± 7 mV for the WT and the L168 mutant at pH 8. The insets in Figure 3.9 show the P^+/P difference spectra determined as the differences of the absolute spectra recorded at two specific applied potentials (labeled as A-F) situated at different regimes of the Nernst curves. It is clearly visible from these insets that in the WT and in the L168 mutant the difference spectra in the dark (F-E) (green) are very similar to those fractions of the samples that had the same potential in the light (D-C) (green).

The difference spectra that represent the population of P with lower potential values (B-A) (maroon color) show smaller electrochromic absorption changes around 800 nm. This observation is in line with the results of Figure 3.5, where during the illumination similar decreases of the electrochromic absorption changes of the bacteriochlorophyll monomer (B) bands were observed in BRCs that exhibited longer recovery kinetics after illumination. The decrease of the electrochromic absorption changes were attributed to light-induced structural changes, which increases the local dielectric constant and are responsible for the altered P/P^+ potential. In Figure 3.9C, the insets for the L131 mutant show the similarities of the spectra obtained in the dark (F-E) (green spectrum) and the major component determined during the weak illumination (D-C) (green spectrum), but for the 8% component the difference spectrum is quite dissimilar (maroon spectrum). It exhibits the electrochromic red shift in the range of the B bands but has very little contribution from P^+. Overall, this difference spectrum in the L131 mutant resembles the double difference spectrum obtained as the difference between two light-minus-dark difference spectra recorded after different illumination times (compare Figure 3.5B). As the electrochemical titrations cannot probe the photo-induced P^+, only those that were generated by the electrical potential, these measurements suggest that even after the charges recovered heterogeneity exists in the BRCs. Figure B2 of the Appendix B shows the near-infrared optical difference spectra recorded at various times up to 7 h after the weak illumination was turned off. The reference spectrum for these measurements was the one that was recorded in the dark prior to the illumination.

Even though the spectral signatures of both P^+ and Q_A^- disappeared in WT within an hour after a prolonged illumination the electrochromic absorption changes around 800 nm, which were indicative of the altered local dielectric constant, remained until 5 h after the light was turned off. Similar, long-lasting spectral features were reported earlier for BRCs dispersed in LDAO[35,67] and in n-dodecyl-β-D-maltoside,[65] indicating that the detergents have no influence on these electrochromic absorption changes. The spectroelectrochemical titrations were also performed in this 7 h dark relaxation in two different time intervals. The titration that was conducted between 1 and 3.5 h after the light was turned off still showed the presence of two different populations of P in accordance with the presence of the electrochromic changes. The fraction of the P with altered potential, however, decreased from 42% to 26% in WT compared to the value determined during the illumination (Figure B3, Table B1 from Appendix B). When the redox titration was conducted between approximately 6.5 and 8.0 h after the illumination was turned off, where the electrochromic changes were not present in the spectra anymore, the data could be described with a single-component Nernst fit with 501 mV midpoint potential for P, as was found before the illumination (Figure B3, Table B1 from Appendix B). Comparison of Figures B2 and B3 (Appendix B) shows that the fraction of the BRCs with an altered redox potential for P disappeared with the same kinetics as the electrochromic absorption changes involving the monomers, indicating that the source for the altered potential of P is the light-induced change of the dielectric constant.

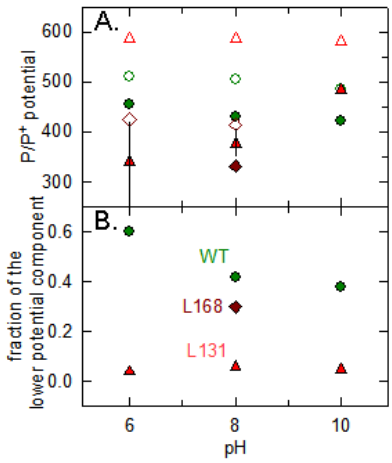

Figure 3.10 Panel A pH dependence of the P/P^+ potential for WT (green circles), the L168 mutant (brown diamonds), and the L131 mutant (red triangles). The potential values determined in the dark and in the presence of weak external illumination are shown with open and filled symbols, respectively. Experimental errors are within the sizes of the symbols unless indicated by vertical lines. **Panel B** pH dependence of the amplitude of the component with lowered P/P^+ potential determined from the titrations performed under weak illumination. Conditions: ~ 300 μM BRCs, 70 mM KCl, 300 μM mediators in 0.05% TX-100.

The P/P^+ midpoint potentials were also determined at pH 6 and 10 and were plotted in Figure 3.10A. In the dark the P/P^+ potentials followed very weak pH dependences corresponding to ~ −6 mV/pH and ~ −1 mV/pH slopes as the pH is raised from pH 6 to 10 in the WT and in the L131 mutant, respectively. In the L168 mutant a trend very similar to WT was observed between pH 6 and 8 as the P/P^+ potential is increased from 415 to 425 mV while the pH was lowered from 8 to 6. In the presence of a weak illumination the decrease of the P/P^+ potential was comparable with the ones measured at pH 8 with values of 55 and 64 mV at pH 6 and 10, respectively. The amplitude of the fraction that exhibited lowered potential in WT, however, increased to 60% at pH 6 and was found to be 38% at pH 10 compared to the 42% at pH 8 (Figure 3.10B).

Contrarily, in the L131 mutant this fraction did not change at pH 10 and decreased at pH 6 to the detection limit of 4% from the value of 8% found at pH 8, making the error of determining the P/P^+ potential for this small component as large as ± 80 mV at pH 6.

3.5.1 Origins of the light-induced decrease of the dimer potential

Earlier studies indicated that the introduction of the H-bonds with His residues as proton donors at the M160, M197, and L131 positions increased the redox midpoint potential of the P/P^+ couple between 65 and 125 mV at pH 8 depending on the position.[93] Similarly, the removal of the H-bond found in the WT by substituting the L168 His with a Phe residue caused a 95 mV drop of the potential in the L168 mutant. Multiple substitutions have an additive effect on the potential, resulting in a 350 mV range for the potential of P between the lowest and the highest potential mutant. The redox midpoint potential of the P/P^+ couple determined in the presence of a weak illumination showed that in the absence of the His residue at the L131 position the illumination caused the potential of the dimer to decrease by 75-79mV in a large fraction of WT and the L168 mutant at pH 8 (Figures 3.9 and 3.10). In contrast, in the presence of the His at the L131 position only a marginal fraction of the BRCs exhibited a decreased dimer potential.

Such a large change in the potential of P should originate from either within the bacteriochlorophyll molecules or from their immediate vicinity. As we reported earlier in section 3.3 that the light-induced structural changes noticeably altered the local dielectric constant near P in WT and in mutants that show long recovery kinetics after continuous illumination but not in the mutants that contained the Leu to His replacement at the L131 position.

The change of the redox potential upon the alteration of the dielectric constant is expected. For example, the difference in the *in situ* redox midpoint potentials of the same ubiquinone-10 molecule in BRCs occupying the hydrophobic, buried Q_A and the water accessible, polar, Q_B binding sites is ~ 60 mV.[2] The P/P^+ potential was shown to be regulated in mutants by the protonational state of introduced Asp and Glu residues to the M199 and L170 and L168 positions, situated within 6 Å from P.[114] A potential drop of ~ 60 mV was observed when the pH was elevated from 6.0 to 9.5, corresponding to a loss of one positive charge through the deprotonation of these Asp and Glu side chains in those mutants. In the WT reaction center there are very few amino acids with protonational side chains in the immediate vicinity of P (Figure 3.11).

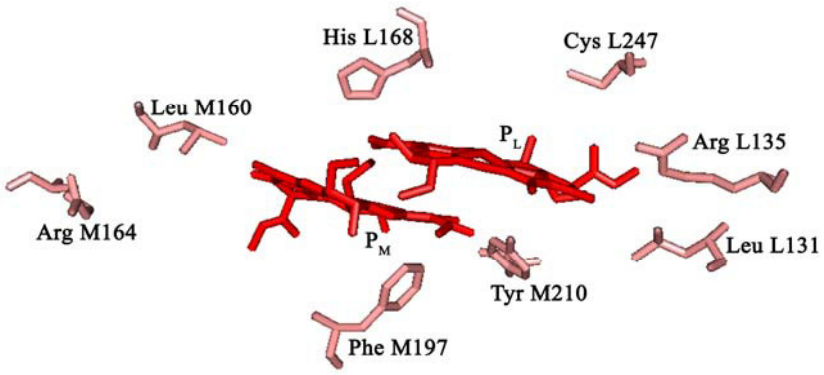

Figure 3.11 Structure of the bacteriochlorophyll dimer P and nearby amino acid residues Leu L131, Leu M160, His L168, and Phe M197. Alteration of each of these residues results in different patterns of hydrogen bonding to P. The residues with protonatable side chains, Arg L135, Cys L247, Arg M164, and Tyr M210 are also shown. This figure is color reproduction from ref. (115) and coordinates were taken from PDB entry code 4RCR[81].

Under normal circumstances the positively charged Arg residues at the L135 and M164 positions are expected to have high pK_a values that should be outside the investigated pH range. In the presence of the positive charge on P about 10 Å away, however, the pK_a values may be shifted downward to values that fall into the investigated range. If replaced by neutral residues the P/P^+ potentials were reported to drop by 12-24 mV in dark-adapted BRCs for the L135 and M164 positions, respectively.[116] The pK_a of the L247 Cys in light-adapted samples was determined to be 8.7 in a tyrosine oxidizing mutant where this residue serves as a proton acceptor to the Tyr L167 residue.[102] Tyr M210 is considered to be one of the key residues in the initial electron transfer process in BRC. Upon its replacement to Trp, Phe, or Leu the initial charge separation drastically slowed down, and the redox potential of the P/P^+ couple in the dark was elevated by up to 50 mV.[117,118] Indirect evidence indicates that if the Trp residue is substituted at the M210 position in mutants with very high P/P^+ potentials that were designed to utilize Tyr residues at various positions as electron donors to P^+, the P/P^+ potential did not drop during continuous illumination.[119-120] The assumption of a deprotonation-mediated stabilization of P^+ requires the P/P^+ potential to be strongly dependent on pH for the light-adapted conformations provided the protons are in equilibrium with the surrounding solution and the pK_a shifts are small.[114] If, however, the interaction energy between the oxidized P and the deprotonating residue is high, then the pK_a shift could be several pH units and the pH dependence should be moderate[121] (Figure 3.10). Tyr M210 is in van der Waals contact with P_M, and the effective local dielectric constant was reported to be only 1.5-4.7 times larger than vacuum.[107] These conditions are extremely favorable to a large pK_a shift upon the oxidation of P.

For example, near Q_B in a medium with an effective dielectric constant of ~ 20, the pK_a of the Glu L212 was reported to be upshifted by ~ 4 pH units to 9.8 due to the negative charge on the Asp L213 residue ~ 5 Å away.[122] The light-induced change in the local dielectric constant not only should alter the P/P^+ potential but also the pK_a values of the nearby residues, since the interaction energies between the charges are inversely proportional to the dielectric constant. For example, the difference in the oxidation potentials of various quinones in organic solvents and *in situ* at the Q_A binding site showed a several hundred millivolts difference, demonstrating the strong dependence of the potential values on the dielectric properties of the environment.[123] The observed 75 mV drop in the potential of the P/P^+ couple and its moderate pH dependence in WT upon prolonged illumination is consistent with the deprotonation of one very close residue plus one or more that have weaker interaction with the dimer. The most likely candidate for the strongly interacting residue is Tyr M210. Whether or not the deprotonation can take place and the released protons can reach the solvent or they are only delivered away from P is dependent upon the existence of a proton conducting pathway that extends from P to the surface. The proton transfer has very slow kinetics of proton release and the accompanying optical changes. This inefficiency is consistent with the proton pathway in WT being not efficient, presumably because it is not physiologically relevant due to the normally fast reduction of P^+ by cytochrome in the cell. A large number of buried protonatable side chains have been reported to equilibrate with the solvent in the minute time scale.[32] Several slow proton conducting pathways were characterized in mutants that were designed to oxidize nearby Tyr residues by P^+ at positions L135, M164, and L167.[102,119,124,125]

The delivery or the trapping of the released phenolic protons were sensitive to the identity of the introduced proton acceptors and the pH. When a His is introduced at L131, the data are consistent with the loss of this proton pathway between Tyr M210 and the surrounding and ultimately the solvent. The loss of the pathway has several consequences for the properties of P^+. The slow kinetics seen in the optical and proton release measurements of WT are now eliminated as the protons can no longer be transferred away from P^+, resulting in only the rapid optical changes being evident. In WT, the long-lived state has a lower P/P^+ midpoint potential due to the redistribution of charges near P, with a loss of positive charge, but for L131 mutants the protons can no longer carried away and there is no redistribution or redox change. As reported earlier the light-induced change of the local dielectric constant upon continuous illumination is much smaller in these mutants than those found in WT (Figure 3.5). The proton pathway presumably involves water molecules rather than just amino acid side chains. The potential role of the structural water molecules near P in facilitating the structural changes was discussed in section 3.3. Two of these five structural water molecules (W736, W737) are very close to P, and one (W723) is very close to Leu L131, while all are within 7 Å distance from P. The introduction of His at the L131 does not allow the decrease of the P/P^+ potential that leads to rapid recovery kinetics. A complementary explanation for the observed light-induced decrease of the P/P^+ potential also assumes the involvement of Tyr M210 and can address why the continuous illumination is unable to drive the entire population of the BRC to the long-lived state. Even though the heterogeneous population of the BRC after continuous illumination was observed in all previous studies, this problem was not scrutinized.

Situating within H-bond distance from the 2-acetyl group of P_M Tyr M210 initially was modeled to be engaged in a H-bond, but later this assumption was dismissed.[118,126] The 2-acetyl group of P_M was also modeled to be a potential ligand to the central Mg^{2+} of P_L both in *Rb. sphaeroides* and earlier in *Blastochloris viridis*.[6,127] These reports suggest the possibility of an axial ligand switch between the L173 His and the 2-acetyl group of P_M to maintain the penta-coordination of the Mg^{2+}, which is reported to be favored in proteins.[110] A ligation of the 2-acetyl group of P_M with the central Mg^{2+} of P_L or an H-bond with Tyr M210 with comparable probabilities could explain why the continuous illumination generated two major populations of the BRCs and was unable to drive the entire BRC population to the long-lived state even after prolonged illumination. Both the ligation to the Mg^{2+} of P_L and the H-bond to Tyr M210 would force the 2-acetyl group out of the molecular plane and thus would not result in the change of the spin density distribution and the position of the Q_Y absorption band of P.[76] In the presence of the H-bond between the His at the L131 position and the 9-keto group of P this switch is disrupted, and a rapid recovery is observed without stabilization of P^+. Redox-induced conformational changes were reported in other proteins as well, for example in the sensor domain of Ec DOS protein and in receptor protein-tyrosine phosphatase.[128,129]

3.6 Proton release

Proton uptake/release measurements were performed in BRCs from WT and the L131 mutant at pH 6 using prolonged, 5 min illumination (Figure 3.12A).

This longer illumination was necessary to reach the saturation values of the proton signals in the set up used for this measurement. After a 5 min illumination, in the WT a large proton release, with ~ 6.5 H^+/BRC was observed. This value is in very good agreement with the proton release reported earlier for the R-26 strain at pH 6.[57] In the L131 mutant, only a small release of ~ 0.3 H^+/BRC was detected that may correspond to a ~ 5% fraction of the BRCs trapped in the longest-lived light-induced conformation. For both samples, the recovery of the proton release followed the recovery kinetics of the optical signals corresponding to the longest-lived states measured under the same 5 min illumination (Figure 3.12B).

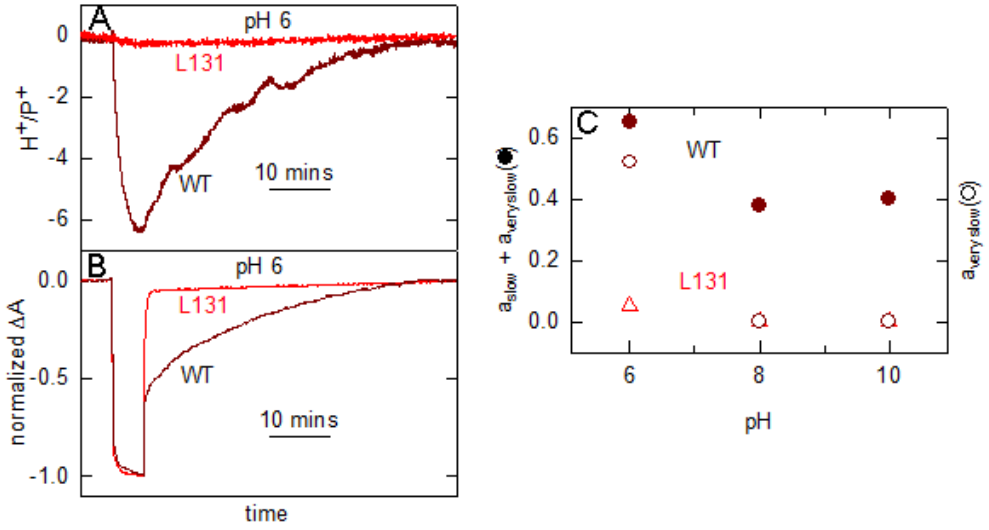

Figure 3.12 Kinetics of the light-induced proton release (A) and absorption changes (B) in WT (brown) and in the L131 (red) mutant at pH 6. The traces for **panel A** are the differences between the unbuffered and the strongly buffered measurements. Conditions for panel A: 2 µM BRCs in 0.05% TX-100, 100mM NaCl, 100 µM terbutryn; for the buffered signal +15mM MES. Conditions for panel B: same as for panel A except 0.1% LDAO instead of TX-100. Illumination time: 5 min through 870 ±15 nm interference filter using water bath as a heat filter. **Panel C:** pH dependence of the amplitude of the trapped states in the recovery kinetics of the absorption changes.

For better comparison, the light-induced kinetic traces were also recorded using a 5 min illumination. In the recovery kinetics after the light was turned off the amplitude of the slowest component increased from 35% to 60% in WT at pH 6 as the illumination time increased from 1 to 5 min (see Figure 3.7 for comparison). The rate constant of the longest-lived component on the other hand dropped only from 2.3×10^{-3} to 1×10^{-3} s^{-1} as the illumination time was increased by 5-fold. The observed kinetics in WT for prolonged illumination recorded here in LDAO is very similar to those found in the carotenoid-less mutant strain R-26 measured in TX-100.[57] The matching kinetics of the proton release measured in TX-100 (Figure 3.12A) and the optical signals recorded in LDAO (Figure 3.12B) for WT and in TX-100 for R-26 indicate that these two detergents do not alter the proposed structural changes or the redox states of the BRCs. The kinetics of the L131 mutant at pH 6 remained almost the same as was seen at 1 min illumination. The vast majority of the reaction centers (95%) recovered immediately, and only the remaining 5% featured the long recovery. At pH 8 even the longer, 5 min illumination could not generate the component with the rate constant of ~ 10^{-3} s^{-1} either in the WT or in the L131 mutant. The pH dependence of the relative extent of the slow and very slow components in WT and in the L131 mutant is displayed in Figure 3.12C and shows remarkable similarities to those that have been obtained from the spectroelectrochemical redox titrations for the fraction with lowered potential P (Figure 3.10B). The stoichiometry of the light-induced proton release at pH 6 correlates with the amplitude of the very slow component that could not have been observed at pH 8 (Figure 3.12).

The conformational state with a large proton release at pH 6 could only be built up significantly in the mutants that showed longer recovery kinetics, exhibited decreases in their P/P^+ potential, and showed decreased electrochromic absorption changes in the B bands. The agreement between the kinetics of the recovery of proton release and the recovery of the charge-separated state at pH 6 is even more pronounced if we compare these data with those reported earlier for R-26.[65]

3.7 Assigning the kinetic components to conformational changes

Most of the earlier conformational studies argued that the origin of the long-lived states upon continuous illumination must stem from conformational changes near the quinones.[35,56,65,67,68] This assumption was supported by structural studies where indeed electron density changes were observed upon illumination near Q_B and the H-subunit.[43,85] These X-ray crystallographic studies used, however, very short (<1 s) illuminations to generate the light-induced states as the crystals would not diffract if exposed to longer illuminations.[85,104] It is obvious from this work as well as earlier illumination time-dependent analyses that accumulation of the really long-lived states requires a much longer illumination time than 1 s.[57,68] We present a model (Scheme 3.1) that explains the results of this work with a minimum of assumptions.

In the scheme the horizontal displacements are redox reactions (D → L_H) and deprotonational steps (L_H → L_0), and the vertical displacements are structural changes between conformational levels (L1 → L2 → L3) from a dark-adapted conformation (L1), to an intermediate light-adapted conformation (L2), and to the final light-adapted conformation (L3).

Scheme 3.1 Minimal model of the light-induced and redox reactions, conformational, and protonational changes in BRCs[a]

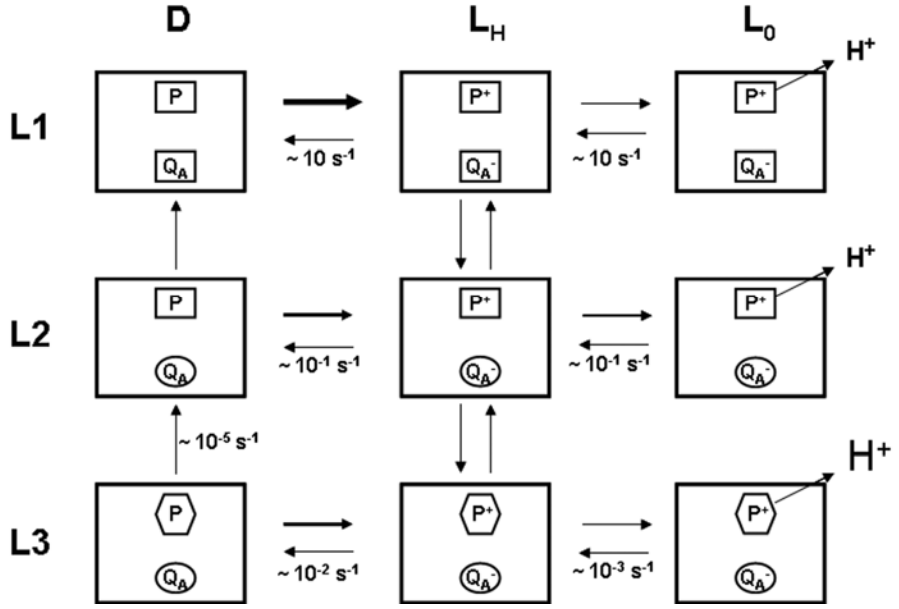

[a] The BRCs are shown as large rectangles. The dark-adapted conformations for both P and Q_A are shown as small rectangles, and the different light-adapted conformations of the protein in the vicinity of P and Q_A are indicated with hexagons and ellipses, respectively. The horizontal changes indicate charge separation (forward arrow) and charge recombination (backward arrow) from the dark (D) to under light (L_H) and the protonational changes between the protonated (L_H) and the deprotonated (L_0) forms of the BRCs are also shown with horizontal arrows. The approximate rate constants for the recovery processes are indicated near the corresponding arrows. A full description is found in the text.

In dark-adapted samples (L1) the charge separation forms the $P^+Q_A^-$ state, and in the vast majority of the samples charge recombination takes place in the ~ 30-100 ms time scale depending on the pH and the mutants (Figure 3.8). Because of the very low quantum yield of the conformational changes, multiple turnovers are needed to build up the different conformational levels indicated by L2 and L3. The multiple turnovers can be achieved either by continuous illumination or trains of flashes as suggested in earlier studies.[35,46,56,57,65,67,68] The populations of the different conformational levels are dependent upon the illumination time and the mutation. At very short illumination times (~ 1 s) the component with a rate constant of ~ 10^{-1} s^{-1} is the first to appear in the recovery kinetics among the slower components in the WT, and this component was predominantly observed even after longer illuminations in the mutants containing His at L131 (at level L2) besides the normal charge recombination. It can also be seen in virtually all mutants if another component with a similar rate constant does not mask it (Figure 3.8). When the reduced quinone was rapidly oxidized by excess ferricyanide after a flash excitation, P^+ has been reported to scavenge an electron from the surroundings with a rate constant of ~ 10^{-1} s^{-1} in R-26 and also in *Blastochoris viridis* reaction centers.[57,113,130] If an early light-induced conformational change around the quinones blocks the return of the electron to P^+, one can assume a similar situation. Thus, we propose that the component with a rate constant of ~10^{-1} s^{-1} is most likely due to the recovery of P^+ caused by the light-induced conformational changes taking place in the vicinity of the quinones, at the cytoplasmic side of the BRC. This assignment is in agreement with the X-ray crystallographic studies where after short illuminations (<1 s) structural changes were only reported near the quinones and in the H-subunit.[43,85]

While the L2 level appears to be populated for WT and all mutants, significant population of L3 is observed only for WT and mutants with the native Leu at L131. The component with rate constants of ~ 10^{-2} s^{-1} (at level L3) was only observed in the mutants that exhibited a large decrease of the P/P^+ potential (Figures 3.8 and 3.9) and was also accompanied by decreased electrochromic absorption changes of the bacteriochlorophyll monomer band upon illumination that was assigned to the increase of the local dielectric constant (Figure 3.5). It should be noted that in the mutants with the M197 Phe to His substitution the recovery kinetics were the fastest in their group (Figure 3.7), but they were not as rapid as in the L131 family of mutants and exhibited some degree of dependence on the P/P^+ potential (Figure 3.8). This is consistent with the models presented above since the M197 His is close to both the 2-acetyl group of P_M and Tyr M210 (Figure 3.11). We assigned the L3 level as the conformational state formed due to structural changes occurring at the periplasmic side, near P. As the amplitude of the very slow component with a rate constant of ~ 10^{-3} s^{-1} at pH 6 was correlated with the extent of the proton release and was predominantly detected in the mutants that lack the L131 His, we conclude that this component should also arise from conformational changes at the periplasmic side but from a different protonational state. The matching kinetics of the recovery of the proton release (Figure 3.12A) and the recovery of the charge-separated state (Figure 3.12B) indicates that the re-protonation step is rate limiting at the L3 level. After flash excitation, at the L1 level, the kinetics of the reuptake of the substoichiometric proton release was also found to be the same as the charge recombination.[113]

The unusual, large proton release that has also been reported earlier for R-26 was attributed to the different pK_as of several protonatable residues near the periplasmic surface in the light- and dark-adapted conformations of the reaction center.[57]

Since the proton release is not coupled with additional decrease of neither the P/P^+ potential nor the electrochromic absorption changes of the monomer bands, most of the proton releasing residues must not be in the immediate vicinity of P or the B monomers. It has been discussed earlier that there are a total of 14 Glu, Asp, and His (not ligated) residues that are at least 10 Å away from P on the periplasmic side of the reaction center and may have their pK_a values in the acidic pH range and can account for the 6.5 H^+/BRC proton release here in WT and for the 6.0 H^+/BRC in R-26 reported earlier.[57] The increase of the local dielectric constant was shown to shift the pK_a values of the side chains of the acidic residues downward and those of the basic residues upward in globular proteins.[131] Because around pH 6 the Asp and Glu residues are more likely expected to undergo protonational changes than the basic ones, the observed proton release in WT and in R-26 is in agreement with the decrease of the pK_as of the 14 possible acidic residues. It was shown earlier that even after flash excitation proton release from near P^+ can only be observed at low pH values.[113,121] This indicates that the pK_a values of the residues near P should be below pH 8 and explains why in this work and after flash excitation proton release was only observed at low pH and not at pH 8. The $L_H \rightarrow L_0$ deprotonation step in Scheme 3.1 is therefore strongly pH dependent in all conformations.

While the proton release in the dark-adapted conformation (at level L1) after a single flash excitation is also caused by the shift of the pK_as of the nearby residues, it can only be substoichiometric since it is due to the interaction of the single positive charge on P with the protonatable side chains.[113,121] This can only provide very moderate stabilization for P^+ due to proton release. At level L3, however, the increased value of the dielectric constant can shift the pK_as of many residues, significantly resulting in a large proton release and almost an order of magnitude longer lifetime of the charge-separated state. According to the proposed Scheme 3.1, there are two different conformations of P: the dark-adapted conformation at levels L1 and L2 (indicated by squares) and the light-adapted conformation, at level L3 (shown as hexagons). The relaxation time from L3 to the L2 (or L1) conformational level in the ground state was found to be ~ 6 h (rate constant of ~ 10^{-5} s^{-1}) after prolonged illumination (Figure B2) and about 1 h after 1 min illumination. These conformational states are the sources for the two populations of P with different redox potentials in WT and in mutants with Leu at L131 (Figure 3.9 and Figure B3). As level L3 is not populated significantly in the mutants containing the His at L131, P predominantly exists only in the dark-adapted conformation (at levels L1 and L2) in these mutants (Figure 3.9 and Figure B3, Table B1).

In summary, we have shown that the rate of the recovery of the oxidized dimer in the $P^+Q_A^-$ state depends systematically on the protein environment of P^+. In particular, replacement of the Leu to His at the L131 position appears to prevent the light-induced conformational changes that result in a very slow recovery of the charge-separated state, the drop of the P/P^+ potential, and a large proton release at pH 6.

These events correlate with the extent of the light-induced change in the local dielectric constant near P. The long-lived P^+ cannot be generated by electrochemical oxidation alone even in the light-adapted conformation (Figure B1) as it requires the presence of the electric field between Q_A^- and P^+ established by the light-induced charge separation and the subsequent structural changes that have low quantum yields. We have also shown that the kinetics of the light-induced conformational changes and the proton release in WT are very similar to those reported earlier in the carotenoid-less R-26 mutant, and they are independent of the detergents used.[57] The extension of the lifetime of the charge-separated state by up to 4 orders of magnitude via light-induced structural and protonational changes provides new opportunities to utilize the BRCs in energy storage as biocapacitors. The charges separated by a low dielectric medium can be prevented from recombination by systematic alteration of the environment of the charges (explained later in chapter 5), and the light can be used as a switch.

Chapter 4

Effect of hydrophobic environment (detergents and lipids) on electronic structure of the primary electron donor

The results in this chapter are based on the following published paper:

Deshmukh, S. S., Akhavein, H., Williams, J. C., Allen, J. P., and Kálmán, L. (2011) Light-induced conformational changes in photosynthetic reaction centers: Impact of detergents and lipids on the electronic structure of the primary donor. *Biochemistry*, *50*, 5249-5262.

Author contributions:

S. S. Deshmukh performed the experiments, analyzed the data, and contributed to writing the paper. H. Akhavein performed experiments in liposomes, which are represented in figure 4.4 and 4.5. J. C. Williams and J. P. Allen supplied the strain from *Rb. capsulatus* and contributed to writing the paper. L. Kálmán designed the research, guided the data analysis, and wrote the paper.

As explained with experimental evidences in Chapter 3, structural changes near P are responsible for the very long lifetime of the charge-separated state after prolonged illumination. A correlation between the type of mutation and several electronic properties, including the redox midpoint potential of P, the light-induced electrochromic absorption changes of the bands of the nearby B molecules due to the increase of the local dielectric constant, and proton release from the periplasmic side, was interpreted in terms of structural changes of P and its local environment. In this chapter, these studies on BRCs from *Rb. sphaeroides* have been extended to BRCs from *Rb. capsulatus*, which shows pronounced spectral changes depending upon the choice of detergents. The structure of the BRC from *Rb. capsulatus* has not been determined, but it is presumed to be very similar to the structure of the BRC from *Rb. sphaeroides* based on the amino acid sequence similarity between the two species.[126,132-134]

The overwhelming majority of the accumulated knowledge about the structure and the coupling between the electron and proton transfer reactions has been obtained using BRCs that were purified in detergents to substitute for the natural membrane environment. The isolation procedure and the selection of the detergent have been found to significantly alter the spectroscopic properties of the BRCs.[135-137]

While in their native membranes the peak position of the Q_Y absorption band of P in both *Rb. sphaeroides* and *Rb. capsulatus* is centered at 865 nm, this position of the P band in BRCs from *Rb. capsulatus* has been reported to be affected by the zwitterionic LDAO detergent, which is the most commonly used detergent for BRC isolation and characterization.[138]

When BRCs are purified using LDAO, the peak position of the P-band in *Rb. sphaeroides* stays at 865 nm, but it was reported to be downshifted by 15 nm in *Rb. capsulatus* to 850 nm. These positions can be systematically switched by selecting detergents with different head-group charges in both strains.[25,138] This spectroscopic difference was identified earlier as an indicator for two different electronic structures of P.[25] Here, the effects of prolonged, continuous illumination on the Q_Y absorption band of P in BRCs from *Rb. capsulatus* are measured using steady-state and transient optical spectroscopy in both detergent micelles and in lipid bilayers. In particular, the light-induced conversion between different spectral states, which has not been reported previously, is investigated. These optical shifts are characterized in terms of structural changes of P involving electrostatic and hydrophobic interactions with the surrounding membrane substituent and compared to those observed for BRCs from *Rb. sphaeroides.*

4.1 Comparison of the light-minus-dark spectra and the recovery kinetics of the dimer in detergent micelles and liposomes

The absolute and light-minus-dark difference optical spectra were recorded during and various different times after the illumination for BRCs from *Rb. capsulatus* that were dispersed in DOC, CTAB, and LDAO detergents (Figure 4.1). The absolute spectra have three absorption bands in the 700-1000 nm region. The band centered at ~ 760 nm is assigned to the H molecules (H-band), the second band centered at ~ 800 to the B molecules (B-band), and the third at 850-870 nm to P (P-band).

The near-infrared absolute absorption spectrum is significantly different if the BRCs are dispersed in positively (CTAB) or negatively (DOC) charged detergent micelles as reported earlier. The most striking effect is a ~ 20 nm blue shift in the position of the P-band that is clearly visible in the absolute spectra. The difference spectrum (thick black solid line in panel A of Figure 4.1) reveals an additional feature, namely a slight broadening of the B-band if the detergent is changed from DOC to CTAB.

The band shift and broadening are two standard electrochromic responses to changes of the local electric field.[101] The light-minus-dark difference optical spectra measured at different times after illumination are shown for DOC and CTAB in panels B and C of Figure 4.1, respectively. In both detergents the difference spectra feature bleaching of the P-band, an electrochromic blue shift of the B-band due to the presence of the positive charge on the nearby P, and an electrochromic red shift of the H-band due to the negative charge on Q_A.[139] After illumination for 1 min, the spectra recovered fully but with different rates for BRCs in CTAB and DOC. In CTAB total recovery was observed within 2 min after the illumination was switched off, while in DOC the full recovery required a ~ 4 times longer time scale. The spectra for DOC and CTAB samples were insensitive to the illumination history of the sample, meaning that subsequent illuminations resulted in the same spectra, but this was not the case for the LDAO-dispersed samples. Using strictly dark-adapted samples, the position of the P-band was 863 nm, a value very close to 865 nm that is observed in TX-100 for *Rb. capsulatus* or for *Rb. sphaeroides* in both TX-100 and LDAO. During the very first illumination, however, the position of the P-band shifted to 855 nm and did not return even after 1 h dark adaptation (panel D of Figure 4.1).

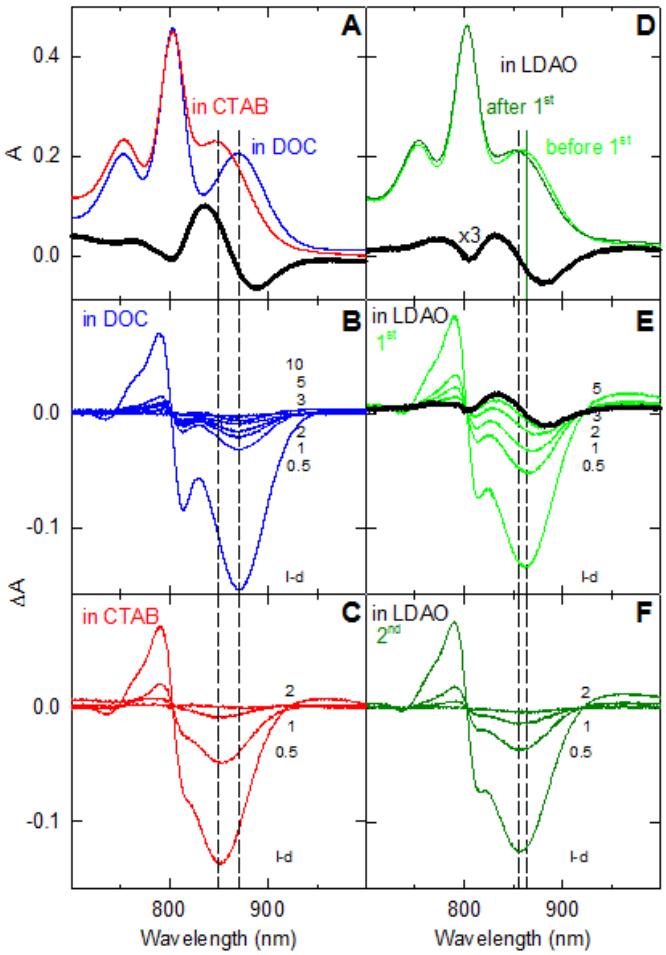

Figure 4.1 NIR absolute (panels **A** and **D**) and light-minus-dark difference optical spectra (recorded at the end of 1 min illumination) and recovery in reaction centers dispersed in DOC (in blue) **(B)**, CTAB (in red) **(C)**, and LDAO during and after the first (in pale green) **(E)** and second (in dark green) **(F)** illumination. The position of the P-band in these samples is indicated by vertical dashed lines. The numbers in the difference spectra in panels B, C, E, and F show what time the spectra were recorded in minutes after the illumination was turned off. In LDAO the position of the P band was found to be different before and after the first illumination. The thick solid black lines in panels A, D, and E represent the difference spectra recorded in DOC and CTAB, before and after the first illumination in LDAO, and the residual spectra after the first illumination, respectively. These difference spectra are consistent with the shift of the P-band from 870 to 850 nm in panel A and from 863 to 855 nm in panels D and E, respectively. Conditions: 1.5 μM BRC, 15 mM Tris-HCl, 1 mM EDTA pH 8. The concentrations of the detergents are listed in the text.

The difference spectrum in LDAO between the spectra collected after and before the first illumination shows the very same features as those determined between CTAB and DOC (panel A of Figure 4.1). Panel E shows the lack of full recovery after the first illumination. Subsequent illuminations, however, did not cause further shifts as the spectral features recovered fully (panel F of Figure 4.1). A single illumination causes only a fraction of the BRCs to be converted to a long-lived, conformationally altered state generating a heterogeneous population of the BRCs. Using subsequent exposures, the position of the P-band eventually shifted to 850 nm after five 1 min long illuminations followed by 10 min dark relaxation periods after each exposure and stayed there even after several hours dark adaptation. One full day in the dark resulted in a few nm red shift in the P-band position, indicating that a very small fraction of P may have returned to the dark-adapted 865 nm position. Such long time storage at room temperature, however, began to take a toll on the stability of the BRC protein as additional changes characteristic to degradation processes also appeared in the spectrum. It has to be noted that the recovery kinetics after the first illumination was slower than after the second illumination in LDAO, in the same manner as in DOC *vs* in CTAB (please compare panels B with E and panels C with F of Figure 4.1).

Complex formation and recovery kinetics during and after illumination (Figure 4.2) indicates that the continuous illumination drives a fraction of the BRCs to a conformationally altered state as described in chapter 3 and previously.[35,56,57,65,68]

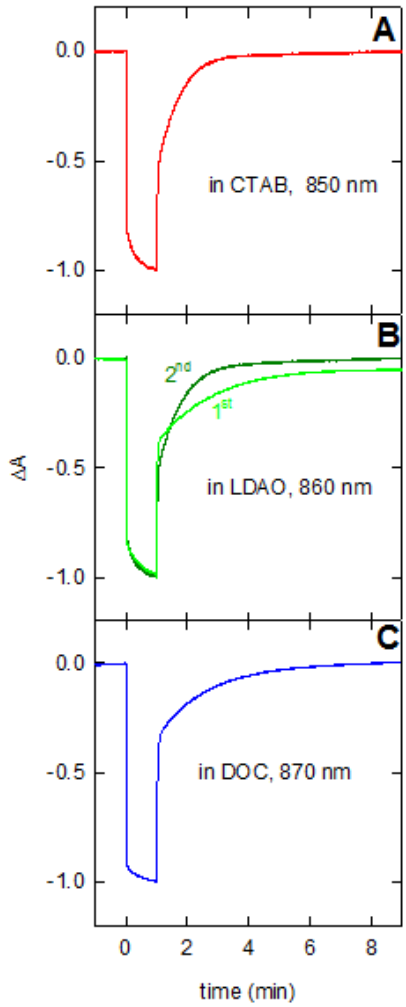

Figure 4.2 Kinetics of the light-induced absorption changes measured in the Q_Y absorption band of P during and after 1 min illumination in the absence of any secondary donor for BRCs in **(A)** CTAB (red), **(B)** LDAO (1^{st} and 2^{nd} illumination in pale and dark green, respectively), and **(C)** DOC (blue). In LDAO the kinetics was dependent on whether the samples were dark-adapted or pre-illuminated. Note that the kinetic trace in LDAO after the first illumination does not recover completely to zero (see panel E in Figure 4.1 for comparison). Conditions as in Figure 4.1.

Analysis of the slow phase in the different detergents yielded rate constants of 9.8×10^{-3} and 2.4×10^{-2} s^{-1} in DOC and CTAB, respectively. A similar, ~ 2-fold difference was observed in LDAO when comparing the slow phases of the first and second illuminations, which had rate constants of 9.4×10^{-3} and 1.9×10^{-2} s^{-1}, respectively. The kinetic parameters are also listed in Table 4.1. These results indicate that the rate constants are essentially the same for BRCs that have the long-wavelength form of P and similar for those that have the short-wavelength form of P regardless of the identity of the detergent. As the position of the P-band in *Rb. sphaeroides* can only be shifted to 850 nm with the addition of cationic detergent (CTAB),[25] the dependence of the recovery kinetics in the presence of CTAB was measured.

Table 4.1 Kinetic parameters of the recovery of the $P^+Q_A^-$ charge-pair after continuous illumination in BRCs from *Rb. capsulatus*[a]

	Head-group charge[b]	name[c]	A_s[e]	$k_s \times 10^2$ (s^{-1})[f]	A_{vs}[e]	$k_{vs} \times 10^3$ (s^{-1})[f]
detergent	+1	CTAB C_{16}	0.53	2.4	ND	ND
	0	LDAO C_{12} 1st	0.41	0.94	ND	ND
	0	LDAO C_{12} 2nd	0.50	1.9	ND	ND
	-1	DOC[d] C_{22}	0.37	0.98	ND	ND
lipid	+1	DOTAP C_{18}	0.24	1.8	0.30	1.7
	0	DOPC C_{18}	0.22	2.0	0.32	2.5
	0	DLPC C_{12}	0.42	1.1	ND	ND
	-1	DOPS C_{18}	0.16	1.4	0.51	0.9

[a] The BRCs were dispersed either in detergent micelles or in liposomes with various head-group charges and the kinetic parameters were determined from Figures 4.2 and 4.5, respectively.

ND: not detectable.

[b] Net charge of the head-group at pH 7.4.

[c] Abbreviated name of the detergent or lipid and the length of the hydrophobic chain.

[d] Effective length C_{12}-C_{13}.

[e] Relative amplitude of the slow (A_s) and very slow (A_{vs}) components in the recovery of the $P^+Q_A^-$ charge pair.

[f] Rate constant of the slow (k_s) and very slow (k_{vs}) components.

The normalized light-minus-dark difference spectra measured at the beginning of the illumination and 1 min after the illumination was turned off in *Rb. capsulatus* in DOC, CTAB, and LDAO are shown in Figure 4.3. The spectra recorded at the beginning of the 1 min illumination are predominantly characteristic of the dark-adapted conformation of the BRC, while those recorded 1 min after the illumination is turned off represent the light-induced conformation in all samples.

The differences between those two spectra are characteristic of the light-induced changes that took place during illumination. A decrease of the electrochromic absorption changes of the B-bands was detected in *Rb. capsulatus* in all three detergents regardless of the position of the P-band, which is similar to the findings for the BRCs from *Rb. sphaeroides* (as discussed in chapter 3). However, in the strictly dark-adapted BRCs in LDAO, the double difference spectrum featured not only the shift in the B-band but also the shift in the P-band (Figure 4.3C).

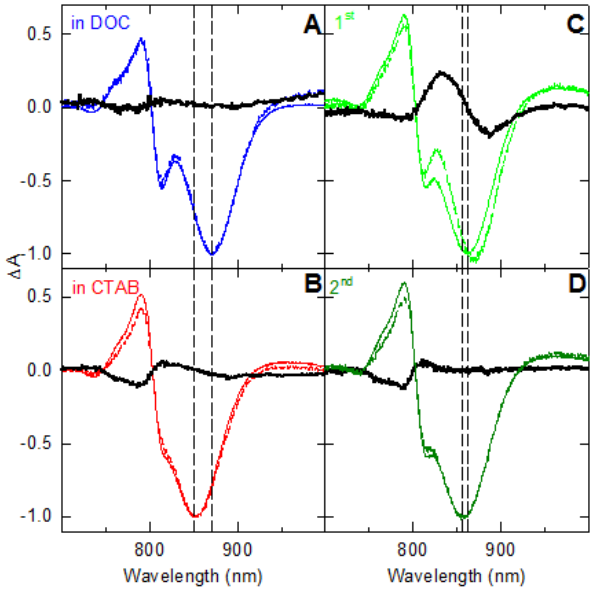

Figure 4.3 Normalized light-minus-dark difference spectra (solid lines) recorded immediately after the onset of the light and 1 min after the illumination was turned off (dashed lines) for BRCs dispersed in DOC (blue) **(A)**, CTAB (red) **(B)**, and LDAO (**C** and **D**, for the first (1st) (pale green) and second (2nd) (dark green) illuminations, respectively). The thick black solid lines show the double difference spectra and feature changes around 800 nm consistent with the decrease of the electrochromic absorption changes involving the monomers during the illumination. The vertical dashed lines show the position of the P-band in DOC, CTAB, and in LDAO before and after the first illumination. Conditions as in Figure 4.1.

Recovery rates of the redox states after prolonged illumination

In *Rb. sphaeroides*, where the position of the P-band in LDAO is 865 nm, the rate constant for the slow component in the recovery kinetics after prolonged illumination without a secondary electron donor was reported to be ~ 2×10^{-2} s^{-1} (Chapter 3). This value is in agreement with the rate constants observed for BRCs from *Rb. capsulatus* dispersed in DOC and LDAO if the samples were dark-adapted.

Upon the light- or detergent-induced shift of the P-band to 850 nm a ~ 2-fold acceleration was observed (Figure 4.2 and Table 4.1). The slow phase is assigned to the fraction of the BRCs that undergo a light-induced conformational change. The amplitudes of the slow phase are comparable (30-50%) in the two species and those found in different detergents in *Rb. capsulatus* (Figure 4.2). These observations suggest a close correlation between the lifetime of the charge-separated state in the light-induced conformation and the position of the P-band and thus the electronic structure of P. The light-induced shift of the P-band in *Rb. capsulatus* appears to be a consequence of conformational changes in the BRC, but the recovery rates change by a factor of 2 compared to a 1000-fold difference between the recovery kinetics in the dark- and light-adapted conformations (Figure 4.3).

4.1.1 Influence of the lipids on the light-induced optical spectra and the kinetics of the recovery of the charge-pair in liposomes

Light-minus-dark optical difference spectra were recorded in BRCs from *Rb. capsulatus* that were reconstituted into liposomes. The liposomes were formed using lipids that all contained the same mono-unsaturated dioleoyl (18 carbon atoms long, C_{18}) fatty acid chain but with different head-groups, cationic (DOTAP), anionic (DOPS), or zwitterionic (DOPC) (Figure 4.4). This selection ensured that all three lipids were in their liquid crystalline phase at room temperature with only differences in their head-group charges. Following the same approach shown in Figure 4.3 for detergent micelles, the normalized spectra taken at the beginning of the illumination (solid lines) and 1 min after the illumination was turned off (dashed lines) are shown in Figure 4.4 for the liposomes.

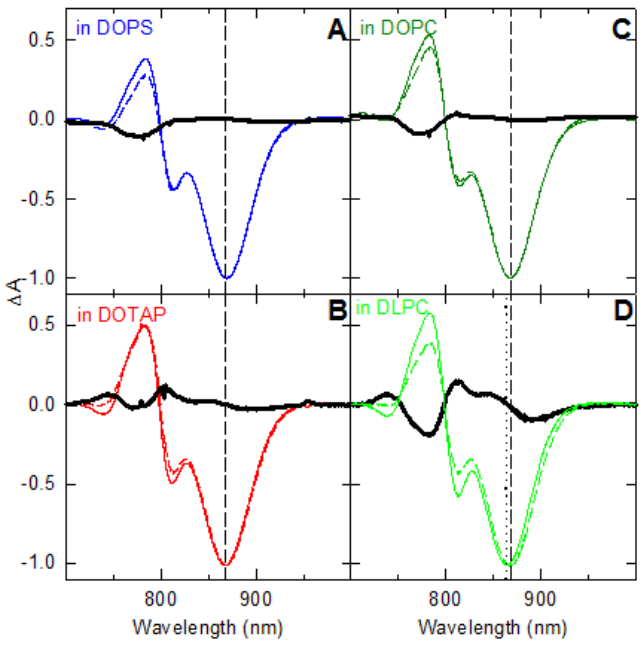

Figure 4.4 Normalized light-minus-dark difference spectra (solid lines) recorded immediately after the onset of the light and 1 min after the illumination was turned off (dashed lines) for BRCs from *Rb. capsulatus* incorporated in DOPS (blue) **(A)**, DOTAP (red) **(B)**, DOPC (dark green) **(C)**, and DLPC (pale green) **(D)** liposomes. The thick black solid lines show the double difference spectra and feature changes around 800 nm, consistent with the decrease of the electrochromic absorption changes involving the monomers during the illumination and in DLPC a marked shift in the P-band. The vertical dashed lines show the position of the P-band in DOPS, DOTAP, and DOPC at 868 nm. The vertical dotted line is indicating the position of the P-band in DLPC at 864 nm. Conditions: ~ 1.5 µM BRC, 15 mM potassium phosphate, 15 mM KCl, 1 mM EDTA, 100 µM terbutryn, pH 7.4.

For comparison, the spectra recorded in BRCs that were incorporated to liposomes from DLPC with zwitterionic head-groups like DOPC but only a C_{12} fatty acid chain are also shown (Figure 4.4D). Unlike for the spectra recorded in detergent micelles (Figure 4.3), the head-group charges had no significant influence on the peak position of the P band as long as the fatty acid chains were C_{18}.

All BRCs exhibited P band positions of 868 ± 1 nm in the dark and at the beginning of the illumination (vertical dashed lines in Figure 4.4, panels A-C). The prolonged illumination of these BRCs did not change the position of this band significantly as indicated by the lack of spectral features in the double difference spectra (thick solid lines) in the 840-900 nm range. If, however, the BRCs were reconstituted into liposomes from DLPC with a zwitterionic head-group and a C_{12} fatty acid chain, the observed position of the P-band at the beginning of the illumination (and in the dark prior to illumination) was already blue-shifted by 4 nm to 864 nm. Upon illumination the observed P band position shifted even further to lower wavelengths, though not as much as observed for reaction centers in zwitterionic LDAO detergent micelles (Figure 4.3C). Analysis of the double difference spectrum (thick solid line in Figure 4.4D) showed a shift of the P-band to 850 nm in 27% of the BRCs. The observed very small, light-induced shift in DOTAP indicated only 7% of the BRCs as being affected (Figure 4.4B). Unlike BRCs in LDAO, the peak position of the P-band during the recovery returned to the value observed before the illumination both in DOTAP and in DLPC liposomes. The spectra recorded after the illumination was turned off were characteristic of the $P^+Q_A^-$ state in the light-adapted conformation and showed decreased electrochromic shifts of the B-bands around 800 nm. The decrease of the electrochromic absorption changes involving the B bands around 800 nm upon illumination were present in all samples but with different extent (Figure 4.4). The recovery kinetics of the $P^+Q_A^-$ charge-pair after illumination is shown in Figure 4.5, and the kinetic parameters are tabulated in Table 4.1 for reaction centers incorporated into liposomes.

The time required for the full recovery of the charge-separated state was found to be much longer in liposomes with C_{18} fatty acid chains (DOTAP, DOPC, and DOPS) than in DLPC liposomes with C_{12} fatty acid chain length. In DLPC liposomes and detergent micelles, the recovery kinetics were biphasic with the slow component being comparable in all detergent micelles and lipids (see also Figure 4.2 and Table 4.1). In liposomes with the lipids with C_{18} fatty acid chains, the recovery kinetics had a third, very slow component. This very slow component had nearly an order of magnitude smaller rate constant than that of the slow component (Table 4.1).

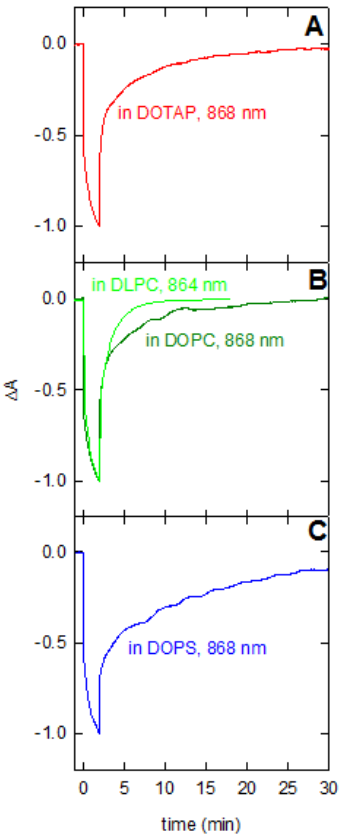

Figure 4.5 Kinetics of the light-induced absorption changes measured in the Q_Y absorption band of P during and after 2 min illumination in the absence of any secondary donor for BRCs in liposomes with different head-group charges: **(A)** DOTAP in red (positive), **(B)** DOPC in dark green and DLPC in pale green (zwitterionic), and **(C)** DOPS in blue (negative). Conditions as in Figure 4.4.

When BRCs from *Rb. capsulatus* were reconstituted into liposomes, the rate constants of the slow component were also found to be similar to those determined in detergent micelles, but further stabilization of the $P^+Q_A^-$ charge-pair was observed in liposomes from lipids with C_{18} fatty acid chains regardless of the head-group charge (Figure 4.5). This stabilization was characterized by the presence of the very slow kinetic component that has a rate constant of ~ 10^{-3} s^{-1} (Table 4.1). When this component was detected the P-band stayed in its long-wavelength form during illumination (Table 4.1 and Figure 4.4 A-C). Contrarily, if DLPC with a C12 fatty acid chain length was used to incorporate the BRCs, the very slow component was not observed and the P-band position has been blue-shifted (Figure 4.4 D, Table 4.1, and Figure 4.5). The very slow component with a rate constant of ~ 10^{-3} s^{-1} was assigned in BRCs from *Rb. sphaeroides* to a stabilization of the conformationally altered state by proton release (Chapter 3). In the proton release Tyr M210 plays a critical role as it is situated within H-bond distance from the 2-acetyl group of P_M. The lack of the very slow component in the recovery kinetics of BRCs reconstituted into DLPC with a blue-shifted P-band is consistent with the rotation of the 2-acetyl group and the loss of the proton pathway between Tyr M210 and the solvent.

4.1.2 Two distinct conformations of P

On the basis of their spectral features, the reaction centers can be divided into two classes depending on the observed position of the Q_Y absorption band of P, with the band being at 865 and ~ 850 nm for first and second classes, respectively.[138]

Under most commonly used BRC purification conditions, the reaction centers from *Rb. sphaeroides* and *Rhodospirillum (Rps.) rubrum* belongs to the first class and *Rb. capsulatus* and *Rps. centenum* were reported to belong to the second group. For BRCs from both *Rb. capsulatus* and *Rb. sphaeroides*, it is possible to shift the P-band position and thus convert one spectral form of P to another by changing the nature of the detergent.[25,138] Positively charged detergents like CTAB fix the position of the P-band at ~ 850 nm while neutral or negatively charged ones adjust the band position to ~ 865 nm. Contrarily to the behavior in LDAO the P-band position for BRCs from both species in chromatophores is reported as 865 nm.[138] Our results showed that in liposomes formed from lipids with C_{18} fatty acid chains the P-band position was also preserved at the long-wavelength form (Figure 4.4). Our results also indicate that illumination can shift the P-band from its long-wavelength form to its short-wavelength form regardless of the identity of the detergent and also in liposomes from DLPC with short fatty acid chain length. The quantum yield of this conversion is reasonably high in LDAO but low in TX-100 and DOC as indicated by the differences in illumination times that are required to induce the shift (Figure 4.2). The conversion of the two spectral forms back and forth indicates that the spectral differences must be due to altered interactions of P with the environment and not due to inherent structural differences. The major difference between these two forms is the ability to delocalize the positive charge over the two halves of P. Extensive electron paramagnetic resonance (EPR) and electron nuclear triple resonance (special TRIPLE) studies have revealed that the observation of the long wavelength form is coupled to a larger degree of delocalization of the positive charge (electron hole) with a ratio of approximately 2:1 favoring P_L over P_M.[140]

Contrarily, the positive charge is almost completely localized on P_L if the band position is found at 850 nm setting the same ratio to 5:1. The observed asymmetry was attributed to the change in the orbital energies of the two halves of the dimer.[141] The change in the delocalization of the positive charge and thus the orbital energies was proposed to be caused by a change of the orientation of the 2-acetyl groups of P_L and/or P_M.[25,45,76,140] These studies indicated that 2-acetyl groups have different orientations when they are free or hydrogen bonded to nearby residues. Whether or not the rotation of the 2-acetyl group causes the shifts in the P-band position and in the spin density distribution between P_L and P_M is not clear. Removal of the native H-bond in *Rb. sphaeroides* between the 2-acetyl group of P_L and the L168 His by substituting this residue with a Phe resulted in the shift of the P-band to 850 nm, but the electron hole became almost evenly shared between the two halves of P instead of the predicted localization on P_L.[76] This is in contrast to what was observed in native BRCs dispersed in positively charged detergents, where the 850 nm P-band position was coupled to an almost total localization of the hole on P_L.[25] Similarly, if H-bonds were introduced in the symmetrical position between the 2-acetyl group of P_M and a residue substituted to the M197 position depending on the identity of the residue different results were obtained. The formation of the H-bond was confirmed with both His and Tyr residues with various techniques.[45,76,142] With His at M197 significant changes could be observed neither in the spin density distribution nor in the position of the P-band in comparison with wild type.[76,93] With Tyr at M197, however, both the blue shift of the P-band and the localization of the hole on P_L were observed.[142]

The picture becomes even more complicated if we compare the changes of the reported P/P^+ potentials caused by the removal or addition of the H-bonds and thus the rotation of the corresponding acetyl groups. The M197 His induced the largest increase of the P/P^+ potential (130 mV) regardless of the lack of the spectral changes, while the Tyr only increased the potential by 30 mV.[93,143] In the symmetrical position, L168, the replacement of His with Phe resulted in a 90 mV decrease in the potential of P.[93]

4.1.3 Influence of the hydrophobic mismatch on the position of the dimer and on the light-induced conformational changes

The position of the Q_Y band of P in the light-minus-dark spectra showed a different sensitivity to the head-group charge when the BRCs were in detergent micelles (Figure 4.3) compared to liposomes (Figure 4.4). For BRCs dispersed in detergent micelles, the charge of the head-group induced a shift in the P-band position not only in BRCs from *Rb. capsulatus* but also in *Rb. sphaeroides*, converting one spectral form of P to another (Figure 4.3).[25,138] The shift was primarily induced by a positively charged (both in *Rb. capsulatus* and in *Rb. sphaeroides*) or zwitterionic (*Rb. capsulatus* only) detergent. Interestingly, this shift was not detected in BRCs from *Rb. capsulatus* that were reconstituted into liposomes with various head-group charges provided the mono-unsaturated fatty acid chain length was C_{18} for which P was in its long-wavelength form as also found in the natural membranes (Figure 4.4 A-C).

Contrarily to the findings in detergents, exposing these BRCs to light did not shift the position of the P band in the zwitterionic DOPC (Figures 4.3C and 4.4C). It was reported earlier that various negatively charged membrane lipids in *Rb. sphaeroides* do not alter the position of the P band if the fatty acid chain lengths are C_{16} or C_{18}.[91] Therefore, it was not expected that the spectrum recorded in the negatively charged DOPS would show any shift in the dimer position, and it is in agreement with the observation obtained in the negatively charged detergent, DOC (Figures 4.3A and 4.4A). In DOTAP liposomes only a tiny fraction (7%) of the BRCs experienced the light-induced hypsochromic shift. However, if we used a shorter lipid (DLPC) with a zwitterionic head-group, a 4 nm blue shift of the P-band was observed even in the dark, which was shifted even further upon prolonged illumination corresponding to 27% of P being converted to its short-wavelength form upon illumination (Figure 4.4D). This fraction is in a reasonable agreement with the amplitude of the long-lived component in the recovery kinetics (Figure 4.4). All other spectral and kinetic features of the light-induced structural changes near P were present in all liposomes, namely the decrease of the electrochromic absorption changes of the B bands and the long-lived charge-separated state.

On the basis of neutron diffraction studies of detergent-grown BRC crystals, the thickness of the detergent belt for LDAO and β-octyl-glucoside micelles is only ~ 23 Å, whereas the thickness of the detergent phase along the transmembrane α-helices of the L and M subunits is ~ 30 Å (Figure 4.6A).[28,72] This difference provides a significant hydrophobic mismatch, which should be compensated for not only by the detergent but also by the protein (Section 1.5).[36]

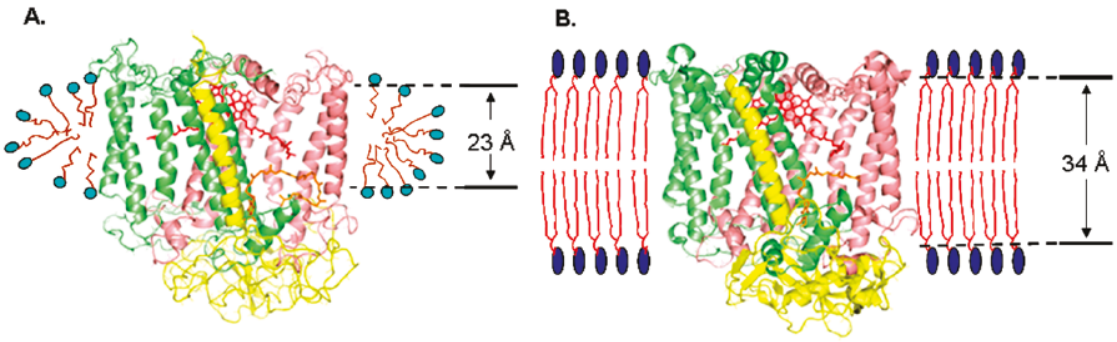

Figure 4.6 Schematic cartoon representation of the BRC in a LDAO detergent micelle **(A)** and in a lipid bilayer with oleoyl fatty acid chains **(B)**. The L, M, and H subunits are labeled with salmon, green, and yellow colors, respectively. The bacteriochlorophyll dimer (P) and the primary quinone (Q_A) are also shown as red and orange sticks, respectively. The differences in the hydrophobic thicknesses between the BRC and the lipid bilayer or detergent belt are shown, and this difference is proposed to alter the electronic structure of P and thus shift the position of the P-band. The coordinates for the BRCs were taken from PDB entry codes 1YST (A) and 1OGV (B).[34,72] The lipids and detergents are not shown as precise molecular structures but rather drawn only as schematic representations. The hydrophobic thicknesses of the detergent belt and the lipid bilayer were taken from refs 28 and 34, respectively.

In the natural membrane environment, from an energetics point of view, it is expected that the hydrophobic thickness are matched; however, there are examples that do not match.[144] For example, in eukaryotic cells the plasma membrane is thicker than the membranes of the endoplasmic reticulum; nonetheless, the proteins found in the plasma membrane are initially integrated in the endoplasmic reticulum.[144] Furthermore, the composition of the natural membrane is not unique in different photosynthetic bacteria.[145] Even within the same strain, for example changes in growth conditions can alter the membrane composition in *Rb. sphaeroides*.[27]

Among the natural lipids the monounsaturated phospholipids are very common in the natural membrane and the thickness of the dioleoyl (C_{18}) fatty acid chain was calculated to be also 30 Å, the same as the length of the α-helices reported in *Rb. sphaeroides*.[28,38] The hydrophobic thickness of the DLPC bilayer in its liquid crystalline and gel phases was reported to be only 19.5 and 27.0 Å, respectively.[38] It is expected that in part of the compensation for the hydrophobic mismatch the phase transition temperature of saturated DLPC at the interface is shifted from ~ 0 °C toward room temperature values. Even if the shift is dramatic, it still cannot match the ~ 30 Å thickness of the hydrophobic length of the transmembrane helices. It was suggested that membrane proteins can compensate for the hydrophobic mismatch by tilting their transmembrane α-helices to reduce their effective thickness or adjust their hydrophobic length by changing the orientation of both the hydrophobic and hydrophilic side chains near the interface (Section 1.5).[144] Recently, the crystal structure of *Rb. sphaeroides* was resolved in a lipidic cubic phase using also mono-unsaturated oleoyl lipids with C_{18} fatty acid chain lengths.[34] Comparison with eight detergent-based structures revealed that the 2-fold symmetry axis passing through P and the non-heme Fe^{2+} is slightly tilted relative to the plane of the membrane, and the crystal contacts were structurally perturbed in the various structures by interactions with the surrounding detergent and lipid molecules. The crystal contacts along the symmetry axis were reported to be mediated by interactions between the periplasmic regions of the L and M subunits not far from P. In the lipid-based structure the membrane was clearly identifiable with a hydrophobic thickness of 34 Å, which is in a reasonable agreement with the predicted value for the thickness of the lipid bilayer and 10 Å larger than the thickness of the detergent belt (Figure 4.6B).[27,38,28]

As mentioned above, the orientation of the 2-acetyl groups of P, which primarily influence the position of the P-band, can systematically be altered by the local electrostatics if hydrophobic residues near P are replaced with charged ones or the nature of the detergent is altered.[45,76] Besides the membrane lipids three integral lipid molecules were identified in one of the detergent-based structures in *Rb. sphaeroides* that most likely influence the rate of the electron transfer and contribute to the energetics of the unidirectional charge separation in the reaction center (Section 1.3).[21] Of these three lipids cardiolipin was also resolved in the lipid-based structure.[34] Even though the polar head-group of the cardiolipin is over 15 Å away from the closest cofactor, it is largely exposed and stabilized primarily by electrostatic interactions with Arg M267, His M145, and several water molecules. The cardiolipin was also proposed to be in contact with the membrane exposed surfaces of the H and M subunits.[146] Thus, the influence of cardiolipin would most likely be different in BRCs isolated in detergents and in liposomes as it interacts with different hydrophobic chains.

4.2 Reversible shifts of the P-band in the presence of secondary electron donors

The possibility of inducing a shift of the P-band reversibly during illumination in BRCs that were dispersed in LDAO was also investigated. For this purpose, a secondary electron donor, 2, 3, 5, 6-tetramethyl-p-phenylenediamine (DAD), was added to strictly dark-adapted samples.

After illumination, the secondary donor reduces P^+ and the measured spectra are characteristic only of the reduced quinone. Such spectra feature an electrochromic red shift of the H-band due to the negative charge on the nearby quinone and a much smaller electrochromic blue shift of the P-band.[147] The influence of the negative charge on the shift of the P-band is very small given the almost 3 times larger distance between Q_A and P compared to the distance between Q_A and H. The requirement for an efficient secondary electron donor is that the electron donation should be faster than the charge recombination as these two processes are parallel reactions. The electron donation time of various, routinely used secondary donors spans over 3 orders of magnitude in time. The native secondary donor, cytochrome c_2, donates an electron to P^+ in one or a few microseconds depending on whether it was already bound to the BRC or it must diffuse to the binding site.[148] Ferrocene donates an electron to P^+ in ~ 250 μs in reaction centers from *Rb. sphaeroides*.[149] DAD is the slowest among the routinely used secondary donors with a donation time of >1 ms.[150] This is still about 100-fold faster than the charge recombination and qualifies DAD as a sufficient secondary donor.

For strictly dark-adapted BRCs after addition of DAD, the light-minus-dark difference spectrum has a pronounced electrochromic shift of the P-band that is strongly dependent upon pH (Figure 4.7A, solid lines). The amplitude of the electrochromic shift was very small at pH 6 and reached its maximum value at pH 8 with a slight decrease at higher pH values (Figure 4.7B, closed symbols). This electrochromic shift corresponds to the shift of the P band from 863 to 855 nm in a varying fraction of the BRCs.

Once the spectral features fully recovered several minutes after illumination, subsequent illuminations resulted in almost the same spectra with slightly smaller amplitudes of the electrochromic shifts on the P-band but without any decrease of the electrochromic shift of the H-band. However, if the BRCs were pre-exposed to illumination prior to the addition of DAD, the large electrochromic shift of the P-band was completely missing and the pronounced pH dependence was also lost (Figure 4.7A, dashed lines; Figure 4.7B, open symbols). Pre-illumination on the other hand did not influence the electrochromic shifts of the H-band (Figure 4.7A).

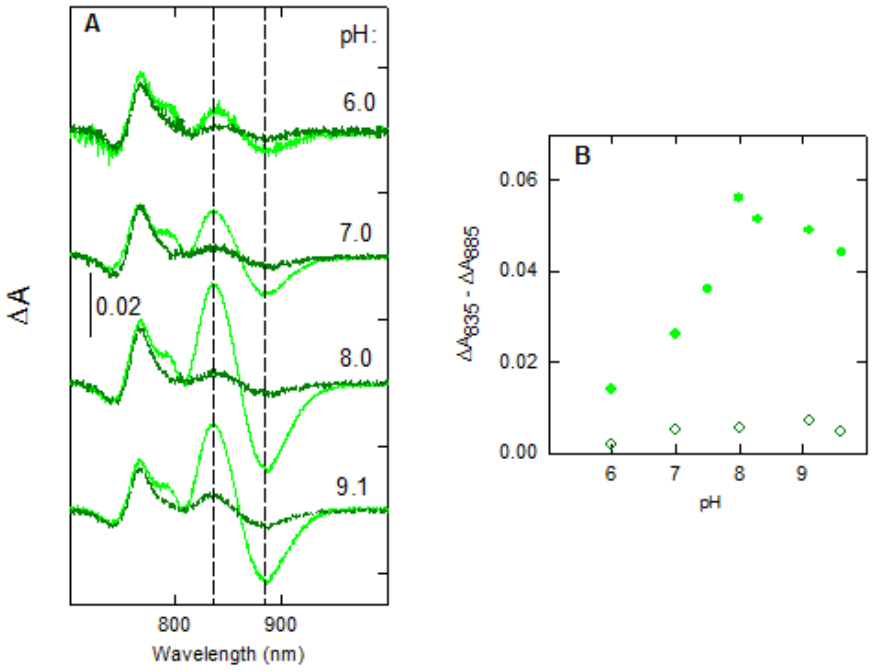

Figure 4.7 (A) Light-minus-dark difference optical spectra of the BRCs in the presence of a secondary donor (DAD) in the dark-adapted (thick solid pale green lines) and pre-illuminated samples (thin solid dark green lines) at the pH values of 6.0, 7.0, 8.0, and 9.1. In the pre-illuminated samples the DAD was added after 10 min dark adaptation. Conditions as in Figure 4.1 except +500 μM DAD. **(B)** pH dependence of the peak-to-trough difference of the shift of the P-band measured at 885 and 835 nm in dark-adapted (closed pale green symbols) and pre-illuminated samples (open dark green symbols).

After illumination, the electrochromic shift of the P-band recovered with biphasic recovery kinetics (Figure 4.8). Kinetic traces were recorded at the maximum values of the spectral changes, namely at 885 and 835 nm (Figure 4.7). For both wavelengths, the recovery had dominant amplitude (87-88%) with a rate constant of (1.2-1.4) × 10^{-1} s^{-1} with the remaining 12-13% component having a rate constant of (1.1-1.5) × 10^{-3} s^{-1}. In the pre-illuminated samples the rate constants were similar but the relative amplitudes differed as 75% recovered with a rate constant of ~ 10^{-1} s^{-1} and 25% with a rate constant of ~ 10^{-3} s^{-1}. Using cytochrome *c* as a secondary donor, the large electrochromic shift of the P-band was not observed, and the recorded spectra were similar to those obtained for the pre-illuminated samples (data not shown). It is not clear whether this is due to electrostatic interactions associated with the docking of the cytochrome or the nearly 3 orders of magnitude faster electron donation time for cytochrome *c* compared to DAD. Using ferrocene, which also donates an electron in a second order process like DAD, intermediate size electrochromic shifts were observed in the P-band, indicating that P^+ should be present for at least a submillisecond time scale to build up the large electrochromic shifts. It should also be mentioned that in the presence of terbutryn, an inhibitor of electron transfer to Q_B, the large electrochromic shifts are not observed, even in dark-adapted samples, but in the presence of a different inhibitor, stigmatellin, the shifts were observed (data not shown).

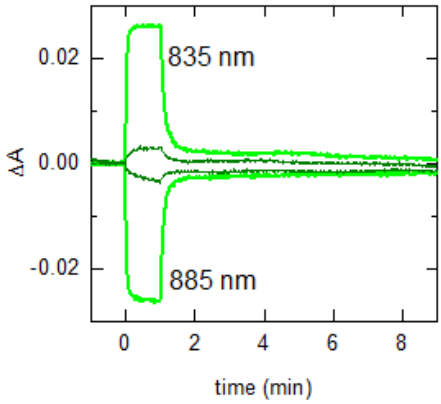

Figure 4.8 Kinetics of the light-induced absorption changes in the presence of DAD as a secondary electron donor in dark-adapted (thick solid pale green lines) and in pre-illuminated (thin solid dark green lines) BRCs. The traces were measured at the maximum values (885 and 835 nm, see Figure 4.7) of the spectral signatures associated with the blue shift of the P-band. Conditions as in Figure 4.7.

In the presence of the secondary electron donor (DAD) the major kinetic component of the recovery associated with the shift of the P-band has a very similar rate constant (~ 10^{-1} s^{-1}) that was assigned to the recovery of P^+ in BRCs with conformational changes only near the quinones due to the use of short light exposure (Figure 4.8) [Chapter 3]. In mutants of BRCs from *Rb. sphaeroides*, where the conformational changes were blocked near P due to the presence of the H-bond between the 9-keto carbonyl group of P_L and the introduced His residue at the L131 position, the rate constant of the recovery after prolonged illumination was also ~ 10^{-1} s^{-1}.

4.2.1 Donor-acceptor interactions

In the presence of a secondary electron donor the Q_A^-/Q_A difference spectrum can be detected during the illumination.[147] A small electrochromic shift of the P band has been routinely observed in BRCs from both *Rb. capsulatus* and *Rb. sphaeroides* and modeled as arising due to a long-range (28 Å) electrostatic interaction between these two cofactors.[147] The large electrochromic shifts reported here (Figure 4.8) have not been observed before. The question arises as to whether these large electrochromic shifts in the P-band are due to strengthened interactions with the quinone during illumination in dark-adapted LDAO-dispersed BRCs. There have been several reports in the literature that suggest stronger interactions between the periplasmic and the cytoplasmic side of the BRCs in *Rb. capsulatus* than in *Rb. sphaeroides*. In WT BRCs from *Rb. capsulatus* and the R-26 strain of *Rb. sphaeroides*, fractional proton uptake and release upon charge-separation has been observed and associated with changes in the pK_a values of the nearby protonatable side chains due to the transient charges on Q_A and P, respectively.[113,121] Amino acid replacements near Q_A at the M246 and M247 positions in BRCs from *Rb. capsulatus* resulted in changes not only in the flash induced proton uptake but also in the proton release.[151] The larger proton release in these mutants was interpreted as being due to a long-range electrostatic interaction between the Q_A binding site and residues near the periplasmic side. The light-induced conformational switch from the long-wavelength form to the short-wavelength form of P was blocked by terbutryn in our experiments but was allowed with the use of stigmatellin even though there was only about 10% Q_B activity in our samples.

The addition of these inhibitors did not prevent the formation of the long-lived charge-separated state and the decreased electrochromic changes in the B-bands during illumination but altered the lifetime of the light-induced state by about a factor of 2 (Figure 4.2). In chromatophores of *Rb. capsulatus*, the binding of various inhibitors that block the electron transfer between Q_A^- and Q_B have been reported to alter the redox potential of P by as much as ~ 50 mV depending on the redox state of Q_A and the identity of the inhibitor.[152] This suggests that only one element of the conformational change was turned on and off by the inhibitors, by the pre-illumination of the samples, or by the selection of the detergent.

The effect of the presence or absence of Q_B on the light-induced conformational changes in *Rb. sphaeroides* is not clear. One group has found no difference,[35] another reported significant differences whether Q_B was present or not,[65] while a third group found only differences at high pH values[57]. These groups used different detergents to disperse the BRCs and also different inhibitors to block the electron transfer to Q_B. Terbutryn and stigmatellin were reported to bind to slightly different positions in the Q_B binding pocket.[153-155] Without any inhibitor the Q_B binding pocket can either be empty or occupied by a distal or a proximal Q_B. In our case without the inhibitors the site has only ~ 10 % Q_B occupancy. When stigmatellin is added, it binds to the proximal position whereas terbutryn binds to a more distal position. Since the observed shifts in the P-band were only seen in dark-adapted samples if this shift is coupled to donor-acceptor interactions, it is most likely disrupted by terbutryn that occupies the place of the dark-adapted quinone and thus prevents the switch to a conformation that would move the quinone to the proximal position.

A coupling between the shift of the 2-acetyl group(s) of P and the distal to proximal repositioning of Q_B upon illumination of the dark-adapted samples is supported by our results. Kinetically resolved electrochromic and electrogenic measurements associated with the reduction of the quinones demonstrated the mobility of this region of the protein.[51-53] These structural changes happen even if Q_B is not present and were associated with the structural changes that eventually facilitate the electron transfer between the quinones. The kinetics of these changes were reported to be in the hundreds of microseconds time scale, a good match to the kinetic limit for the shift of the P-band observed in the present study with the use of different secondary donors with a wide range of donation times. One might assume that the difference in the hydrophobicity of the applied secondary electron donors could also have some influence on the local electrostatics and thus on the shift of the P-band. Both DAD and ferrocene are neutral and sparingly soluble in water and can be expected to partition into a non-aqueous environment within the BRC-detergent complex. Upon oxidation they could create a local cation analogous to the CTAB head-group effect. The use of the water-soluble cytochrome *c* should not have this effect. Unlike in *Rb. capsulatus* the use of the same external electron donors in BRCs from *Rb. sphaeroides* did not result in large shifts of the P-band.[147] Thus, we assume that the local electrostatic interactions with the oxidized forms of the secondary donors do not contribute to the large spectral features observed in LDAO.

The pH dependence of the electrochromic shifts (Figure 4.7B) complements the pH dependence of the proton release reported in chapter 3 for BRCs from *Rb. sphaeroides* upon continuous illumination.[57]

At pH 6, where a large proton release was observed, a negligible shift of the P-band was detected (or more precisely, the shift was observed only in a very small fraction of the BRCs). At pH 8, where the proton release is reported to be the smallest the electrochromic signals associated with the shift of the P-band were the largest (Figure 4.7). This indicates that the effect arises from the combination of various electrostatic interactions that participate in the solvation of the charges.

4.3 Potential of the P/P^+ couple in the light-induced states

Similar to earlier redox measurements done in chapter 3 the P/P^+ oxidation/reduction midpoint potential was measured for BRCs from *Rb. capsulatus* in TX-100 and DOC using spectroelectrochemical titrations (Figure 4.9). Without any external illumination the data were well described using the Nernst equation assuming only one population of P, yielding midpoint potentials (E_m) of 500 and 480 mV in TX-100 and DOC, respectively. Under these conditions, the peak position of the P-band was at 865 and 870 nm for TX-100 and DOC, respectively (Figure 4.1). The error is estimated to be ± 5 mV based upon the results obtained from different titrations in the dark.

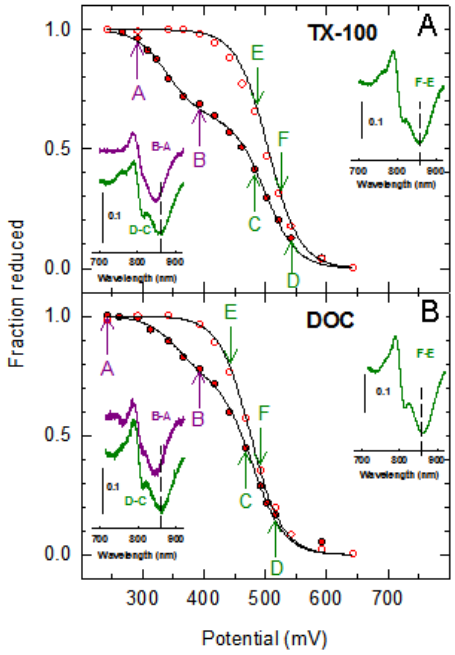

Figure 4.9 Spectroelectrochemical redox titrations of the BRCs in the absence (open red circles) and in the presence (closed red circles) of a weak external illumination in TX-100 and DOC. The data were fitted with a standard Nernst equation assuming one (in the dark) or two (in the presence of illumination) components. The fit yielded the following values for the P/P^+ potentials: TX-100: 500 mV (100%) in the dark and 500 mV (60%) and 340 mV (40%) in the presence of illumination; in DOC: 480 mV (100%) in the dark and 480 mV (75%) and 360 mV (25%) in the presence of illumination. The inserts show the difference spectra between two absolute spectra recorded at two different applied potentials in the appropriate range indicated by the arrows and letters from A to F with respective color code (green for the dark-adapted and maroon for the light-adapted state). The vertical dashed lines in the insets are drawn at 865 nm. Note the shifted P-band positions and the decreased electrochromic shifts in the spectra of the light-induced conformations. Conditions ~ 300 µM BRC, 70 mM KCl, 1 mM EDTA, 0.05% TX-100 or 0.05% DOC.

The dependence of the fraction reduced on the potential required the use of a two-component Nernst equation assuming two populations of P with different E_m values as previously found for BRCs from *Rb. sphaeroides* (Chapter 3).

One population represents the BRCs that are in the dark-adapted conformation, and another fraction is characteristic of the light-adapted conformation. While the potentials of the fractions with an unchanged P-band position did not change, those with blue shifted P-band positions exhibited much lower P/P^+ potentials with values of 340 and 360 mV in TX-100 and DOC, respectively. These decreases of the E_m value in BRCs from *Rb. capsulatus* are about twice as large as the values of the decreases reported in *Rb. sphaeroides* where the P-band position remained at 865 nm even in the light-adapted conformation (Chapter 3). Unlike in *Rb. sphaeroides*, prolonged illumination of BRCs from *Rb. capsulatus* results in the position of the P-band shifting in one fraction of the BRCs to 850 nm in TX-100 and DOC in addition to the decrease of the electrochromic shifts of the B-bands (see insets in Figure 4.9). The spectroelectrochemical redox titrations could not be performed for BRCs in LDAO due to an undermined but earlier reported interaction between the LDAO and the electrodes.[93] Also, measurements could not be performed in CTAB due to instability of the samples.

The orientations of the acetyl groups are proposed to influence the position of the P-band and the potential of P in the light-adapted conformation (Figure 4.9). Previously, the rotation of the acetyl group during light-induced conformational changes had been proposed in *Rb. sphaeroides*, but a shift of the P band was not observed for those BRCs (Chapter 3). It appears that only certain orientations cause the shift of the P-band. The possible influence of different orientations of the 2-acetyl groups of P_L in BRCs from different organisms on the P-band position is supported by FT Raman investigations as the vibrational frequencies of the H-bonded acetyl groups of P_L show small but significant variations when comparing *Rb. sphaeroides* and *Rb. capsulatus*.[77]

A similar two-state conformational model was proposed for a mutant reaction center from *Rb. capsulatus* for which amino acid residues M205 to M210 were replaced with the corresponding L subunit residues.[137] In this mutant the shift of the P-band was even more pronounced, from 853 to 820 nm, and the potential of the P/P^+ couple (in the dark) increased by ~ 50 mV. Similar changes were observed in a mutant of *Rb. sphaeroides* containing the replacement of Tyr M210 with Trp.[117] In *Rb. sphaeroides* the phenol group of Tyr M210 is within H-bonding distance to the 2-acetyl group of P_M and its possible involvement in the conformational change was proposed as a potential source for the light-induced rotation of the 2-acetyl group of P_M.[3,6,126,] The residue Tyr M210 is conserved in *Rb. capsulatus* and is likely to be at a comparable distance to the 2-acetyl group of P_M. Two amino acid residues near P, Phe M208, which is ~ 3 Å away from Tyr M210, and Val M192, which is ~ 10 Å from P, are Ala and Asp in BRCs from *Rb. capsulatus*.[126] Given the closeness of Phe M208 to Tyr M210, the difference between Phe and Ala might influence the rotational freedom of the 2-acetyl group of P. The light-induced decrease of the P/P^+ potential was measured to range from 55 to 79 mV in *Rb. sphaeroides* depending upon the pH (Chapter 3), while in *Rb. capsulatus* the decrease was twice as large at pH 8 (Figure 4.9) as discussed below.

The 500 mV E_m value from BRCs from *Rb. capsulatus* without external illumination is, within error, the same as the E_m value of 505 mV determined for *Rb. sphaeroides* under the same conditions.[93] The slight decrease of 20 mV in the potential for BRCs in DOC is attributed to an electrostatic stabilization of P^+ by the negatively charged detergent head-groups compared to the neutral head-groups in TX-100.

Such electrostatic stabilization of P^+ can be observed in TX-100 at higher pH values where many amino acid side chains become deprotonated.[113,114] The decrease of the P/P^+ potential in the light-adapted conformation was ~ 120-160 mV in BRCs from *Rb. capsulatus* depending on the detergent, where the position of the P-band in this population was found centered at 850 nm (Figure 4.9). In BRCs from *Rb. sphaeroides*, where the P-band position remained at 865 nm even in the light-induced conformation, the decrease of the potential was only 75 mV under the same conditions (Chapter 3). Since the dark-adapted conformations resulted in very similar potentials for the two species with the P-band position at ~ 865 nm, we conclude that the differences in the potentials in the light-adapted conformations are associated with the shift in the P-band position from 865-870 to 850 nm and arising from different orientations of the acetyl groups of P. Even though the decrease of the potential in the light-adapted conformation in TX-100 is about twice as large if the band position is shifted to 850 nm than if it remains at 865 nm after 1 min illumination, the trend in the recovery rates was found to be the opposite. The rate constants were found to be about twice as large in BRCs with P-band position at 850 nm than in those with the P-band at 865 nm, indicating that the recovery from the light-induced conformation is not electron transfer limited.

These results revealed that the conformations of the dimer in the isolated BRCs of *Rb. sphaeroides* and *Rb. capsulatus* in zwitterionic LDAO micelles are essentially the same in the dark-adapted samples as indicated by the identical wavelength of the dimer band at 865 nm. The same position is measured for BRCs in their native membrane environments and in liposomes with long (C_{18}) hydrophobic chain lengths.

The band is blue shifted in *Rb. capsulatus*, but not in *Rb. sphaeroides*, for BRCs in zwitterionic detergent micelles and liposomes with short hydrophobic chains upon illumination. The P-band for BRCs from *Rb. capsulatus* was observed at 850 nm and thought to be irreversible, but these results show that the two spectral forms of P can interconvert with the proper selection of detergent or lipid and also by using light as a switch. The two optical states also have different redox potentials and lifetimes of the charge-separated state in addition to the previously reported differences in the distribution of the unpaired electron of P^+.

The electronic state of P is very sensitive to the properties of the lipids and detergents that surround the protein and demonstrates the utility of the BRC as a model system for membrane proteins. Alteration of the native lipid environment has a significant effect on P, including the energetics of the excited and oxidized states that are critical for the function. In addition to the previously identified influence of electrostatic interactions, hydrophobic interactions have a critical role in establishing the properties of P. In particular, the hydrophobic mismatch between the thickness of the detergent micelle and the length of the transmembrane helices is most likely responsible for the reported functional differences of the BRC in detergent micelles, liposomes, and natural membranes.[62,151,156] These effects are expected to be general for all integral membrane proteins, in particular the properties of the primary electron donor of PS II.

Chapter 5

Optimization of light-induced conformational changes to stabilize charge-separated state by lipid binding and phase transition of the membrane lipids

The results in this chapter are based on the following published paper:

Deshmukh, S. S., Tang, K., and Kálmán, L. (2011) Lipid binding to the carotenoid binding site in photosynthetic reaction centers. *J. Am. Chem. Soc. 133*, 16309-16316.

Author contributions:

S. S. Deshmukh performed the experiments, analyzed the data, and contributed to writing the paper. K. Tang performed preliminary experiment in DLPC liposome (data not included). L. Kálmán designed the research, guided the data analysis, and wrote the paper.

As discussed in chapter 3 and 4, the generation of a long-lived charge-separated state can be achieved by a single enzyme with the transfer of only one electron. The BRC from purple photosynthetic bacteria has been used widely as a structural and functional model for examining the general principles of biological electron transfer for decades.[112] It has also played an important role in the design and construction of artificial photosynthetic complexes.[157,158] As mentioned in the chapter 1 the WT BRC also incorporates a tightly bound carotenoid molecule in the close vicinity of the inactive bacteriochlorophyll monomer (B_M) that is responsible for photoprotection of the BRC (Figure 5.1). This binding site was successfully reconstituted earlier with various carotenoids, and as demonstrated in Figure 5.1, detergent molecules, such as LDAO or octyl β-glucoside (BOG) were also reported to bind to this site in the carotenoid-less mutant, R-26.[81,159,160]

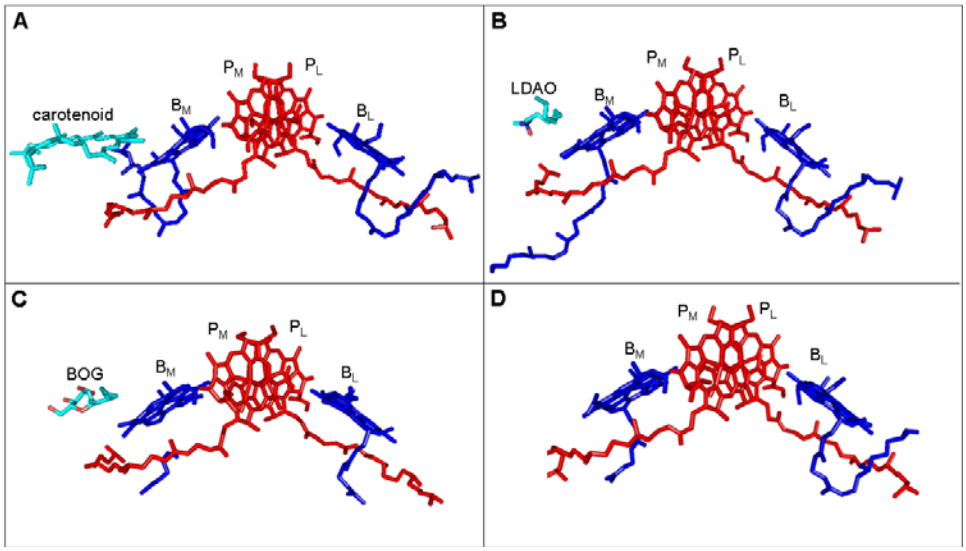

Figure 5.1 Structural view of the four bacteriochlorophylls constituting two halves of the dimer in red (P_L and P_M) and the monomers in blue (B_L and B_M) with the bound molecules near B_M. The bound molecules are color-coded by their atoms: carbon (cyan), nitrogen (blue), and oxygen (red). The site near B_M is shown occupied by a carotenoid (A), an LDAO (B), and an octyl β-glucoside (BOG) (C), molecule. The empty pocket is also shown (D). Coordinates were taken from the following PDB entry codes for each panel: (A) 1PCR, (B) 1RG5, (C) 4RCR, and (D) 1OGV.

We have demonstrated (in chapter 3 and 4) that the lifetime of the $P^+Q_A^-$ charge-pair can be increased from 100 ms to 16 min by the combination of systematic alteration of the environment of the charges and light-induced structural changes near P in BRCs from both *Rb. sphaeroides* and *Rb. capsulatus*. In this work we combine lipid binding to the carotenoid binding site near B_M and replacement of the detergent micelles with liposomes to increase the lifetime of the $P^+Q_A^-$ state even further to hours in the R-26 strain. Although the BRC is arguably the most studied integral membrane protein, very little is known about how individual lipid molecules influence the function of the protein. As mentioned earlier high resolution X-ray structures identified three integral lipid molecules (Figure 1.5), but a definite functional role could not be assigned to them unambiguously.[21,146] In this chapter we report the effects of lipid binding near B_M on the light-induced structural changes.

5.1 Influence of added lipids on lifetime of the $P^+Q_A^-$ state after prolonged illumination

The BRCs from anaerobically grown WT and R-26 strains dispersed in TX-100 detergent micelles were illuminated in the presence and absence of various lipids, and the kinetics of absorption changes after prolonged, sub-saturating illumination was monitored at the center of the P-band at 865 nm at pH 7. Figure 5.2 shows these recovery kinetic traces recorded at two different temperatures: 22 °C (panel A) and 8 °C (panel B).

The illumination time was selected at both temperatures to meet the following criteria: (i) saturation of the signals in all samples before the illumination was terminated, (ii) fully recovering absorption changes at 865 nm, and (iii) maximizing the lifetime of the charge-separated state.

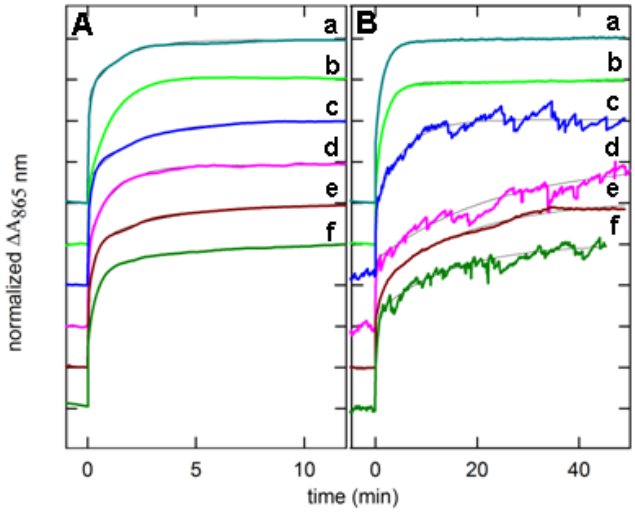

Figure 5.2 Kinetics of light-induced absorption changes at (A) 22 °C and (B) 8 °C, measured at the center of the Q_Y absorption band of P after the illumination was turned off. The following samples were used: (a) R-26 (dark cyan), (b) R-26 + DOPC (green), (c) R-26 + DMPC (blue), (d) R-26 + DLPC (pink), (e) WT (dark brown), and (f) WT + DLPC (dark green). The illumination time was 5 and 20 min for panels A and B, respectively. The traces were normalized to the maximum absorbance changes at time = 0 and were shifted vertically for clarity. Thin solid lines are the best fits to the curves. The results of the fits are tabulated in Table C1 (Appendix C). Conditions: 1 μM BRCs, 15 mM Bis-tris-propane, pH 7.0, 1 mM EDTA, and 0.05% TX-100.

The complex recovery kinetics after the illumination indicates that long-lived, conformationally altered forms of the $P^+Q_A^-$ charge-pair were formed in fractions of the BRCs besides the unresolved (in the minute scale) transient changes as reported earlier in chapter 3, 4 and also by many other studies.[35,56,57,65]

At 22 °C, the overall recovery kinetics was faster in the R-26 (trace a in dark cyan) than in WT (trace e in dark brown), and the fraction of BRCs that underwent light-induced structural changes was also smaller in R-26 than in WT. A similar observation was made for semi-aerobically grown WT and R-26 (Figure C1 in Appendix C). Rate constants and relative amplitudes for the slower kinetic components for the anaerobically grown samples are tabulated in Table C1 (Appendix C). In R-26 only the component with a rate constant of ~ 10^{-2} s^{-1} was detected, while in WT an additional, slower component with a rate constant of ~ 10^{-3} s^{-1} was also observed in a small fraction of BRCs. These long-lived kinetic components were identified in chapter 3 and 4 in BRCs from semiaerobically grown WT from *Rb. sphaeroides* and *Rb. capsulatus* as arising from conformational changes near P. The chosen lipids all had the same zwitterionic phosphocholine (PC) head-group with zero net charge at the selected pH to avoid electrostatic perturbations in the BRCs. The length of the fatty acid chain and the saturation level was altered by using dilauroyl (12 carbon atoms long chain with zero double bonds, C12:0), dimyristoyl (C14:0), and dioleoyl (C18:1) chains in DLPC, DMPC, and DOPC, respectively. Addition of lipids at 22 °C had only a minor effect on the kinetics in R-26, except for DMPC, and had practically no effect at all in WT (Figure 5.2A). In the presence of DMPC (trace c in blue), a slight increase of the lifetime was observed. At 8 °C the difference between the recovery kinetics in R-26 (trace a in dark cyan) and in WT (trace e in dark brown) became even more pronounced and the influence of the lipids altered the lifetime of the charge-pair very differently in R-26. The presence of DOPC (trace b in green) did not induce any change but both DMPC (trace c in blue) and DLPC (trace d in pink) increased the lifetime of the $P^{+}Q_{A}^{-}$ state.

The effect was especially pronounced for DLPC where the recovery kinetics became unexpectedly longer in R-26 than in WT with rate constants of 7.0×10^{-4} s^{-1} and 1.1×10^{-3} s^{-1} for the slowest components in R-26+DLPC and in WT, respectively. It must be noted that the pronounced effect of the saturated lipids were observed only if the samples were cooled with a slow, 0.2 °C/min, rate. Unlike in R-26 the addition of DLPC did not induce any further change in the lifetimes for WT regardless of the cooling rate (trace f dark green).

5.1.1 Spectral signatures associated with bound carotenoid and lipid

Room-temperature light-minus-dark optical difference spectra of dark-adapted BRCs from WT and R-26 dispersed in TX-100 are expected to be similar in the near-infrared spectral region, as major differences are observed only in the 450-600 nm range due to absorption of the carotenoid in WT.[161] Figure 5.3 shows these absorption changes recorded in anaerobically grown WT and R-26 (panels A and B) and in R-26 in the presence of DLPC lipid at 22 °C (panel C) and at 8 °C (panel D).

Comparison of the presented spectra recorded immediately after the illumination started (solid lines) reveals that the extent of electrochromic absorption change of the B-band is considerably larger in WT (panel A), which binds a carotenoid molecule near B_M, than in the carotenoid-less R-26 (panel B). A similar trend can be observed in BRCs from semi-aerobically grown cells (Figure C2, Appendix C).

Although the presence of DLPC at room temperature did not alter the light-induced spectra of R-26 (panel C) at 8 °C, the extent of electrochromic absorption change of the B-band has increased significantly (panel D).

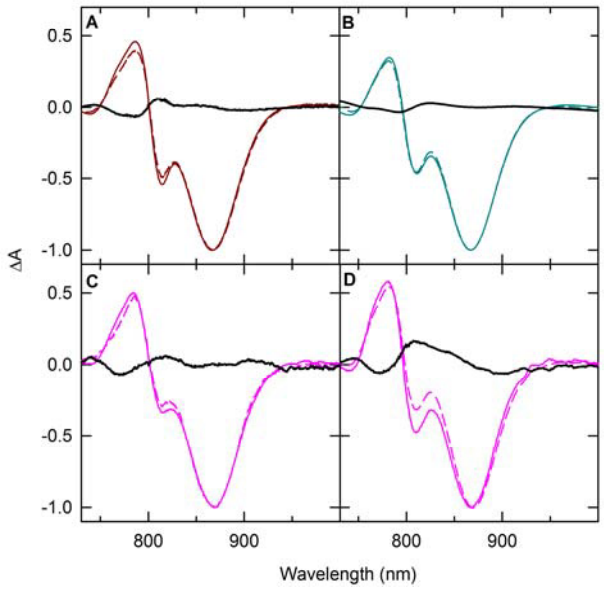

Figure 5.3 Normalized light-minus-dark difference optical spectra, recorded (thin solid line) immediately after the onset of the light and (dashed line) 1 min after the illumination was turned off, for BRCs isolated from anaerobically grown cells: (A) WT (brown spectra); (B) R-26 (dark cyan spectra); and R-26 + DLPC (pink spectra) at (C) 22 °C and (D) 8 °C. The thick solid lines (black) show the double difference spectra (dashed-minus-solid) and feature changes around 800 nm consistent with the decrease of electrochromic absorption changes involving the monomers during the illumination. Conditions were as described for Figure 5.2.

Figure 5.3 also shows the normalized spectra recorded immediately after the prolonged illumination was turned off (dashed lines).

While the spectra recorded at the beginning of the illumination are characteristic to dark-adapted reaction centers those collected after the prolonged illumination can be attributed to BRCs that underwent light-induced structural changes (Chapter 3).

The decrease of electrochromic absorption change of the B-band during the prolonged illumination was also much smaller in R-26 than in WT, as indicated by the double difference spectra (thick solid lines). The extent of prolonged light-induced electrochromic absorption changes of the B_M band was found to be a sensitive probe of the local electric field and of the light-induced structural changes near P in BRCs from both *Rb. sphaeroides* and *Rb. capsulatus* (Chapter 3 and 4). Corresponding to the smaller light-induced spectral changes in R-26, the amplitude of the long-lived $P^+Q_A^-$ state in the recovery kinetics recorded at 865 nm was also smaller in the carotenoid-less mutant without added lipids (see Figure 5.2A, traces a and e, and Figure C1 and Table C1 in Appendix C). In the presence of DLPC at room temperature, the prolonged illumination-induced decrease remained small but at 8 °C this decrease of the electrochromic absorption change of the B-band became very large.

Since the peak-to-trough amplitude of the electrochromic absorption change was sensitive to the presence or absence of the hydrophobic carotenoid molecule, growth conditions, and added lipids, this parameter was measured as a function of temperature in the 6-30 °C range in BRCs mostly dispersed in TX-100. Moreover, this spectral feature was found to be correlated with the local dielectric constant near B_M (Chapter 3).

As shown in Figure 5.4, the amplitude of this absorption change was large and was found, within error, to be independent of the temperature in both anaerobically and semi-aerobically grown WT and in anaerobically grown R-26 dispersed in relatively high (1%) concentrations of LDAO.

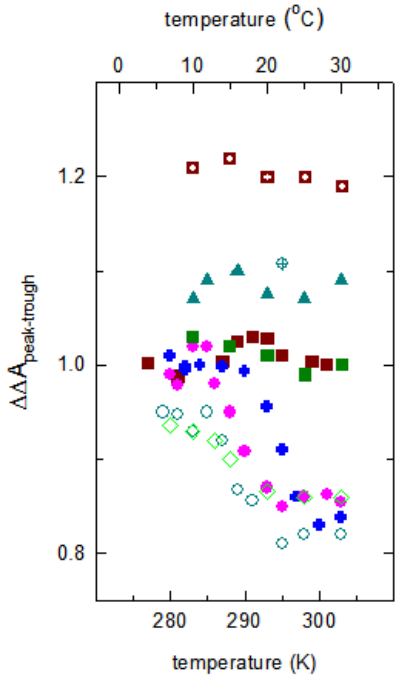

Figure 5.4 Temperature dependence of the peak-to-trough amplitude of the electrochromic absorption changes around 800 nm for BRCs isolated from anaerobically grown cells: (solid brown squares) WT, (solid dark green squares) WT + DLPC, (open dark cyan circles) R-26, (open green diamonds) R-26 + DOPC, (blue cross) R-26 + DMPC, (solid pink circles) R-26 + DLPC, and (solid dark cyan triangles) R-26 in 1% LDAO. For comparison, the same parameters in WT (brown crossed squares) and R-26 (dark cyan crossed circle) from semi-aerobic growth are also shown. The data were taken from light-minus-dark difference absorption spectra recorded immediately after the onset of illumination and normalized to the maximum of the P band. The error of the measurements is ± 0.02 absorbance unit. Conditions were as described for Figure 5.2 except for (solid dark cyan), where 0.05% TX-100 was replaced with 1% LDAO.

In general, the electrochromic absorption changes in BRCs from semi-aerobically grown cells were larger than those found in BRCs from anaerobically grown cells for both WT and R-26 in TX-100 (see Figure 5.3 and Figure C2 in Appendix C).

The presence of added DLPC did not change this value in WT. LDAO was specifically selected because an LDAO molecule was reported earlier to occupy the carotenoid binding site in R-26 for samples dispersed in LDAO detergent micelles (Figure 5.1C). In the presence of added DLPC and DMPC, the extent of electrochromic absorption change showed pronounced temperature dependence in anaerobically grown R-26. As the temperature was lowered, the initially small spectral changes in the 24-18 and 20-12 °C temperature ranges increased and then leveled off at lower temperatures in the presence of DMPC and DLPC, respectively. Interestingly, with decreasing temperature a moderate increase was also observed in the anaerobically grown R-26 even without added lipids, and DOPC also caused only moderate temperature dependence. The absorption changes in the presence of the saturated lipids were sensitive to the cooling rate as stated above.

5.1.2 Carotenoid binding pocket

The bound carotenoid in WT is located ~ 11 Å from P, and it is in van der Waals contact with B_M.[162] Its closeness to both B_M and P justifies the pronounced differences in both kinetics (Figure 5.2 and Figure C1 in Appendix C) and spectra (Figure 5.3 and Figure C2 in Appendix C) between WT and R-26. The B_M also has the single largest surface area contribution in the binding pocket.[159] Besides B_M, the pocket is composed of 29 mostly hydrophobic amino acids.

Both the natural and the reconstituted carotenoids bind to the same position, adopting the 15-15'-cis configuration. The carotenoids used for reconstitution, however, were in all-trans isomeric configuration upon addition, indicating that the isomerization must take place upon binding.[159]

The molecules to be bound to the pocket should enter only from the entrance with tail-in-first orientation since the other end was reported to be blocked by Phe M162, which serves as a gatekeeper.[159] The binding pocket is quite flexible, as significant differences in the tunnel shape and diameter were reported in the presence and absence of the carotenoid.[159] The much shorter LDAO molecule, with its chain length of 12 carbons, was reported to occupy the central portion of the pocket only 3.6 Å away from the acetyl group of B_M.

5.1.3 Dependence of binding on phase behavior of the lipid

Comparison of the recovery kinetics of WT and R-26 BRCs dispersed in detergent micelles suggests that the presence of the bound carotenoid molecule in WT provides a larger degree of stabilization than the empty binding site in R-26 for the $P^+Q_A^-$ charge-pair in the light-adapted conformation (Figure 5.2 and Figure C1 in Appendix C). Of the three lipids used in this study, addition of DMPC to R-26 BRCs increased the lifetime of the charge-separated state at both 22 and 8 °C; DLPC had the greatest influence but only at 8 °C; and DOPC did not provide any stabilization at either temperature (Figure 5.2). As none of the lipids induced any change in either the spectra or kinetics in WT, our results are consistent with binding of the lipids to the carotenoid binding site in their ordered but not in their disordered phase.

In the liquid crystalline phase the acyl chains are disordered, requiring more space than in the ordered phase, where the chains become parallel and fully extended.

The phase transition temperature of pure DMPC determined by light scattering measurements was reported as 24.7 °C, and the presence of the reaction center with a 4000:1 lipid:BRC ratio in liposomes caused it to shift to 27 ± 2 °C.[39,163] The same parameters for DLPC are 0 and 11 ± 3 °C, respectively.[39] In the presence of the BRC protein, the phase transition curves of these lipids were also reported to be broadened by 2.5-4 °C compared to the phase transition behavior of pure lipids. Due to these factors, the complete phase transition in the presence of the BRC protein was reported to occur at ~ 28-25 °C and at ~ 17-7 °C for DMPC and DLPC, respectively.[163] These reported ranges are in reasonable agreement with the temperature dependences of the electrochromic absorption changes of the B-bands that exhibited a pronounced increase in the ~ 24-18 °C range for DMPC and ~ 20-10 °C range for DLPC in mixed micelles (Figure 5.4). Besides the two main phases an intermediate phase, the ripple phase, was also observed in various saturated phospholipids upon phase transition.[164,165] The structure of the ripple phase for DLPC was found to be heavily dependent upon the cooling rate.[166] Slow cooling with rates between 0.1 and 1 °C/min favored the formation of a long ripple phase with higher degree of hydration than the short ripple phase obtained with rapid cooling (Figure 5.5). The lateral diffusion coefficients ($D_{P\beta}$') were reported to be dependent upon the hydration level with nearly 2 orders of magnitude slower values in the gel phase than in the liquid-crystalline phase.[167] The faster diffusion reported earlier in DLPC than in DMPC supports the longer lifetime caused by the presence of DLPC in this study (Figure 5.2).[168]

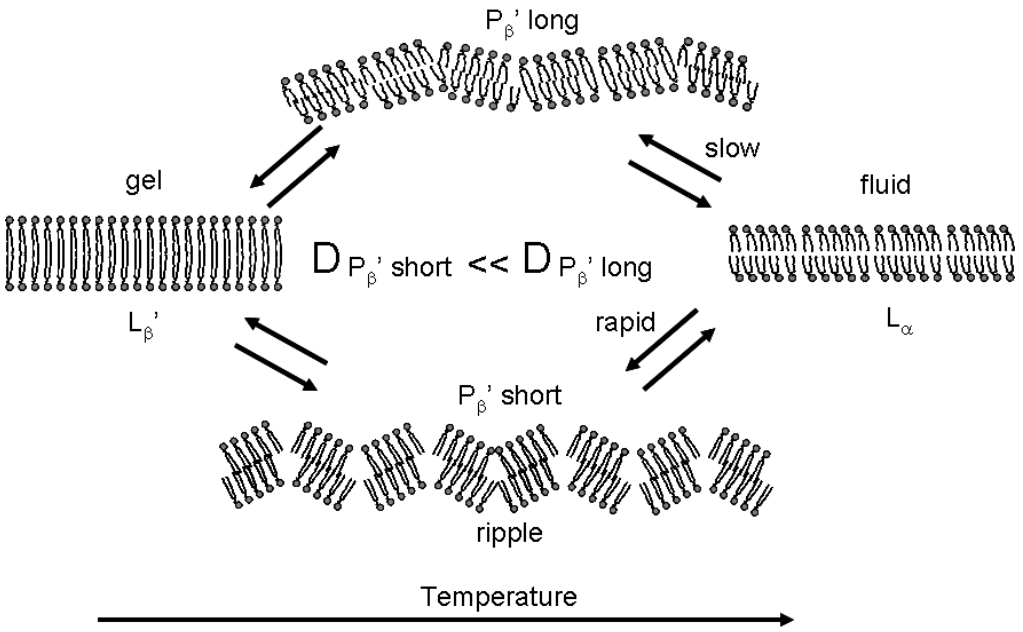

Figure 5.5 Schematic representation of the lipid membrane upon phase transition and the influence of cooling rate on the formation of the ripple phases.

The absence of any influence of DOPC on the recovery kinetics in the detergent-solubilized BRCs is consistent with the lack of binding of this lipid, as the phase transition temperature of DOPC (~ −20 °C) is well below the investigated temperature range. The lack of DOPC binding is also supported by the same temperature dependence of the electrochromic absorption change in the presence and absence of DOPC in R-26 (Figure 5.4).

5.1.4 Orientation of the acetyl group of B_M

A correlation between the orientation of the 2-acetyl group of B_M and the extent of the electrochromic absorption changes can be established by comparing structural details with our results presented in Figure 5.4.

Structural studies based on X-ray crystallography modeled the orientation of the acetyl group of B_M differently, depending on the occupation of the carotenoid binding site (Figure 5.6, Table 5.1). In all cases the acetyl group was assumed to be more or less in the plane of the tetrapyrrole macrocycle and thus, part of the conjugation. This is in agreement with earlier spectroscopic studies and our present results that detected no significant blue shift in the absorption band of B_M in the absolute optical spectra (Figure 5.3 and Figure C2 in Appendix C). When the site was occupied with a spheroidenone molecule in BRCs from semi-aerobically grown WT (Figure 5.6A), the oxygen atom of the acetyl group was modeled facing inward.[82,109,169,170] If, however, the site was occupied with spheroidene in WT (Figure 5.6B) from anaerobic growth, the oxygen of the acetyl group was modeled facing outward.[6,44,72] Corresponding to these orientations, the electrochromic absorption changes in the semi-aerobically grown WT were significantly larger than in WT from anaerobically grown cells. In both cases these changes were temperature-independent, suggesting that the rotation of the acetyl group is not favored if a carotenoid molecule occupies the binding site (Figure 5.4 and Figure C2 in Appendix C).

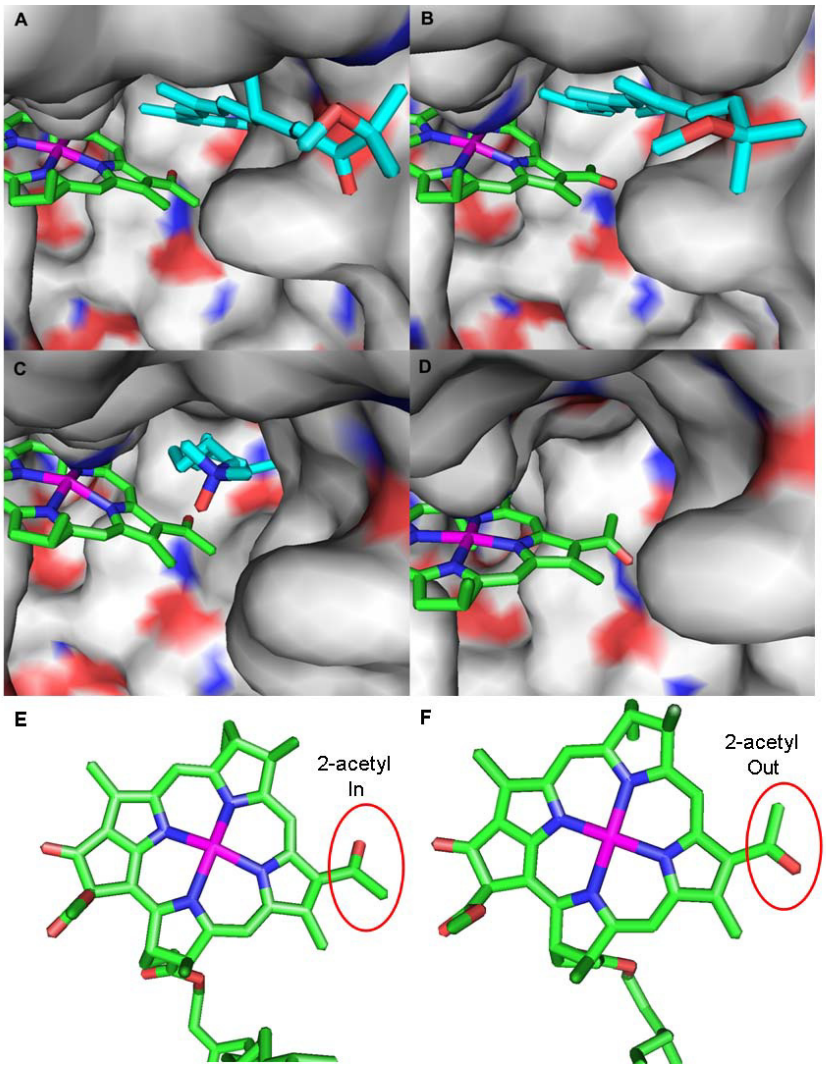

Figure 5.6 Surface representation of the carotenoid binding site near B_M as viewed from the entrance of the cavity that has access to the surrounding (A-D) and top view of B_M (E and F). Negatively charged regions are indicated with red, positively charged ones with blue, and neutral areas with gray. The B_M molecule is color-coded by its atoms: carbon (green), nitrogen (blue), oxygen (red), and the central Mg^{2+} (magenta). The hydrophobic chains of the bound molecules are indicated with cyan. The site is shown occupied by a spheroidenone (A), a spheroidene (B), and an LDAO (C), molecule. The empty pocket is also shown (D). Top view of B_M is shown with oxygen atom of 2-acetyl group oriented inside (E) and outside (F) as represented by red circle. Left (A, C, and E) and right (B, D, and F) panels show inward and outward orientations of oxygen atom of 2-acetyl group, respectively. Coordinates were taken from the following PDB entry codes for each panel: (A) 2GMR, (B) 1PCR, (C) 1RG5, (D) 1OGV, (E) 1PCR, and (F) 1RGN.

It must be noted that the inward orientation was proposed in all cases when the binding site was reconstituted in the carotenoid-less R-26 mutant with spheroidene or 3,4-dihydrospheroidene or when an LDAO molecule (Figure 5.6C, Table 5.1) was modeled to occupy this site.[159] In contrast, the opposite orientation was found when the binding site was empty (Figure 5.6D) in R-26 when the crystals were grown from a lipidic cubic phase.[34] The different levels measured for electrochromic absorption changes in TX-100 and in the presence of 1% LDAO for R-26 are consistent with the proposed rotation of the acetyl group from "out" to "in" upon binding of LDAO. Our results in LDAO also suggest that the acetyl group should be oriented inward in the semi-aerobically grown R-26. Since the electrochromic absorption changes are inversely proportional to the local dielectric constant around the interacting P and B_M molecules, these changes in WT are expected to be larger than in R-26 due to the presence of a hydrophobic carotenoid molecule in the immediate vicinity of B_M in WT (Figure 5.3 and Figure C2 in Appendix C). Our results also support the rotation of the acetyl group from the "out" to the "in" orientation in the 20-15 °C range as the temperature is lowered in the anaerobically grown R-26 (Figure 5.4). This rotation appears to be required for the binding of a lipid molecule, as in the presence of DLPC and DMPC the electrochromic absorption changes followed similar temperature dependence, although with larger differences between the two extremes. The slight differences in this temperature dependence for DLPC and DMPC are most likely due to the different *in situ* phase transition temperatures of the lipids as discussed earlier. The inward orientation for lipid binding is also supported by crystallographic studies that modeled this conformation for any bound molecules other than the naturally synthesized spheroidene (Table 5.1). [6,44,72,159,160]

Table 5.1 List of PDB codes for representative structures that show orientation of the acetyl group of B_M depending on the molecule occupying the carotenoid binding site

Strain	Bound Molecule near B_M	θ^a	PDB code	Reference
WT	spheroidenone	in	2GMR, 2BOZ, 1UMX, 1K6L, 3DSY	82 109 169 170 unpublished
	spheroidene	out	1RVJ, 1PCR, 1YST, 1KBY, 2J8C, 2UWS	171 6 72 21 44
R-26	3,4-dihydro spheroidene	in	1RQK	159
	spheroidene	in	1RGN	159
	LDAO	in	2HG3, 2HG9, 1RG5	160 159
	-	out	1OGV	34

[a] θ is the orientation of oxygen atom of the acetyl group of B_M viewed from the entrance of the binding pocket.

Even though the correlation appears to be strong, it should also be mentioned that in moderate-resolution crystal structures (>2 Å), such as those available for the BRCs from *Rb. sphaeroides*, it could be challenging to determine the orientation of the acetyl group directly from the electron density. Since the expected electron density difference between the "in" and "out" orientations is very small, the best bet is usually based on identification of potential hydrogen-bonding partners for the carbonyl oxygen. Unfortunately, for B_M a potential hydrogen-bond donor is absent in most of the cases.

Therefore the proposed orientation may suffer from bias by the molecular replacement starting model or automatic choice of chemical restraints, where one torsion angle is favored over the other. For example, in the case of the special pair, where His L168 and Tyr M210 were suggested to be hydrogen-bond donors for the carbonyl oxygen atoms, in some models the carbonyl oxygen is modeled pointing away from the potential hydrogen-bond donor.[82,171] In chapter 3 we proposed Tyr M210 to be hydrogen-bonded to the acetyl group of P_M but only in the light-induced conformation. This indicates that the experimental conditions, in particular the dark adaptation of the BRCs, may have significant influence on this structural detail.

5.2 Influence of liposomes on light-induced conformational changes

Figure 5.7 shows the kinetics of recovery of the $P^+Q_A^-$ charge-pair at 22 °C (panel A) and 8 °C (panel B) in BRCs from anaerobically grown WT and R-26 that have been incorporated into liposomes formed from various lipids with different hydrophobic thicknesses and saturation levels. The kinetic traces were generated by plotting the absorption changes at 868 nm taken from the spectra recorded at different times during and after the illumination, as demonstrated for three data points in Figure 5.7B. Rate constants and relative amplitudes of the kinetic components in the recovery kinetics are tabulated in Table C2 (appendix C). At 22 °C, the lifetime of the $P^+Q_A^-$ state in R-26 was found to be 2.5-fold longer in liposomes from DOPC, which has a long fatty acid chain (C_{18}), than in liposomes from DLPC with a shorter (C_{12}) chain.

When BRCs from WT with the hydrophobic spheroidene molecule near B_M were incorporated into the same DLPC liposomes, the lifetime was nearly a factor of 2 longer than in R-26. The relative amplitude of this long-lived component was also larger in WT than in R-26, in agreement with the observations made in detergent-dispersed BRCs (Figure 5.2 and Figure C1 in Appendix C). This relationship became radically different at 8 °C, where the lifetimes were extremely long (~ 2 h) in DLPC liposomes for both WT (trace b) and R-26 (trace c), with rate constants of 1.5×10^{-4} s^{-1} and 1.3×10^{-4} s^{-1}, respectively. Moreover, the fraction of the component with this ultra long lifetime reached 93% in R-26 as compared to 58% in WT. As seen from the inset in Figure 5.7B, the electrochromic absorption changes of the B-band were still observable even after complete recovery of the $P^+Q_A^-$ charge-pair 8 h after the illumination was turned off (trace c). This very long lifetime, however, could be achieved only if the BRCs were cooled at a slow rate of 0.2 °C/min. Rapid cooling (4 °C/min rate) of BRCs from R-26 in DLPC liposomes resulted in exactly an order of magnitude faster recovery with a rate constant of 1.3×10^{-3} s^{-1} and in only 36% of the BRCs (trace c'). The same temperature decrease in DOPC liposomes caused the lifetime of the charge-separated state to change only by ~ 1.4-fold in R-26 BRCs. Unlike in DLPC, the cooling rate had no influence of the recovery kinetics in DOPC liposomes.

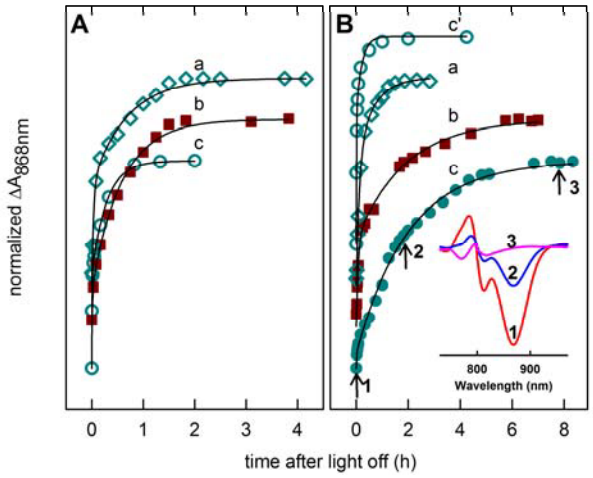

Figure 5.7 Kinetics of the light-induced absorption changes at (A) 22 °C and (B) 8 °C, measured at the center of the Q_Y absorption band of P after the prolonged, continuous illumination was turned off in BRCs reconstituted into liposomes from various lipids. The following samples were used: (a, open dark cyan diamonds) R-26 in DOPC, (b, solid brown squares) WT in DLPC, (c, open and solid dark cyan circles) R-26 in DLPC, and (c', open dark cyan circles) R-26 in DLPC with rapid cooling. The traces were normalized to the maximum absorption changes at time = 0 and were shifted vertically for clarity. Thin solid lines are the best fits to the curves (equation 1). The results of the fits are tabulated in Table C2 (Appendix C). Conditions: ~ 1.5 μM BRCs, 15 mM phosphate (mono- and disodium) buffer, pH 7, 15 mM KCl, 100 μM terbutryn.

In R-26 at 8 °C in DLPC liposomes, the lifetime of the longest-lived charge-separated state was more than 5-fold longer than in TX-100 micelles mixed with DLPC (Figures 5.2 and 5.7; Tables C1 and C2, Appendix C). Additionally, the amplitude of the longest-lived component rose from 60% in detergent to 93% in liposomes. Thus, it is obvious that binding of DLPC to the carotenoid binding site alone cannot account for the very long lifetime of the charge-separated state measured at 8 °C in DLPC liposomes.

It has been shown that the lifetime of the $P^+Q_A^-$ state at room temperature in the light-induced conformation could be increased by 2-fold if the BRCs from *Rb. capsulatus* were incorporated into DOPC liposomes, where the lipid bilayer thickness was matched by the hydrophobic thickness of the BRC, but not in DLPC liposomes, with shorter than desired bilayer thickness (Chapter 4). As at 22 °C, neither DOPC nor DLPC is expected to bind to the carotenoid binding site; the nearly 2.5-fold longer lifetime in DOPC liposomes for R-26 is consistent with this earlier finding (Figure 5.7A and Table C2, Appendix C). A similar 2-fold difference in the rate constants could still be observed at 8 °C if the DLPC liposomes were cooled rapidly, suggesting that rapid cooling in DLPC liposomes prevents the binding of the lipid due to the dramatically decreased diffusion rate of the lipid as discussed above (trace c' in Figure 5.7B). In the gel phase the thickness of the DLPC bilayer was reported to be 27.0 Å, as opposed to 19.5 Å in the liquid crystalline phase, indicating that at 8 °C the DLPC bilayer may provide a reasonable hydrophobic thickness for the transmembrane α-helices of the BRCs with a thickness of ~ 30 Å.[38,72]

Chapter 6

Inhibition of light-induced conformational changes due to manganese binding

The results presented in this chapter are part of a manuscript under preparation:

Author contributions:

S. S. Deshmukh performed the experiments, and analyzed the data. M-Alexandru Ivanescu performed the experiments (data not included). L. Kálmán designed the research and guided the data analysis.

In earlier chapters we have demonstrated that by controlling light-induced structural changes systematically in the vicinity of the dimer the lifetime of the charge-separated state can be increased by up to 5 orders of magnitude. The BRC and PS II are evolutionarily related and share structural similarities such as the core cofactors and subunits are arranged symmetrically.[20,172] Even though both complexes transfer electrons and protons across the membrane in similar way, they utilize different secondary electron donors. In PS II water is used as the electron donor, while BRC can only utilize a lower potential cytochrome. Despite these structural and functional similarities, PS II has unique ability to oxidize water into molecular oxygen. The oxidation of water in PS II is achieved by the following three key components: (i) the primary electron donor with high oxidizing potential, (ii) presence of Tyr residues at key position, which results transfer of electrons and protons, and (iii) presence of manganese cluster that can store four electron equivalents required for the overall reaction.

It has been demonstrated that manganese ions can serve as an electron donor in photosynthetic organisms, which may have been an intermediate step in the evolution of water oxidation at a manganese complex.[173,174] Manganese is often found in surface sediments and its wide scale availability might have provided primitive photosynthetic organisms as an electron source.

Moreover, manganese is an essential trace element that has many different functions in the protein. It often plays important role in biological redox reactions in enzymes such as manganese superoxide dismutase, manganese peroxidase, manganese catalase etc. In these enzymes redox activity of manganese is established through protonatable amino acid residues or water as ligands.[175]

Binding of other transition metal ions (copper, cobalt) to a local protein environment has been shown to modulate the forward electron transfer and the charge recombination.[176] Some of the above-mentioned key components such as highly oxidizing P, electron and proton transfer through Tyr residue, and manganese oxidation can be introduced in the BRCs by genetic manipulation.[70,119] Here in this work we attempted an alternative approach to explore the effect of manganese ion as a potential secondary donor by systematically altering the immediate surrounding of the BRC and in particular the assumed binding site of manganese ion. In order for Mn^{2+} to serve as a secondary electron donor to P^+ its *in situ* oxidation-reduction potential (Mn^{2+}/Mn^{3+}) should be lower than that of the P/P^+ redox couple. Since in WT or in R-26 the P/P^+ midpoint potential was reported to be ~ 505 mV, physiologically it can only use secondary electron donors that have midpoint potentials lower than the dimer potential. The cytochrome c is such a molecule with a ~320 mV potential.[177] In order to utilize manganese as a secondary electron donor, it is necessary to either increase the P/P^+ midpoint potential of the BRC and/or lower the Mn^{2+}/ Mn^{3+} potential. In the hexa-aquo complex the Mn^{2+}/ Mn^{3+} potential is (~ 1.3 V) much higher than the dimer of the BRC. When one or more water molecule(s) are replaced by different anions such as bicarbonate, acetate, citrate, or malate the net positive charge decreases with each substitution and the oxidation of manganese in such complex becomes energetically more favorable (Figure 6.1).[98] For example bicarbonate anion can form manganese-bicarbonate complexes that have one or two bicarbonate molecules replacing the water resulting in Mn^{2+}/ Mn^{3+} potentials in these complexes, as 920 and 650 mV, respectively (Figure 6.1).[178]

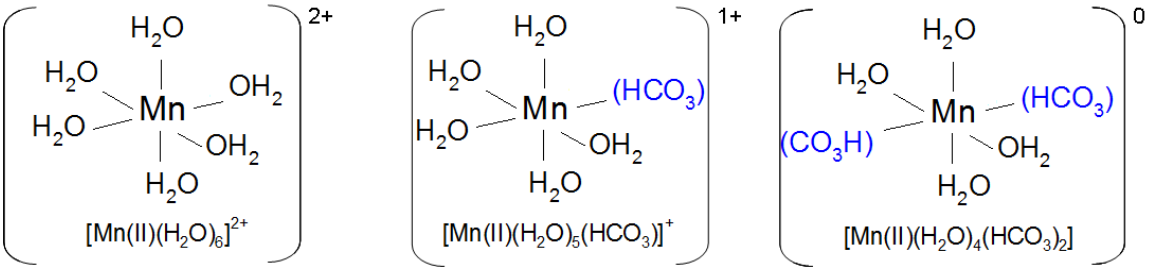

Figure 6.1 Coordination of manganese (II) ion with six ligands to form octahedral geometry. The central Mn^{2+} coordinates with water molecules in solution but upon availability of bicarbonate (negatively charged) residue (blue text) binding affinity can be increased by lowering the net positive charge of the complex.

In these complexes the potential is lowered by electrostatic stabilization of the manganese ion upon coordination with bicarbonate.[179] The pH buffer bis-tris propane is also known to form complex with manganese ion and thereby would lower its potential.[180]

Different transition metal ions, such as Zn^{2+}, Cd^{2+}, Ni^{2+} or Cu^{2+} have been proven to bind near the Q_B and therefore inhibiting the proton uptake from the environment[181-183]. However, Mn^{2+} is known not to bind to any of the known sites near the quinones and none of the above transition metals were reported to bind near P.[96,184] Recent studies focused on the design of metal binding sites in BRCs analogous to those found in PS II and other manganese binding proteins.[70,97,99] Binding of Mn^{2+} ion in native BRCs was not accomplished so far. In this chapter, manganese ion binding in native BRCs from *Rb. sphaeroides* was studied to understand the effect of bound Mn^{2+} ion on light-induced conformational changes and whether it can alter the P/P^+ potential.

6.1 Changes in light-minus-dark optical difference spectrum upon manganese binding

Near-infrared light-minus-dark difference spectra were recorded at prompt after the illumination turned on, 5 min after the illumination turned on , and 1 min after the illumination was turned off in BRCs with and without the presence of added manganese. As the spectral intensities correlate with the fractions of the BRCs trapped in various conformational states the normalized spectra are displayed for better comparison in Figure 6.2A and B. Inset of the Figure 6.2 indicate the times at which the spectra were recorded. Spectra recorded at the beginning of the illumination are predominantly characteristic of the dark-adapted conformation, while further illumination generates the mixture of the spectra characteristic to both the dark- and light-adapted conformations. Spectra recorded 1 min after the illumination turned off correspond exclusively to the light-induced conformations of the BRCs. The double difference spectra between those recorded at the beginning and the end of the illumination (black dotted spectra-minus-red solid spectra in Figure 6.2) indicate the light-induced changes that occurred during illumination. A decrease in the electrochromic absorption changes around 800 nm with increasing illumination time was detected in BRCs without added manganese (red solid and black dotted traces in Figure 6.2A). This is in agreement with the previous findings for BRCs and characteristic to long-lasting conformational substates (Figure 3.5, 4.3 and 4.4). The double difference spectrum (solid black trace in Figure 6.2A) also shows structural changes associated with the bacteriochlorophyll monomers (around 800 nm).

In contrast, these spectral features were absent in the presence of added manganese indicating that the metal ion inhibits the light-induced conformational changes in the vicinity of the dimer (Figure 6.2B).

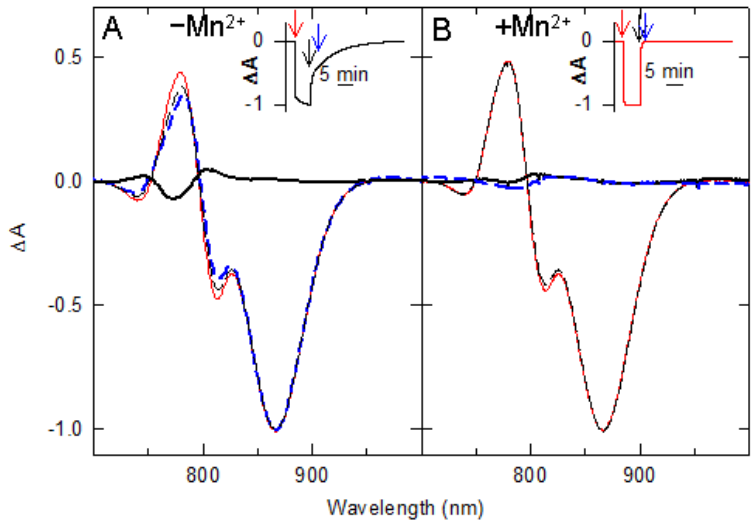

Figure 6.2 Normalized light-minus-dark optical difference spectra of R-26, in the absence **(A)** and presence **(B)** of bound Mn^{2+}, recorded immediately after the light had been turned on (red solid trace), after illumination for 5 min (black dotted trace), and 1 min after the illumination had been turned off (blue dotted trace). The inset shows the time dependence of the absorption changes and indicates the times at which the spectral traces were recorded. The thick solid lines (black) show the double difference spectra (black dotted-minus-red solid trace) and feature changes around 800 nm, consistent with the decrease of the electrochromic absorption changes involving the monomers during the illumination in **(A)** whereas these changes were not observed in **(B)**. Conditions: ~ 1 µM BRC, 15 mM bis-tris propane, 0.1 % LADO, 100 µM terbutryn, 5mM $MnCl_2$ for Mn^{2+} samples, pH 8.0.

6.2 Effects of bound transition metal ion on kinetics of the recovery of the charge-separated states

The kinetics of the absorption changes caused by 5 min illumination with subsaturating light intensity were recorded at the center of Q_Y band of the dimer as different transition metal ions were titrated in the BRC protein. The recovery of the oxidized dimer showed a complex kinetics with three components. The fastest phase was attributed to the charge-recombination in the dark-adapted conformation, while the slow and the very slow components were assigned to recoveries observed in various altered (light-adapted) conformations established in Chapter 3. The fraction of the slow (intermediate) component is plotted as a function of the applied metal ion concentration (Figure 6.3A) to determine dissociation constant (K_D) of metal ions using equation 3 and 4 (Chapter 2).

The K_D values for Cu^{2+}, Ni^{2+}, Zn^{2+}, and Co^{2+} are 4 μM, 7 μM, 4 μM, and 4 μM, respectively whereas for Mn^{2+} it is much higher, 282 μM and 125 μM, in the absence and presence of bicarbonate, respectively. Also the fraction of the slow component in the presence of Mn^{2+} increases to 50 % while other metal ions showed only less than 10 % increase in the fraction of the slow component (Figure 6.3A). The rate constants of both slow and very slow components were found to be independent of the metal ion concentration clearly separating two populations (Figure 6.3B). At very high concentration of Mn^{2+} (1 mM and above) the very slow component was not detected. These observations suggest that while the structural changes near the quinones (slow component) are not affected by the manganese, the presence of manganese ion completely blocks the structural changes near P.

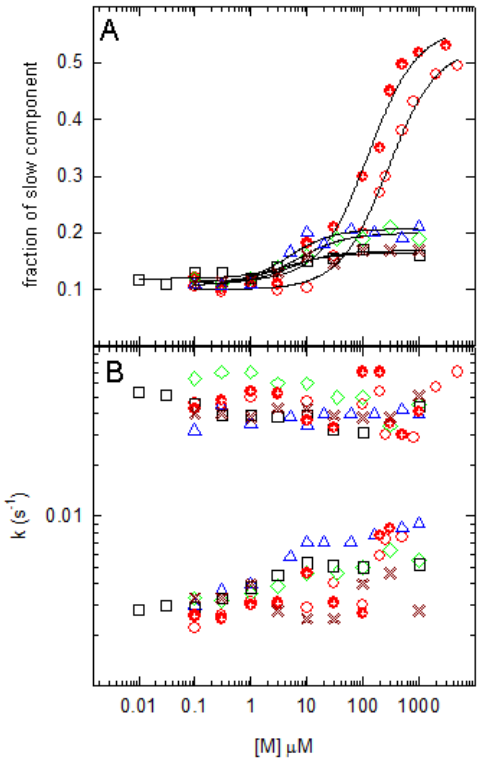

Figure 6.3 Dependence of the kinetic parameters obtained from the recovery kinetics of the oxidized dimer on the metal ion concentration. A. amplitude of the slow component, continuous lines are the best fits to the measured data points (using equation 3 and 4 from Chapter 2) and **B.** rate constants of the slow and very slow components in the 5 min illumination induced recovery kinetics. The following transition metal ions were used: Mn^{2+} (open red circles), Cu^{2+} (open blue triangles), Ni^{2+} (open green diamonds), Co^{2+} (brown cross), and Zn^{2+} (open black squares). In the presence of bicarbonate the K_D value lowered for manganese (solid crossed red circles). Results are described in the text. Conditions as in Figure 6.2 except respective metal ions were used for binding study.

It should be noted that the relative fraction of slow component increases in the presence of manganese and hence the formation of very slow component becomes inhibited (Figure 6.3A).

Since other metal ions that have known binding sites near Q_B show only very minor effect, their binding near P can be excluded. This conclusion has also been scrutinized by the effect of the metals on the P/P^+ potential and will be presented later.

The results indicate the manganese becomes associated with the BRC at high concentrations but the relatively high dissociation constant of ~ 282 μM (and 125 μM in the presence of bicarbonate) are consistent with the manganese not being tightly coordinated to the BRC. Use of anions such as bicarbonate enhances the binding of divalent metal ion. The binding is expected to be weak if many of the coordinating residues are protonated. The bicarbonate ions may increase the surface pH and facilitate the deprotonation of the residues in the binding pocket by altering the local pH.

Since, all other studied transition metal ions have known binding site near Q_B, the high binding affinity (K_D < 10 μM) site was attributed to the quinone side while low binding affinity site (for Mn^{2+}) was attributed to the dimer side. The results of the kinetic analysis indicate that manganese binding inhibits the formation of L3 conformational state, associated with structural changes in the vicinity of the dimer, in scheme 3.1 (Chapter 3). If Mn^{2+} ion binds close to P^+ then the association of the manganese with the BRC is expected to alter the P/P^+ potential due to electrostatic interactions.

6.3 P/P^+ oxidation-reduction midpoint potential

The oxidation-reduction midpoint potential of the P/P^+ redox couple was measured in the presence of added Mn^{2+} (Figure 6.4). Without any external illumination the data were well described using Nernst equation assuming only a dark-adapted population of P that yields a midpoint potential of 606 mV at pH 8 (open symbols in Figure 6.4B).

This measurement was also carried out in the presence of added 50 mM and 100 mM bicarbonate. These bicarbonate concentrations facilitate the formation of the $[Mn(II)(H_2O)_5(HCO_3)]^+$ and $[Mn(II)(H_2O)_4(HCO_3)_2]$ complexes, respectively that reduce and neutralize the net positive charge of the divalent metal ion. As a consequence of the bicarbonate effect the midpoint potential of P/P^+ couple dropped to 548 mV and 516 mV, respectively (open symbols in Figure 6.4C and D). The midpoint potentials were also measured while the samples were weakly illuminated according to the method described in Chapter 3. Under weak illumination the data required the use of three-component Nernst equation assuming three different populations of P (Mn^{2+} bound, dark-, and light-adapted) in the presence of Mn^{2+}. While the P/P^+ midpoint potential of fraction that has bound Mn^{2+} remained unchanged, those that do not have bound Mn^{2+} showed values of 505 mV (38 %) and 420 mV (12 %) (closed symbols in Figure 6.4B). Also in the presence of 50 mM bicarbonate we observed lowered potentials of 508 mV (20 %) and 420 mV (11 %) along with 548 mV (69 %) for the fraction that has bound Mn^{2+} (closed symbols in Figure 6.4C), but in the presence of 100 mM bicarbonate lower value of potential was not observed (Figure 6.4D). For comparison purpose the P/P^+ midpoint potentials of the WT BRC in the dark and under weak illumination was also presented here (Figure 6.4A; the data are taken from Figure 3.9B).

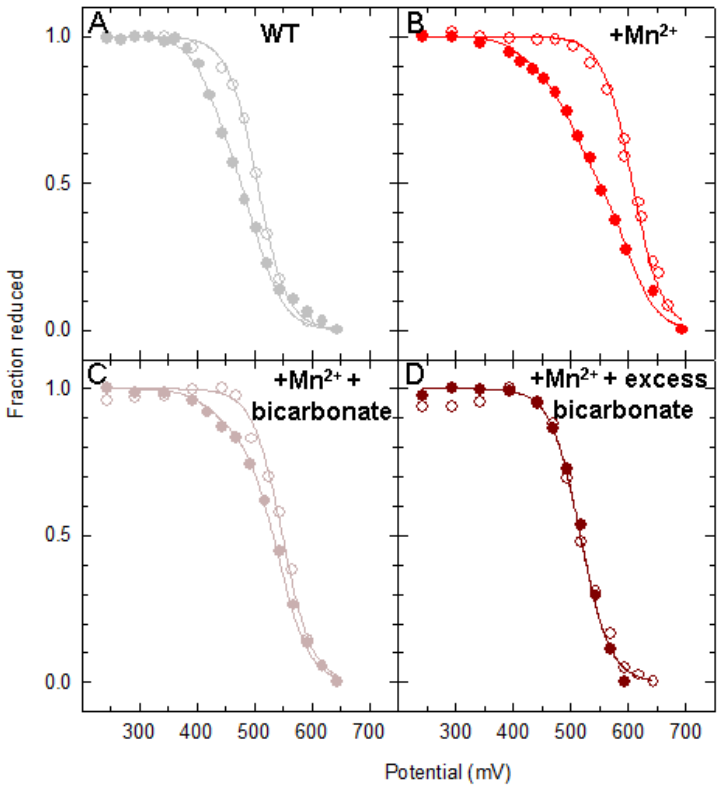

Figure 6.4 Spectroelectrochemical redox titrations of the BRCs in the absence (open symbols) and in the presence (closed symbols) of a weak external illumination in **(A)** WT (gray) (from Figure 3.9 for comparison), **(B)** R-26 + 5 mM Mn^{2+} (red), **(C)** R-26 + 5 mM Mn^{2+} + 50 mM bicarbonate (pale brown), and **(D)** R-26 + 5mM Mn^{2+} + 100 mM bicarbonate (dark brown). The data were fitted with a standard Nernst equation assuming one (in the dark), two or three (in the presence of illumination) components. Results of the fit are described in the text. Conditions as in figure 6.2 except: ~ 300 µM BRC, 70 mM KCl, 0.05 % TX-100.

A potential drop of ~ 60 mV was observed due to loss of one positive charge (Figure 6.4A and Chapter 3). However, in the presence of divalent metal ion the midpoint potential was increased by ~ 100 mV which would be equivalent to addition of two positive charges in the close vicinity of the dimer (Figure 6.4B open symbols).

Since the net positive charge of the manganese decreases with each substitution of bicarbonate, two different concentrations of bicarbonate were studied to identify whether the increase in the dimer potential was due to only electrostatic interactions between P^+ and Mn^{2+}. The spectroelectrochemical redox titrations require high concentration of the BRC samples therefore relatively high concentration of bicarbonate was used.

The presence of 50 mM bicarbonate lowers the P/P^+ potential to ~ 548 mV, which is also in agreement with the loss of one positive charge due to the manganese-bicarbonate complex formation whereas in the presence of 100 mM bicarbonate the P/P^+ potential dropped to 516 mV indicating loss of two positive charges in the vicinity of P^+ (Figure 6.4C and D open symbols). Excess bicarbonate is known to increase P/P^+ midpoint potential by ~ 15mV,[185] which is in line with the above-mentioned results.

In the presence of weak illumination, however, Mn^{2+} becomes unbound in a fraction of BRCs due to over 2 h of prolonged illumination during the long experiments. As a result of this the fraction of BRCs that do not have bound Mn^{2+} show altered conformational state with lower potential resembling to WT BRCs (Compare Figure 6.4A and B closed symbols). This result was also observed in the presence of 50 mM bicarbonate (Figure 6.4C), but in the presence of excess bicarbonate the lower potential was not observed with altered state mostly due to high binding affinity of the complex (Figure 6.4D). The P/P^+ potential remained unchanged under weak illumination in the presence of excess bicarbonate. Experimental limitations hinder the measurements of the P/P^+ potential at higher manganese concentration due to the change in optical quality of the sample. Thus to estimate the upper limit for the dimer potential in the presence of manganese, previously established model by Tommos and Babcock was used.[100]

Figure 6.5 shows the P/P^+ potential as a function of pM (-log [M]; where [M]: added Mn^{2+} concentration in moles). The P/P^+ couple has a pM dependent potential that increases by ~ 60 mV per pM unit and can have lower and upper limits of ~ 610 mV and ~ 643 mV, respectively as determined by extrapolating the fits. Actual fitting to the measured data points yields P/P^+ potential of ~ 625 mV, which is equivalent to two positive charges in the close vicinity of the dimer.

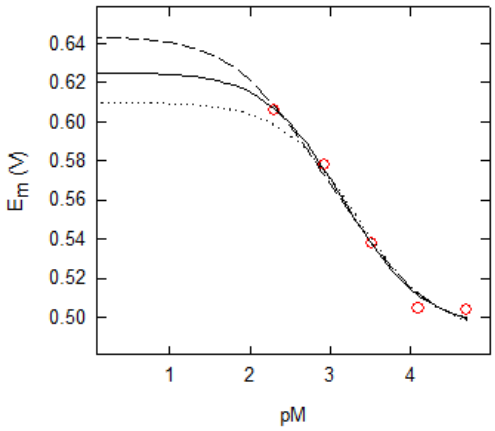

Figure 6.5 P/P^+ potentials measured by spectroelectrochemical redox titrations as a function of pM. The fit of the data is described by equation 8 (Chapter 2) that gives lower and upper limit for the increase in P/P^+ potential (dotted and dashed lines, respectively). Solid line is the best fit to the measured data. The results are described in the text. Conditions as in figure 6.4.

Since there is a large, 110 mV increase in the P/P^+ potential in the presence of bound Mn^{2+}, was detected it is also expected that the energy levels of the charge-separated ($P^+Q_A^-$) and/or of the ground state (PQ_A) are also shifted. To test this the flash-induced charge recombination from the primary quinone was studied in the presence of bound Mn^{2+}.

The kinetics of the flash-induced charge recombination were measured by the recovery of the bleaching of the Q_Y band of P in the presence of terbutryn (Figure 6.6). Without the addition of Mn^{2+} the $P^+Q_A^-$ → PQ_A charge recombination occurred with a lifetime of ~ 86 ms, while in the presence of bound Mn^{2+} it decreased to ~ 66 ms (red trace in Figure 6.6). It has been shown earlier that substitutions of positively charged amino acids near the dimer increase not only the P/P^+ potential but also the rate of the charge recombination.[93] For example, in the case of the mutant that contained the Leu to His substitution 5 Å from P at the M197 position (Figure 1.15, Chapter 1) the potential of the dimer has increased to 630 mV and the lifetime of the charge recombination was measured to be 65 ms.[93] Our result recorded in the presence of Mn^{2+} is in an exceptionally good agreement with those measured in the M197 mutant. This indicates that binding of Mn^{2+} destabilizes P^+ leading to rapid charge recombination and confirm the presence of a binding site for Mn^{2+} near P.

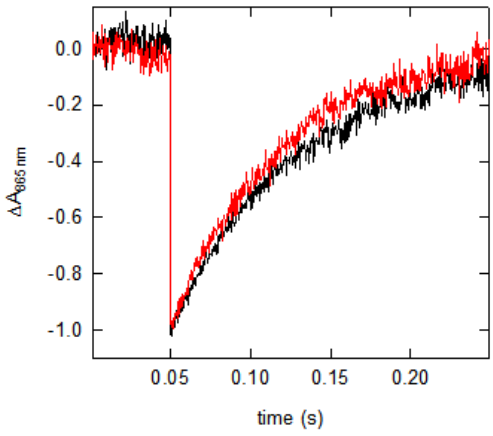

Figure 6.6 Normalized kinetic traces of the flash-induced charge recombination in R-26 reaction centers monitored at 865 nm with (red trace) and without (black trace) added Mn^{2+}. The results are described in the text. Conditions as in figure 6.2 except ~ 4 μM BRC.

6.4 Modeling of the proposed manganese binding site

At most seven manganese(II)-ions were estimated to bind to the entire BRC based on an EPR (Electron Paramagnetic Resonance) study .[70] All the experimental evidences suggest that the proposed binding site must be in the vicinity of the dimer. To model the binding site of Mn^{2+} in BRC, Q-site finder server (University of Leeds, Leeds, UK) was used, which predicted two such sites in the proximity of the dimer (Figure 6.7A). One site (Site 1) is on top of the dimer along the Q_X of the bacteriochlorophylls and the another site (Site 2) is near B_M where carotenoid is known to bind (Figure 6.7A). Site 1 involves Ser L158, Tyr L162, Ser M190, Gly L161, and Gly L165 amino acid residues along with three water molecules W736, W737, and W810 and Site 2 contains Ser M119, Met M122, and Tyr M177. None of these residues in either site are negatively charged that could electrostatically stabilize the binding of the divalent manganese(II), thus the elevated potential of P^+ reported in our work is in a good agreement with the lack of electrostatic stabilization. It also explains why the binding of the manganese is found to be weak (K_D = 282 μM). Enzymes such as manganese peroxidase, manganese superoxide dismutase or manganese catalase have strong manganese binding sites due to coordination to Asp, Glu or His residues, while residues in our proposed site can only weakly coordinate metal ion.[186,187] Among the potential ligands to manganese Tyr L162 is known to play important role in electron transfer process from external electron donor (cyt c_2) to P^+.[24]

Since the P/P^+ potential was increased by 110 mV, and the acceleration of the flash induced charge recombination was also modest we can conclude that manganese can bind predominantly to only one of the two proposed sites.

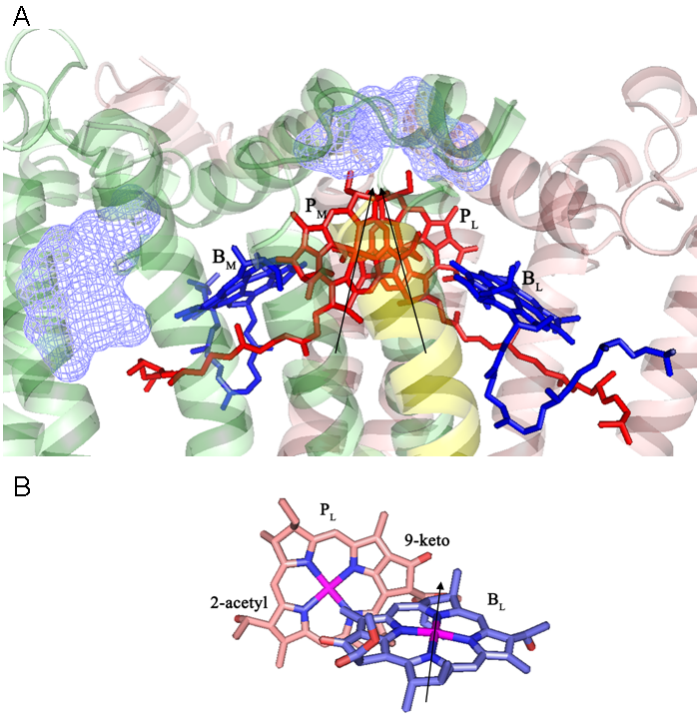

Figure 6.7 A. Cartoon representation of the BRC that shows two halves of the dimer (P_L and P_M in red sticks) and two monomers (B_L and B_M in blue sticks) with two predicted binding sites (Site 1 and 2) for the metal ion (slate colored mesh). The amino acid residues representing the mesh are listed in the text. The L, M, and H subunits are shown in salmon, green and yellow, respectively. The transparency of the subunits is increased for clarity of the cofactors. Arrows indicate the Q_X transition moment of the two halves of the dimer. **B.** The structure of L-half of the dimer (P_L) (salmon sticks) and monomer B_L (slate sticks). The Q_X transition moment of the B_L (shown by arrow) is in the plane of 9-keto carbonyl group of the P_L. Coordinates were taken from PDB entry code 1PCR.[6]

To study which of the two sites is more likely accommodating the manganese ion light-minus-dark optical difference spectra of the BRC was recorded in the spectral range corresponding to the Q_X electronic transition of the bacteriochlorines (500-700 nm). Any structural change along the Q_X transition of bacteriochlorophylls would be expected to cause a shift in the Q_X absorption band of these pigments.

The spectra were recorded during and after the illumination in the Q_X region, where all four bacteriochlorophylls have absorption around ~ 600 nm. The spectra are shown in Figure 6.8 in the 500−700 nm region. Spectra recorded at the beginning of the illumination are characteristic to the pigments in BRCs in their dark-adapted conformation, while those recorded 1 min after the illumination turned off represent light-adapted conformation. The spectral intensities mirror the fractions of the BRCs found in the corresponding conformational states. In the spectrum that was recorded 1 min after the illumination turned off without added metal ion, there was 16 nm blue shift in the bacteriochlorophyll band from 601 to 585 nm with almost half of fraction in altered conformational state, which recovers in long time-scale (Figure 6.8A). After addition of metal ion, this fraction became negligible and it recovered rapidly (Figure 6.8B). This observation is in line with the relative amplitudes of the kinetic components of Figure 6.2. Since structural water molecules W737 and W736 are along the Q_X transitions of P_L and P_M (Figure 3.6), any displacement of these molecules would be expected to cause a shift in the Q_X band of bacteriochlorophylls around 600 nm. This light-induced structural change along the Q_X transition of bacteriochlorophylls was absent upon Mn^{2+} addition. This indicates that Mn^{2+} most likely has a binding site along the Q_X transition of one of the four bacteriochlorophylls, which is in agreement with Site 1 modeled with the Q-site finder server.

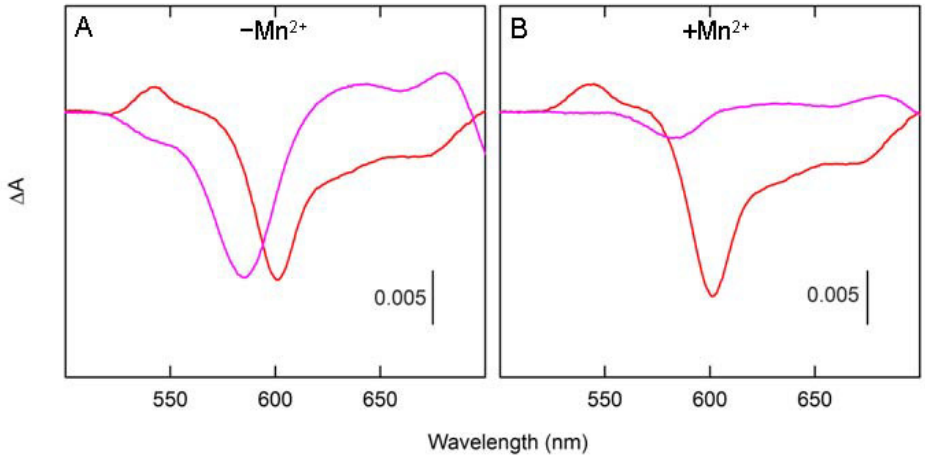

Figure 6.8 Light-minus-dark optical difference spectra recorded immediately after the onset of the light (red trace) and 1 min after the illumination turned off (pink trace) for R-26 BRCs in the absence (A) and presence (B) of Mn^{2+} in the Q_X region of the bacteriochlorophylls. Pink trace shows the light-adapted conformational state that was observed to be blue-shifted by 15 nm from 601 nm of the dark-adapted state (red trace) in (A) whereas this conformational change was not observed in the presence of bound Mn^{2+} in (B). Conditions as in figure 6.2.

In addition also within Site 1 the 9-keto group of the L-half of the dimer (P_L) is also along the Q_X transition of monomer B_L (Figure 6.7B). When Leu is mutated to His at L131 position to introduce H-bond with the dimer through 9-keto group then light-induced structural changes were blocked. The lack of structural changes were explained by the loss of proton conducting pathway from the dimer to the solvent (Chapter 3). Thus, one can speculate that the manganese-binding to Site 1 can also block the proton-conducting pathway to the solvent.

The Site 2 near the B_M (Ser M119, Met M122, and Tyr M177) lies where carotenoid, detergent, and lipid molecules can bind, but no spectral feature was observed in the light-minus-dark optical difference spectra in the presence of Mn^{2+} that leads to confirm this as a possible binding site. Since manganese binding to the native BRC can be achieved at high concentrations that leads to an increased in P/P^+ potential, it is interesting to study the role of manganese as a secondary electron donor (discussed later in future plan).

Chapter 7

Conclusion

Nature's photosynthetic apparatus offers at least three different model examples for solar energy conversion that can inspire humanity to develop artificial light-driven energy converters for future energy production and storage: (i) creation of long-lived, energetic charge-separated states in many photosynthetic enzymes, (ii) generation of proton-electrochemical gradient in both oxygenic (PSII) and anoxygenic systems (BRCs), and (iii) catalytic splitting of water in oxygenic photosynthetic organisms. These model examples depend on electron and proton transfers and subsequent conformational changes. In the frame of this thesis we have localized the conformational changes in the BRCs at molecular level in the vicinity of P with the use of the wild type and 11 different mutants of *Rb. sphaeroides*. We have determined that the light-induced conformational changes that favor long-lived charge-separated states involve: (i) a dielectric relaxation of the protein that stabilizes the charge on the dimer (Chapter 3)[108], (ii) decrease in the P/P^+ potential and large proton release through a proton conducting pathway from the dimer to the solvent (Chapter 3)[115] and, (iii) rotation of the 2-acetyl group of P_M[108,115,188]. We discovered and reported a novel lipid binding site near the dimer and through lipid binding we were able to extend the lifetime of the charge-separated state by an unprecedented 5 orders of magnitude from sub seconds to hours (Chapter 5).[189] This expansion of the lifetime of the charge-pair at a convenient temperature range presented within this work provides new opportunities to utilize the BRC as a light-driven biocapacitor in energy storage (Figure 7.1).

Based on the different abilities of the BRCs to undergo structural changes with and without a bound hydrophobic molecule (lipid or carotenoid) we concluded that the light-induced structural change serves as a protective mechanism against oxidative damage if, due to excess light, the BRC becomes saturated and the cyt c_2 and/or quinone pools become exhausted (Chapter 5).[189] We also demonstrated that the light-induced conformational changes are also sensitive to the hydrophobic membrane environment, such as types of detergent and liposomes in terms of their hydrophobic thicknesses or head-group charges (Chapter 4).[188]

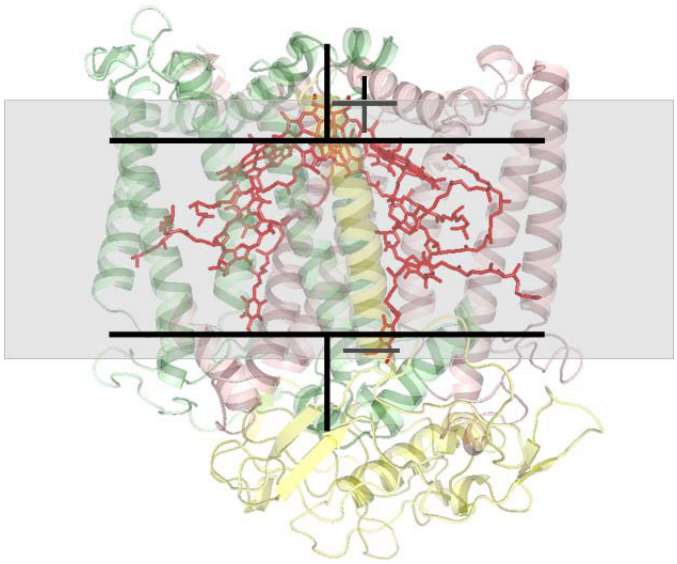

Figure 7.1 BRC as a biocapacitor. Cartoon representation of structure of the BRC with 9 cofactors (red sticks). The L, M, and H subunits (with increased transparency) are shown in salmon, green, and yellow colors, respectively. Light-induced charge-separated state is shown by charges only at approximate positions. The membrane is represented by gray shaded area.

The principles leading to the ability of the BRC to store electric potential on an extended time-scale can be inspiring for the development of biomimetic systems that can form the basis of molecular-scale optoelectronic devices. It will give insights of how solar energy can be converted into chemical potential under laboratory conditions. Moreover, this may open the stage for widespread artificial methods to develop man-made solar energy converters. On the other hand, as demonstrated in Chapter 6, light-induced long-lived conformational states can be blocked by transition metal binding without genetical modifications, This makes BRC to gain some specific functional features that are similar to PS II.

Chapter 8

Future work

The zwitterionic lipid molecule with short acyl chain length (C_{12}: DLPC) was shown to bind near B_M in the carotenoid binding pocket of R-26 BRC. Binding of hydrophobic molecule and formation of ripple phase of lipid bilayer in proteoliposomes can stabilize the light-induced charge-separated state substantially. In order to extend the lifetime of charge-separated state further, systematic study will be done to identify whether binding of a lipid molecule with negatively charged head-group with same acyl chain length (C_{12}: DLPS) is possible along with the formation of ripple phase of lipid bilayer in proteoliposomes.

Evolutionarily related PS II utilizes manganese cluster as external electron donor in the process of water oxidation because manganese-bicarbonate complex has much lower oxidation potential (~ 0.8 V) than that of primary donor of PS II (~ 1.1 V) (Figure 8.1). The P/P^+ potential of BRCs can be increased up to ~ 0.76 V by genetic alteration of hydrogen bonding pattern of the dimer (shown as shaded area in Figure 8.1) so that manganese-bicarbonate complex can be utilized as secondary electron donor. On the other hand it was demonstrated in Chapter 6 that binding of Mn^{2+} to the native BRC alone can increase the P/P^+ potential by ~ 120 mV. Manganese was found to bind BRC at the similar site, where cyt c_2 is known to bind. In order to use Mn^{2+} as a secondary electron donor besides increasing the P/P^+ potential, Mn^{2+}/Mn^{3+} potential has to be lowered. Even though manganese-bicarbonate complex has significantly lower midpoint

potential than the hexa-aquo form (Figure 8.1), it is still not low enough to use it as secondary electron donor to the P^+ in Mn^{2+} bound native BRC. As the presence of bicarbonate, bis-tris propane, and higher pH were known to further lower Mn^{2+}/Mn^{3+} potential, potentially Mn^{2+} can serve as a secondary electron donor to P^+ in native BRCs under optimum conditions. This Mn^{2+} binding study can further be extended to the liposomes with different net head-group charge (DOTAP: +1, DOPS: -1, DOPC: 0) to study the changes in the midpoint potential of the dimer, lifetime of the light-induced charge-separates states, and subsequent structural changes.

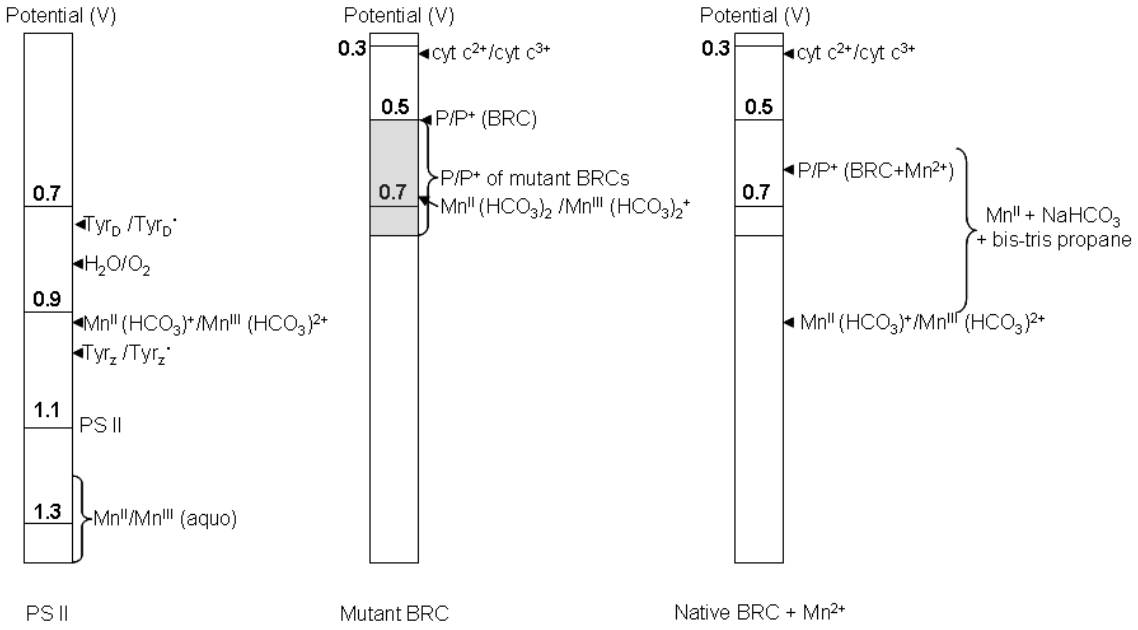

Figure 8.1 Relative comparison of the midpoint potentials of the primary and secondary electron donors in PS II, mutant BRC, and BRC with bound Mn^{2+}. The P/P^+ potential of the BRC can be elevated by genetic alterations in the BRC (shown in shaded area). To use manganese as a secondary electron donor in native BRCs under optimized conditions, further studies will be done which may make BRC protein to gain some specific functional features of the evolutionary related PS II.

References

(1) Des Marais, D. J. (2000) *Science*, *289*, 1703-1705.

(2) Hunter, C. N., Daldal, F., Thurnauer, M. C., and Beatty, J. T. (Eds.) (2008) The Purple Phototropic Bacteria, Springer Verlag, Dordrecht, The Netherlands.

(3) Allen, J. P., Feher, G., Yeates, T. O., Komiya, H., and Rees, D. C. (1987) *Proc. Natl. Acad. Sci. U.S.A. 84*, 5730-5734.

(4) Allen, J. P., Feher, G., Yeates, T. O., Komiya, H., and Rees, D. C. (1987) *Proc. Natl. Acad. Sci. U.S.A. 84*, 6162-6166.

(5) Bacon Ke, *Advances in photosynthesis*, *10*, chapter 11, 199-212.

(6) Ermler, U., Fritzsch, G., Buchanan, S. K., and Michel, H. (1994) *Structure, 2*, 925-936.

(7) McElroy, J. D., Feher, G., and Mauzerrall, D. C. (1969) *Biochim. Biophys. Acta, 172*, 180-183.

(8) Norris, J. R., Uphaus, R. A., Crespi, H. L., and Katz, J. J. (1971) *Proc. Natl. Acad. Sci. U.S.A. 68*, 625-628.

(9) Feher, G., Hoff, A. J., Isaacson, R. A., and Ackerson, L. C. (1975) *Ann. N. Y. Acad. Sci. 244*, 239-259.

(10) Feher, G., Okamura, M. Y., and McElroy, J. D. (1972) *Biochim. Biophys. Acta, 267*, 222-226.

(11) Okamura, M. Y., Isaacson, R. A., and Feher, G. (1975) *Proc. Natl. acad. Sci. U.S.A. 72*, 3491-3495.

(12) Tiede, D. M., Prince, R. C., Reed, G. H., and Dutton, P. L. (1976) *FEBS Lett. 65*, 301-304.

(13) McPherson, P. H., Okamura, M. Y., and Feher, G. (1990) *Biochim. Biophys. Acta*, *1016*, 289-292.

(14) Paddock, M. L., Rongey, S. H., Feher, G., and Okamura, M. Y. (1989) *Proc. Natl. acad. Sci. U.S.A.*, *86*, 6602-6606.

(15) Paddock, M. L., Rongey, S. H., McPherson, P. H., Juth, A., Feher, G., and Okamura, M. Y. (1994) *Biochemistry*, *33*, 734-745.

(16) Takahashi, E. and Wraight, C. A. (1991) *Biochemistry*, *31*, 855-866.

(17) Paddock, M. L., McPherson, P. H., Feher, G., and Okamura, M. Y. (1990) *Proc. Natl. acad. Sci. U.S.A. 87*, 6803-6807.

(18) Takahashi, E. and Wraight, C. A. (1992) *Biochim. Biophys. Acta*, *1020*, 107-111.

(19) McPherson, P. H., Schoenfeld, M., Paddock, M. L., Okamura, M. Y., and Feher, G. (1994) *Biochemistry*, *33*, 1181-1193.

(20) Feher, G., Allen, J. P., Okamura, M. Y., and Rees, D. C. (1989) *Nature, 339,* 111-116.

(21) Cámara-Artigas, A., Brune, D., and Allen, J. P. (2002) *Proc. Natl. acad. Sci. U.S.A. 99,* 11055-11060.

(22) Paddock, M. L., Flores, M., Isaacson, R., Chang, C., Abresch, E. C., Selvaduray, P., and Okamura, M. Y. (2006) *Biochemistry*, *45,* 14032-14042.

(23) Nabedryk, E. and Breton, J. (2008) *Biochim. Biophys. Acta. 1777*, 1229-1248.

(24) Axelrod, H. L. and Okamura, M. Y. (2005) *Photosynth. Res. 85*, 101-114.

(25) Müh, F., Rautter, J., and Lubitz, W. (1997) *Biochemistry*, *36*, 4155-4162.

(26) Berry, E. A., Huang, L. S., Saechao, L. K., Pon, N. G., Valkova-Valchanova, M. and Daldal, F. (2004) *Photosynthesis Research*, *81*, 251-275.

(27) Donohue, T. J., Chain, B. D., and Kaplan, S. (1982) *J. Bacteriol. 152*, 595-606.

(28) Roth, M., Arnoux, B., Ducruix, A., Reiss-Hussan, F. (1991) *Biochemistry*, *30,* 9403-9413.

(29) Trotta, M., Milano, F., Nagy, L., and Agostiano, A. (2002) *Mat. Sci. Eng. C, 22,* 263-267.

(30) Trotta, M., Peira, E., Debernardi, F., and Gallarate, M. (2002) *Int. J. Pharm. 241*, 319-327.

(31) Piazza, R., Pierno, M., Vignati, E., Venturoli, G., Francia, F., Mallardi, A., and Palazzo, G. (2003) *Phys. Rev. Lett. 90,* 208101.

(32) Kálmán, L., Gajda, T., Sebban, P., and Maróti, P. (1997) *Biochemistry*, *36*, 4489-4496.

(33) Rosen, M. J. (2004) *Surfactants and Interfacial Phenomena, 3*, 105-136.

(34) Katona, G., Andréasson, U., Landau, E. M., Andréasson, L-E, and Neutze, R. (2003) *J. Mol. Biol. 331*, 681-692.

(35) van Mourik, F., Reus, M., and Holzwarth, A. R., (2001) *Biochim. Biophys. Acta, 1504*, 311-318.

(36) Bowie, J. U. (2005) *Nature*, *438*, 581-589.

(37) Sperotto, M. M. and Mouritsen, O. G. (1991) *Biophys. J. 59*, 261-270.

(38) Dumas, F., Lebrun, M. C., and Tocanne, J. F. (1999) *FEBS letters*, *458,* 271-277.

(39) Sperotto, M. M. and Mouritsen, O. G. (1988) *Eur. Biophys. J. 16*, 1-10.

(40) Bowie, J. U. (1997) *J. Mol. Biol. 272*, 780-789.

(41) Yeates, T. O., Komiya, H., Rees, D. C., Allen, J. P., and Feher, G. (1987) *Proc. Natl. acad. Sci. U.S.A. 84*, 6438-6442.

(42) Clayton, R. K. and Straley, S. C. (1972) *Biophys. J. 12*, 1221-1234.

(43) Stowell, M. H. B., McPhillips, T. M., Rees, D. C., Soltis, S. M., Abresch, E., and Feher, G. (1997) *Science 276*, 812-816.

(44) Koepke, J., Krammer, E-M, Klingen, A. R., Sebban, P., Ullmann, G. M., and Fritzsch, G. (2007) *J. mol. Boil. 371*, 396-409.

(45) Müh, F., Schulz, C., Schlodder, E., Jones, M. R., Rautter, J., Kuhn, M., and Lubitz, W. (1998) *Photosynth. Res.*, *55,* 199-205.

(46) Kleinfeld, D., Okamura, M. Y., and Feher, G. (1984) *Biochemistry*, *23*, 5780-5786.

(47) Nicholls, D. G. (1982) in *Bioenergetics: An Introduction to the Chemiosmotic Theory.* pp. 114-115 Academic Press, London.

(48) Lanyi, J. K. (1998) *Struct. boil. 124*, 164-178.

(49) Lanyi, J. K. (2004) *Mol. Membr. boil. 21*, 143-150.

(50) Müh, F., Williams, J. C., Allen, J. P., and Lubitz, W. (1997) *Biochemistry 37,* 13066-13074.

(51) Tiede, D. M., and Hanson, D. K. (1992) in *The Photosynthetic Bacterial Reaction Center II: Structure, Spectroscopy and Dynamics* (Breton, J., and Vermeglio, A., Eds.) pp. 341-350, Plenum Press, New York and London.

(52) Kálmán, L., Turzó, K., and Maróti, P. (1993) *Photosynthetica 28,* 185-194.

(53) Brzezinski, P., Okamura, M. Y., and Feher, G. (1992) in *The Photosynthetic Bacterial Reaction Center II: Structure, Spectroscopy and Dynamics* (Breton, J., and Vermeglio, A., Eds.) pp. 321-330, Plenum Press, New York and London.

(54) Maróti, P., and Wraight, C. A. (1997) *Biophys J. 73,* 367-381.

(55) Puchenkov, O. V., Kopf, Z., and Malkin, S. (1995) *Biochim. Biophys. Acta, 1231*, 197-212.

(56) Goushcha, A. O., Kharkyanen, V. N., and Holzwarth, A. R. (1997) *J. Phys. Chem. B 101*, 259-265.

(57) Kálmán, L. and Maróti, P. (1997) *Biochemistry 36*, 15269-15276.

(58) Peloquin, J. M., Williams, J. C., Lin, X., Alden, R. G., Taguchi, A. K. W., Allen, J. P., and Woodbury, N. W. (1994) *Biochemistry*, *33*, 8089-8100.

(59) Moser, C. C., Keske, J. M., Warncke, K., Farid, R. S., and Dutton, P. L. (1992) *Nature*, *355*, 796-802.

(60) Malkin, S., Churio, M. S., Shochat, S., and Braslavsky, S. E. (1994) *J. Photochem. Photobiol. B, 23,* 79-85.

(61) Mauzerall, D. C., Gunner, M. R., and Zhang, J. M. (1995) *Biophys. J. 68*, 275-280.

(62) Tiede, D. M., Vazquez, J., Cordova, J., and Marone, P. A. (1996) *Biochemistry, 35*, 10763-10775.

(63) Li, J., Gilroy, D., Tiede, D. M., and Gunner, M. R. (1998) *Biochemistry, 37*, 2818-2829.

(64) Graige, M. S., Feher, G., and Okamura, M. Y. (1998) *Proc. Natl. Acad. Sci. U.S.A. 95*, 11679-11684.

(65) Andréasson U., Andréasson, L-E. (2003) *Photosynth. Res. 75*, 223-233.

(66) Wang, H., Lin, S., Allen, J. P., Williams, J. C., Blankert, S., Laser, C., and Woodbury, N. W. (2007) *Science 316*, 747-750.

(67) Xu, Q. and Gunner, M. R. (2001) *Biochemistry, 40,* 3232-3241.

(68) Olenchuk, M. and Berezetska, N. (2008) *Mol. Cryst. Liq. Cryst. 497*, 121-128.

(69) Clayton, R. K. (2000) *Photosynth. Res.73,* 63-71.

(70) Kálmán, L., LoBrutto, R., Allen, J. P., and Williams, J. C. (2003) *Biochemistry*, *42,* 11016-11022.

(71) Chang, C. H., El-Kabbani, O., Tiede, D., Norris, J. R., and Schiffer, M. (1991) *Biochemistry 30*, 5352-5360.

(72) Arnoux, B., Gaucher, J. F., Ducruix, A., and Reiss-Husson, F. (1995) *Acta Crystallogr. D 51*, 368-379.

(73) Allen, J. P. and Williams, J. C. (1995) *J. Bioenerg. Biomembr. 27*, 275-281.

(74) Mattioli, T. A., Williams, J. C., Allen, J. P., and Robert, B. (1994) *Biochemistry, 33*, 1636-1643.

(75) Nabedryk, E., Allen, J. P., Taguchi, A. K. W., Williams, J. C., Woodbury, N. W., and Breton, J. (1993) *Biochemistry, 32*, 13879-13885.

(76) Rautter, J., Lendzian, F., Shulz, C., Fetsch, A., Kuhn, M., Lin, X., Williams, J. C., Allen, J. P., and Lubitz, W. (1995) *Biochemistry, 34*, 8130-8143.

(77) Mattioli, T. A., Lin, X., Allen, J. P., and Williams, J. C. (1995) *Biochemistry, 34*, 6142-6152.

(78) Williams, J. C., Alden, R. G., Murchison, H. A., Peloquin, J. M., Woodbury, N. W., and Allen, J. P. (1992) *Biochemistry, 31*, 11029-11037.

(79) Frank, H. A., Cogdell, R. J. (1993) *Carotenoids in Photosynthesis*; Young, A. J., Britton, G., Eds.; Chapman and Hall: London, pp. 252.

(80) Pan J., Lin S., Allen J. P., Williams J. C., Frank H. A., and Woodbury N. W. (2011) *J. Phys. Chem. B*, *115*, 7058-7068.

(81) Yeates, T. O.; Komiya, H.; Chirino, A.; Rees, D. C.; Allen, J. P.; Feher, G. (1988) *Proc. Natl. Acad. Sci. U.S.A. 85*, 7993-7997.

(82) Hermes, S., Stachnik, J. M., Onidas, D., Remy, A., Hofmann, E., and Gerwert, K. (2006) *Biochemistry*, *45*, 13741-13749.

(83) Lawlor, D. W. (1993) second edition, *Photosynthesis*, Chapter 1, 1-15, Longman Scientific and Technical Publications, England, UK.

(84) Borisov, A. Yu. (1979) in *Photosynthesis in relation to model systems*, (Barber, J. Eds.), Elsevier, *3*, 2-26.

(85) Katona, G., Snijder, A., Gourdon, P., Andréasson, U., Hansson, Ö., Andréasson, L. E., and Neutze, R. (2005) *Nat. Struct. Mol. Biol. 12*, 630-631.

(86) Feher, G. and Okamura, M. Y. (1978) in *The photosynthetic bacteria* (Clayton, R. K. and Sistrom, W. R., Eds.) pp. 349-386 Plenum Press, New York.

(87) Muller, M. G., Griebenow, K., Holzwarth, A. R. (1991) *Biochim. Biophys. Acta*, *1098*, 1-12.

(88) Maróti, P. and Wraight, C. A. (1987) *Prog. Photosynth. Res. 2*, 401-404.

(89) Williams, J. C., Alden, R. G., Coryell, V. H., Lin, X., Murchison, H. A., Peloquin, J. M., Woodbury, N. W., and Allen, J. P. (1992) in *Research in Photosynthesis,* (Murata, N. Ed.) *1*, pp. 377-380, Kluwer, Dordrecht, The Netherlands.

(90) McPherson, P. H., Okamura, M. Y., and Feher, G. (1993) *Biochim. Biophys. Acta, 1144*, 309-324.

(91) Agostiano, A., Milano, F., and Trotta, M. (2005) *Photosynth Res*, *83*, 53-61.

(92) Murchison, H. A., Alden, R. G., Allen, J. P., Peloquin, J. M., Taguchi, A. K. W., Woodbury, N. W., and Williams, J. C. (1993) *Biochemistry*, *32,* 3498-3505.

(93) Lin, X., Murchison, H. A., Nagarajan, V., Parson, W. W., Allen, J. P., and Williams, J. C. (1994) *Proc. Natl. Acad. Sci. U.S.A. 91,* 10265-10269.

(94) Moss, D. A., Leonhard, M., Bauscher, M., and Mäntele, W. (1991) *FEBS Lett. 283*, 33-36.

(95) O'Reilly, J. E. (1973) *Biochim. Biophys. Acta*, *292*, 509-515.

(96) Gerencsér, L. and Maróti, (2001) *Biochemistry, 40*, 1850-1860.

(97) Thielges, M., Uyeda, G., Cámara-Artigas, A., Kálmán, L, Williams, J. C., and Allen J. P. (2005) *Biochemistry, 44*, 7389-7394.

(98) Tang, K., Williams, J. C., Allen, J. P., and Kálmán, L. (2009) *Biophys. J., 96*, 3295-3304.

(99) Kálmán, L., Thielges, M. C., Williams, J. C., and Allen, J. P. (2005) *Biochemistry, 44*, 13266-13273.

(100) Tommos, C. and Babcock, G. T. (2000) *Biochim. Biophys. Acta*, *1458*, 199-219.

(101) Parson, W. W. (2007) Electronic absorption. In Modern Optical Spectroscopy, pp 182-188, Springer-Verlag, Berlin.

(102) Kálmán, L., LoBrutto, R., Narváez, A. J., Williams, J. C., and Allen, J. P. (2003) *Biochemistry*, *42*, 13280-13286.

(103) Kleinfeld, D., Okamura, M. Y., and Feher, G. (1984) *Biochim. Biophys. Acta*, *766*, 126-140.

(104) Fritzsch, G., Koepke, J., Diem, R., Kuglstatter, A., and Baciou, L. (2002) *Acta Crystallogr. D 58*, 1660-1663.

(105) Breton, J. (2004) *Biochemistry*, *43*, 3318-3326.

(106) Breton, J. (2007) *Biochemistry*, *46*, 4459-4465.

(107) Steffen, M. A., Lao, K., and Boxer, S. G. (1994) *Science*, *264*, 810-816.

(108) Deshmukh, S. S., Williams, J. C., Allen, J. P., and Kálmán, L. (2011) *Biochemistry, 50*, 340-348.

(109) Potter, J. A., Fyfe, P. K., Frolov, D., Wakeham, M. C., van Grondelle, R., Robert, B., and Jones, M. R. (2005) *J. Biol. Chem. 280*, 27155-27164.

(110) Frolov, D., Marsh, M., Crouch, L. I., Fyfe, P. K., Robert, B., van Grondelle, R., Hadfield, A., and Jones, M. R. (2010) *Biochemistry*, *49*, 1882-1892.

(111) Kálmán, L. and Maróti, P. (1994) *Biochemistry*, *33*, 9237-9244.

(112) Marcus, R. A. and Sutin, N. (1985) *Biochim. Biophys. Acta*, *811*, 265-322.

(113) Maróti, P. and Wraight, C. A. (1988) *Biochim. Biophys. Acta 934*, 329-347.

(114) Williams, J. C., Haffa, A. L. M., McCulley, J. L., Woodbury, N. W., and Allen, J. P. (2001) *Biochemistry*, *40*, 15403-15407.

(115) Deshmukh, S. S. Williams, J. C., Allen, J. P., and Kálmán, L. (2011) *Biochemistry, 50*, 3321-3331.

(116) Johnson, E. T. and Parson, W. W. (2002) *Biochemistry*, *41*, 6483-6494.

(117) Nagarajan, V., Parson, W. W., Davis, D., and Schenck, C. C. (1993) *Biochemistry*, *32*, 12324-12336.

(118) Wachtveitl, J., Huber, H., Feick, R., Rautter, J., Müh, F., and Lubitz, W. (1998) *Spectrochim. Acta, Part A 54*, 1231-1245.

(119) Kálmán, L., LoBrutto, R., Allen, J. P., and Williams, J. C. (1999) *Nature*, *402*, 696-699.

(120) Kálmán, L., Narváez, A. J., LoBrutto, R., Williams, J. C., and Allen, J. P. (2004) *Biochemistry*, *43*, 12905-12912.

(121) McPherson, P. H., Okamura, M. Y., and Feher, G. (1988) *Biochim. Biophys. Acta*, *934*, 348-368.

(122) Okamura, M. Y., Paddock, M. L., Graige, M. S., and Feher, G. (2000) *Biochim. Biophys. Acta*, *1458*, 148-163.

(123) Woodbury, N. W., Parson, W. W., Gunner, M. R., Prince, R. C., and Dutton, P. L. (1986) *Biochim. Biophys. Acta*, *851*, 6-22.

(124) Kálmán, L., Williams, J. C., and Allen, J. P. (2003) *FEBS Lett. 545*, 193-198.

(125) Narváez, A. J., Kálmán, L., LoBrutto, R., Allen, J. P., and Williams, J. C. (2002) *Biochemistry*, *41*, 15253-15258.

(126) Komiya, H., Yeates, T. O., Rees, D. C., Allen, J. P., and Feher, G. (1988) *Proc. Natl. Acad. Sci. U.S.A. 85*, 9012-9016.

(127) Deisenhofer, J., Epp, O., Miki, K., Huber, R., and Michel, H. (1984) *J. Mol. Biol. 180*, 385-398.

(128) El-Mashtoly, S. F., Takahashi, H., Kurokawa, H., Sato, A., Shimizu, T., and Kitagawa, T. (2008) *J. Raman Spectrosc. 39*, 1614-1626.

(129) van derWijk, T., Blanchetot, C., Overvoorde, J., and den Hertog, J. (2003) *J. Biol. Chem. 278*, 13968-13974.

(130) Shopes, R. and Wraight, C. A. (1986) *Biochim. Biophys. Acta*, *848*, 364-371.

(131) van Holde, K. E., Johnson, W. C., Ho, P. S. (2006) *Principles of Physical Biochemistry*, Pearson-Prentice Hall, Upper Saddle River, NJ.

(132) Williams, J. C., Steiner, L. A., Ogden, R. C., Simon, M. I., and Feher, G. (1983) *Proc. Natl. Acad. Sci. U.S.A. 80*, 6505-6509.

(133) Williams, J. C., Steiner, L. A., Feher, G., and Simon, M. I. (1984) *Proc. Natl. Acad. Sci. U.S.A. 81*, 7303-7307.

(134) Youvan, D. C., Alberti, M., Begusch, H., Bylina, E. J., and Hearst, J. E. (1984) *Proc. Natl. Acad. Sci. U.S.A. 81*, 189-192.

(135) Clayton, R. K. (1978) *Biochim. Biophys. Acta 504*, 255-264.

(136) Debus, R. J., Feher, G., and Okamura, M. Y. (1985) *Biochemistry 24*, 2488-2500.

(137) Eastman, J. E., Taguchi, A. K. W., Lin, S., Jackson, J. A., and Woodbury, N. W. (2000) *Biochemistry*, *39*, 14787-14798.

(138) Wang, S., Lin, S., Lin, X., Woodbury, N. W., and Allen, J. P. (1994) *Photosynth. Res. 42*, 203-215.

(139) Clayton, R. K. (1980) *Photosynthesis: Physical Mechanisms and Chemical Patterns*, Cambridge University Press, New York.

(140) Rautter, J., Lendzian, F., and Lubitz, W. (1994) *Biochemistry*, *33*, 12077-12084.

(141) Plato, M., Lendzian, F., Lubitz, W., and Mobius, K. (1992) *Photosynth. Bact. React. Cent. II 237*, 109-118.

(142) Kuglstatter, A., Hellwig, P., Fritzsch, G., Wachtveitl, J., Oesterhelt, D., Mäntele, W., and Michel, H. (1999) *FEBS Lett. 463*, 169-174.

(143) Wachtveitl, J., Farchaus, J. W., Das, R., Lutz, M., Robert, B., and Mattioli, T. A. (1993) *Biochemistry*, *32*, 12875-12886.

(144) Killian, J. A. (1998) *Biochim. Biophys. Acta*, *1376*, 401-416.

(145) Wood, B. J. B., Nichols, B. W., and James, A. T. (1965) *Biochim. Biophys. Acta*, *106*, 261-273.

(146) McAuley, K. E., Feyfe, P. K., Ridge, J. P., Isaacs, N. W., Cogdell, R. J., and Jones, M. R. (1999) *Proc. Natl. Acad. Sci. U.S.A. 96*, 14706-14711.

(147) Dutton, P. L. and Jackson, J. B. (1972) *Eur. J. Biochem. 30*, 495-510.

(148) Osváth, S., and Maróti, P. (1997) *Biophys. J. 73*, 972-982.

(149) Kálmán, L., Haffa, A. L. M., Williams, J. C., Woodbury, N. W., and Allen, J. P. (2007) *J. Porphyrins Phthalocyanines*, *11*, 205-211.

(150) Kleinfeld, D., Abresch, E. C., Okamura,M. Y., and Feher,G. (1984) *Biochim. Biophys. Acta 765*, 406-409.

(151) Tandori, J., Miksovska, J., Valerio-Lepiniec, M., Schiffer, M., Maróti, P., Hanson, D. K., and Sebban, P. (2002) *Photochem. Photobiol. 75*, 126-133.

(152) Ginet, N. and Lavergne, J. (2000) *Biochemistry*, *39*, 16252-16262.

(153) Lancaster, C. R. D. (1998) *Biochim. Biophys. Acta 1365*, 143-150.

(154) Lancaster, C. R. D. and Michel, H. (1999) *J. Mol. Biol. 286*, 883-898.

(155) Allen, J. P., Lous, E. J., Feher, G., Chirino, A., Komiya, H., and Rees, D. C. (1990) in *Curr. Res. Photosynth*., *Proc. Int. Conf. Photosynth., 8th*. (Baltscheffsky, M. Ed.), 1:611-64. Dordrecht: Kluwer.

(156) Lavergne, J., Matthews, C., and Ginet, N. (1999) *Biochemistry*, *38*, 4542-4552.

(157) Gust, D., Moore, T. A., and Moore, A. L. (2001) *Acc. Chem. Res. 34*, 40-48.

(158) Hammarström, L., Sun, L. C., Åkermark, B., and Styring, S. (2001) *Spectrochim. Acta, Part A 57*, 2145-2160.

(159) Roszak, A. W., McKendrick, K., Gardiner, A. T., Mitchell, I. A., Isaacs, N. W., Cogdell, R. J., Hashimoto, H., and Frank, H. A. (2004) *Structure*, *12*, 765-773.

(160) Roszak, A. W., Gardiner, A. T., Isaacs, N. W., and Cogdell, R. J. (2007) *Biochemistry*, *46*, 2909-2916.

(161) Cogdell, R. J., Celis, S., Celis, H., and Crofts, A. R. (1977) *FEBS Lett. 80*, 190-194.

(162) McAuley, K. E., Fyfe, P. K., Ridge, J. P., Cogdell, R. J., Isaacs, N. W., and Jones, M. R. (2000) *Biochemistry*, *39*, 15032-15043.

(163) Riegler, J. and Möhwald, H. (1986) *Biophys. J. 49*, 1111-1118.

(164) Rappolt, M. and Rapp, G. (1996) *Eur. Biophys. J. 24*, 381-386.

(165) Sun, W-J., Tristram-Nagle, S., Suter, R. M., and Nagle, J. F. (1996) *Proc. Natl. Acad. Sci. U.S.A. 93*, 7008-7012.

(166) Dahbi, L., Arbel-Haddad, M., Lesieur, P., Bourgaux, C., and Ollivon, M. (2006) *Chem. Phys. Lipids*, *139*, 43-53.

(167) Ratto, T. V. and Longo, M. L. (2002) *Biophys. J. 83*, 3380-3392.

(168) Vaz, W. L. C., Goodsaid-Zalduondo, F., and Jacobson, K. (1984) *FEBS Lett. 174*, 199-207.

(169) Fyfe, P. K., Isaacs, N. W., Cogdell, R. J., and Jones, M. R. (2004) *Biochim. Biophys. Acta*, *1608*, 11-22.

(170) Pokkuluri, P. R., Laible, P. D., Deng, Y. L., Wong, T. N., Hanson, D. K., and Schiffer, M. (2002) *Biochemistry*, *41*, 5998-6007.

(171) Xu, Q., Axelrod, H. L., Abresch, E. C., Paddock, M. L., Okamura, M. Y., and Feher, G. (2004) *Structure, 12*,703-715.

(172) Zouni, A., Witt, H. T., Kern, J., Fromme, P., Krauss, N., Saenger, W., and Orth, P. (2001) *Nature*, *409*, 739-743.

(173) Pierson, B. K. (1994) in *Early Life on Earth* (Bengston, S., Ed) pp 161-180, Columbia University Press, New York, USA.

(174) Sauer, K. and Yachandra, V. K. (2002) *Proc. Natl. Acad. Sci. U.S.A., 99*, 8631-8636.

(175) Sundaramoorthy, M., Kishi, K., Gold, M. H., and Poulos, T. L. (1994) *J. Boil. Chem. 269*, 32759-32767.

(176) Utschig, L. M., Poluektov, O., Schlesselman, S. L., Thurnauer, M. C., and Tiede, D. M. (2001) *Biochemistry*, *40,* 6132-6141.

(177) Fritz, F., Moss, D. A., and Mäntele, W. (1991) in *Spectroscopy of biological molecules*, *94*, 81-82. Royal society of chemistry special publications.

(178) Kozlov, Y. N., Kazakova, A. A., and klimov, V. V. (1997) *Membr. Cell Biol. 11*, 115-120.

(179) Dismukes, G. C., Klimov, V. V., Baranov, S. V., Kozlov, Y. N., DasGupta, J., and tyryshkin, A. (2001) *Proc. Natl. Acad. Sci. U.S.A., 98,* 2170-2175.

(180) Ferguson, A., Darwish, A., Graham, K., Schmidtmann, M., Parkin, A., and Murrie, M. (2008) *Inorg. Chem. 47*, 9742-9744.

(181) Keller, S., Beatty, J. T., Paddock, M., Breton, J., and Leibl, W. (2001) *Biochemistry, 40,* 429-439.

(182) Paddock, M. L., Sagle, L., Tehrani, A., Beatty, J. T., Feher, G., and Okamura, M. Y. (2003) *Biochemistry, 42,* 9626-9632.

(183) Axelrod, H. L., Abresch, E. C., Paddock, M. L., Okamura, M. Y., and Feher, G. (2000) *Proc. Natl. Acad. Sci. U.S.A. 97,* 1542-1547.

(184) Paddock, M. L., Graige, M. S., Feher, G., and Okamura, M. Y. (1999) *Proc. Natl. Acad. Sci. U.S.A. 96,* 6183-6188.

(185) Terentyev, V. V., Shkuropatov, A. Ya., Shkuropatov, V. A., Shuvalov, V. A., and Klimov, V. V. (2011) *Biochemistry (Moscow)*, *76*, 1360-1366.

(186) Khodabandeh, M. H., Davari, M. D., Zahedi, M., and Ohanessian, G. (2010) *Int. J. Mass Spec. 291,* 73-83.

(187) Diner, B. A. (2001) *Biochim. Biophys. Acta, 1503*, 147-163.

(188) Deshmukh, S. S., Akhavein, H., Williams, J. C., Allen, J. P., and Kálmán, L. (2011) *Biochemistry*, *50*, 5249-5262.

(189) Deshmukh, S. S., Tang, k., and Kálmán, L. (2011) *J. Am. Chem. Soc. 133*, 16309-16316.

Appendix A

Identification of molecular mechanism behind the light-induced conformational changes using site-directed mutant reaction centers from *Rhodobacter sphaeroides*

The results in this section are color reproduction of the supporting information of the following published paper:

Deshmukh, S. S., Williams, J. C., Allen, J. P., and Kálmán, L. (2011) Light-induced conformational changes in photosynthetic reaction centers: Dielectric relaxation in the vicinity of the dimer. *Biochemistry*, *50*, 340-348.

Author contributions:

S. S. Deshmukh performed the experiments, analyzed the data, and contributed to writing the paper. L. Kálmán designed the research, guided the data analysis, and wrote the paper. J. C. Williams and J. P. Allen designed, constructed, and supplied the mutants and contributed to writing the paper.

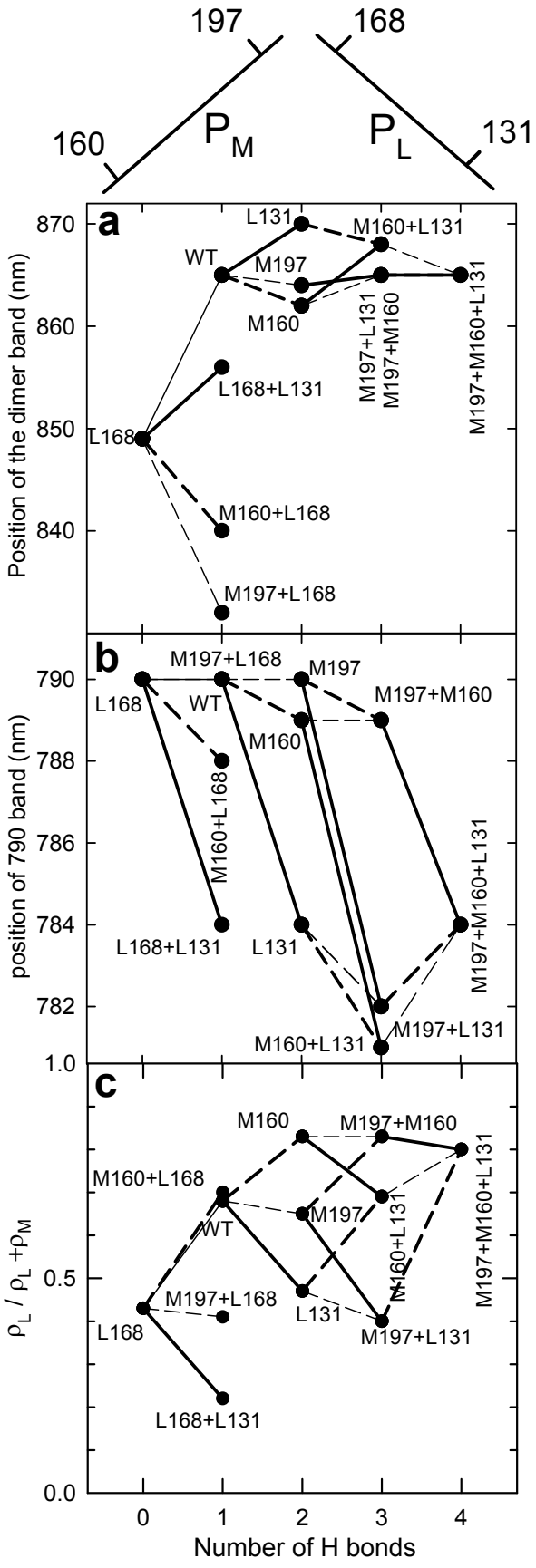

Figure A1. Properties of the WT and the 11 mutant reaction centers. The position of the mutation (and the H-bond created or removed with it) is shown by the simplified structural model of P showing P_L and P_M at the top. Panel a: The position of the Q_Y absorption band (panel a), the positive absorption peak near 790 nm (panel b) in the light-minus-dark difference optical spectra, and the spin density distribution (panel c) as a function of the number of H-bonds in the mutants. The lines represent the direction of the change upon introducing the H-bonds at the positions of L131 (thick solid line), M160 (thick dashed line), M197 (thin dashed line), and L168 (thin solid line). Data of panels a and b were taken from Figure 3.1. To construct panel c the data were taken from reference (76).

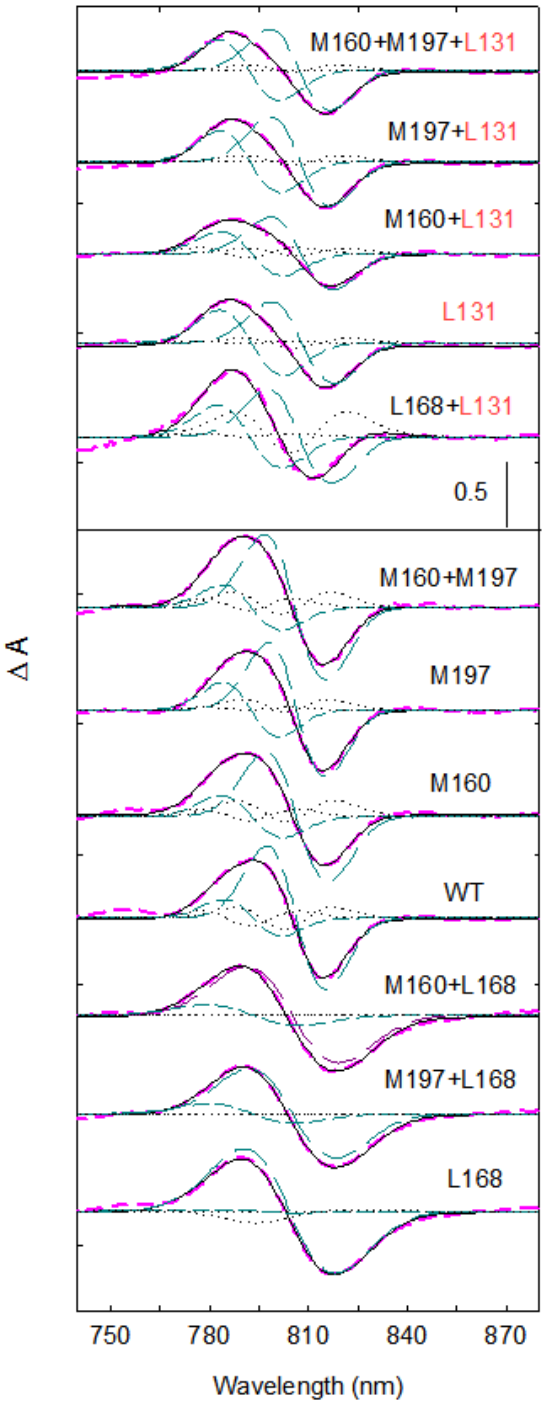

Figure A2. Light-induced electrochromic absorption changes in B_M and B_L (thick pink dashed lines) deducted from near-infrared light-minus-dark absorption difference spectra of reaction centers isolated from wild type and 11 H-bonding mutants after removing contributions from reduced quinone and oxidized dimer (as shown in Figure 3.3A). The spectra were taken using non-saturating (30% of the saturating value for wild type) continuous illumination and were normalized to the dimer band position before removing contributions from reduced quinone and oxidized dimer. These deducted spectra were best fitted by the shifts (thin dark cyan dashed lines) and broadenings (thin black dotted lines) of B_M and B_L and thick solid lines represent the best fit to the spectra (fitting parameters are shown in Table A1). These mutants are categorized in two families: those which have L131 mutation and those which do not have this mutation (separated by the line). The mutants which have the L131 mutation show comparable shifts in B_M and B_L whereas the mutants which do not have this mutation show larger shifts in B_M. L168 mutant shows the shift in monomer band primarily from B_M.

Table A1. Fitting parameters of bacteriochlorophyll monomer B_M and monomer B_L for wild type (WT) and 11 H-bonding mutants (for Figure A2).

Mutant	B_M						B_L					
	A_I [a]	A_D [b]	W_I [c]	W_D [d]	B_I [e]	B_D [f]	A_I [a]	A_D [b]	W_I [c]	W_D [d]	B_I [e]	B_D [f]
M160+M197 + L131	0.92	0.93	804.90	810.00	9.60	9.00	0.93	0.93	790.20	794.00	9.00	9.00
M197+L131	1.07	1.10	805.20	810.00	9.80	9.10	1.10	1.10	790.70	794.00	9.10	9.10
M160+L131	1.05	1.07	805.90	810.00	10.00	9.40	1.04	1.07	791.50	794.00	10.10	9.40
L131	1.06	1.10	806.00	810.50	10.00	9.40	1.10	1.10	790.90	794.50	9.50	9.40
L168+L131	0.98	1.10	804.70	810.00	13.00	9.60	1.10	1.10	790.50	794.00	9.90	9.60
M160+M197	1.05	1.10	802.00	810.00	10.70	9.00	1.08	1.10	791.60	794.00	9.90	9.00
M197	1.08	1.10	803.10	810.00	9.50	8.50	1.10	1.10	791.30	794.00	8.70	8.50
M160	1.09	1.13	803.00	810.00	11.00	9.30	1.10	1.13	791.80	794.00	10.10	9.30
WT	1.04	1.13	802.60	810.00	10.00	8.70	1.07	1.13	792.20	794.00	9.50	8.70
M160+L168	0.90	0.90	800.40	810.00	13.70	13.70	0.90	0.90	792.00	794.00	13.70	13.70
M197+L168	0.80	0.80	800.50	810.00	12.90	12.90	0.80	0.80	792.00	794.00	12.90	12.90
L168	1.00	1.00	798.70	810.00	13.50	13.50	0.91	1.00	793.70	794.00	14.00	13.50

[a, b] Amplitude 1 minute after the illumination (A_I) and before the illumination (A_D) respectively;

[c, d] Band position 1 minute after the illumination (W_I) and before the illumination (W_D) respectively;

[e, f] Full width at half maximum 1 minute after the illumination (B_I) and before the illumination (B_D) respectively.

Appendix B

Identification of molecular mechanism behind the light-induced conformational changes using site-directed mutant reaction centers from *Rhodobacter sphaeroides*

The results in this section are reproduction of the supporting information of the following published paper:

Deshmukh, S. S., Williams, J. C., Allen, J. P., and Kálmán, L. (2011) Light-induced conformational changes in photosynthetic reaction centers: Redox-regulated proton pathway near the dimer. *Biochemistry*, *50*, 3321-3331.

Author contributions:

S. S. Deshmukh performed the experiments, analyzed the data, and contributed to writing the paper. L. Kálmán designed the research, guided the data analysis, and wrote the paper. J. C. Williams and J. P. Allen designed, constructed, and supplied the mutants and contributed to writing the paper.

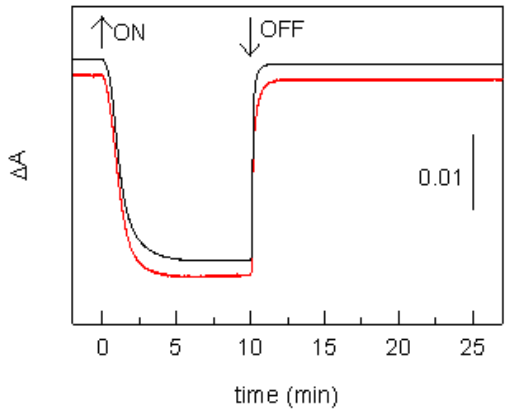

Figure B1. Equilibration of the BRC in response to the onset and offset of the +600 mV applied potential monitored as the bleaching of the Q_Y absorption band of the dimer centered at 865 nm. Black and red traces represent the kinetics in the dark and under weak continuous illumination that generated only 6% of the BRCs to be in charge-separated state, respectively. The nearly matching response to the sudden change for the two traces indicates that the illumination has no effect on the equilibration time.

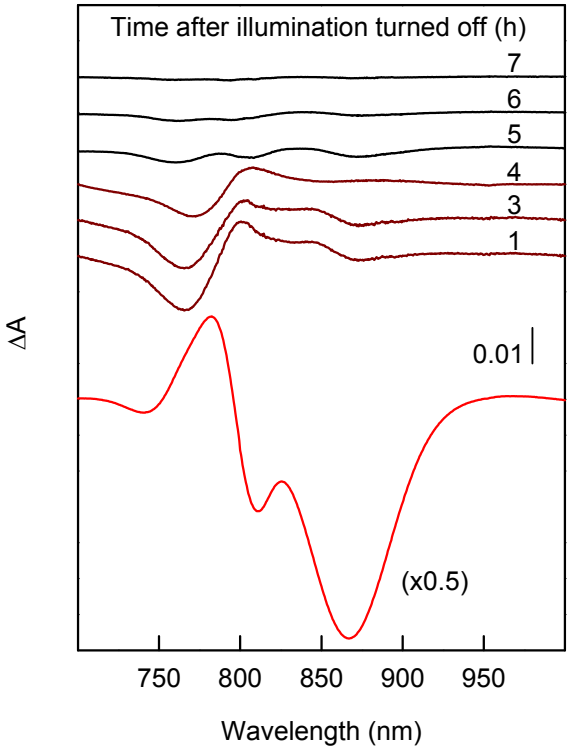

Figure B2. Near-infrared optical difference spectra of WT BRCs recorded immediately after the illumination turned on (red trace) and up to 7 hours after the illumination that lasted for 2.5 hours was ceased (maroon and black traces). The numbers indicate the time in hours after illumination, at which that particular spectrum was recorded. For better comparison of the spectral features the spectrum recorded during the illumination was scaled down to half of its original size and the spectra were vertically shifted for clarity. The intensity of the weak illumination was selected to be the same as used for the redox titrations. As seen from the maroon traces the electrochromic absorption changes of the monomers (near 800 nm) are still present after 5 hours that is long after the spectral features of both P^+ and Q_A^- disappeared.

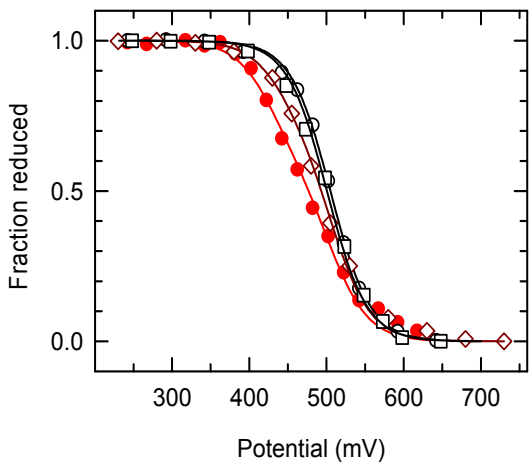

Figure B3. Spectroelectrochemical oxidation-reduction titrations of the dimer in WT reaction centers at pH 8. Open circles, closed circles, open diamonds, and open squares represent the data collected before any illumination, during the weak illumination, in time intervals of approximately 1-3.5 hours, and 6.5-8 hours after the illumination turned off, respectively; Solid lines show the best fit to Nernst curves with one or two components. The parameters of the fit are tabulated in Table B1. The data determined before (open black circles) and during (closed red circles) the illumination were taken from Figure 3.8 to show all the titrations for better comparison.

Condition	Conformation			
	Dark-adapted		Light-adapted	
	A_1 [a]	E_{m1} [b] (mV)	A_2 [c]	E_{m2} [d] (mV)
D1	1	505	-	-
L	0.58	505	0.42	430
D2	0.74	507	0.26	443
D3	1	501	-	-

[a, c] Amplitudes (A1, A2) in the dark- and light-adapted conformations, respectively;

[b, d] Midpoint potential values (E_{m1}, E_{m2}) of the dimer in the dark- and light-adapted conformations, respectively;

Table B1. Fitting parameters of spectro-electrochemical oxidation-reduction titrations of the dimer in WT BRCs before (D1), during (L), between 1 and 3.5 hours (D2), and between 7 and 9.5 hours (D3) after the weak illumination. Where needed two component Nernst-fit was applied resulting in two populations of the dimer with different fractions (A) and midpoint potential values (E_m) representing the dark- and light-adapted conformations, respectively.

Appendix C

Optimization of light-induced conformational changes to stabilize charge-separated state by lipid binding and phase transition of the membrane lipids

The results in this section are color reproduction of the supporting information of the following published paper:

Deshmukh, S. S., Tang, K., and Kálmán, L. (2011) Lipid binding to the carotenoid binding site in photosynthetic reaction centers. *J. Am. Chem. Soc. 133*, 16309-16316.

Author contributions:

S. S. Deshmukh performed the experiments, analyzed the data, and contributed to writing the paper. K. Tang performed preliminary experiment in DLPC liposome (data not included). L. Kálmán designed the research, guided the data analysis, and wrote the paper.

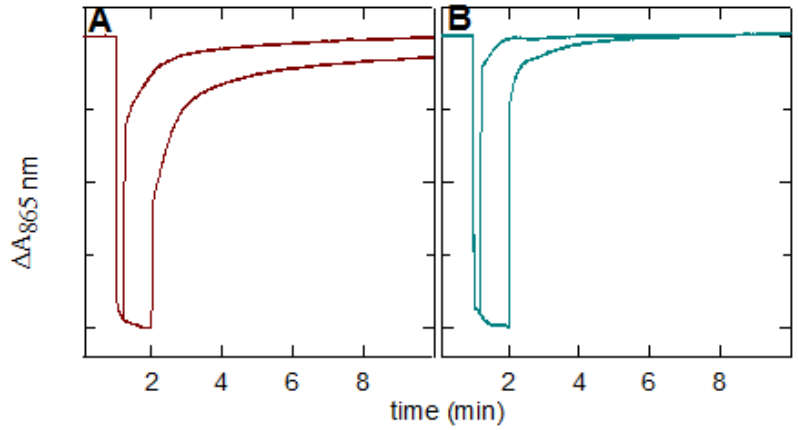

Figure C1. Kinetics of the light-induced absorption changes in BRCs from semiaerobically grown WT (panel A in dark brown) and R-26 (panel B in dark cyan) measured at the center of the Q_Y absorption band of P. The kinetic traces were recorded at two different illumination times for both BRCs: 0.2 and 1 min. Note the much larger amplitude of the longer lived components in WT. Conditions: 1 μM BRCs, 15 mM Bis-tris propane pH 7.0, 1 mM EDTA, 0.05 % TX-100.

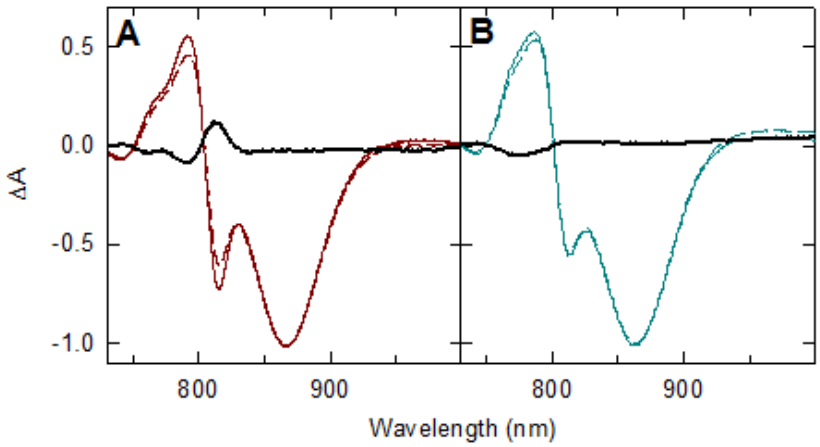

Figure C2. Normalized light-minus-dark difference spectra (solid lines) recorded immediately after the onset of the light and 1 minute after the illumination was turned off (dashed lines) for BRCs isolated from semiaerobically grown cells from WT (dark brown) (A) and R-26 (dark cyan) (B). The thick black solid lines show the double difference spectra (dashed-minus-solid) and feature changes around 800 nm consistent with the decrease of the electrochromic absorption changes involving the monomers during the illumination. Note the larger decrease in WT than in R-26. Conditions as in Figure C1.

Table C1. Fitting parameters of the kinetic traces recorded in TX-100 and presented in Figure 5.2

sample	$k_{(22\ ^\circ C)}$[a] (s^{-1}) $\times 10^3$	$A_{(22\ ^\circ C)}$[b]	$k_{(8\ ^\circ C)}$[c] (s^{-1}) $\times 10^3$	$A_{(8\ ^\circ C)}$[d]
WT	48 4	0.33 0.23	75 1.1	0.45 0.55
R-26	12	0.34	9.6	0.6
R-26+DOPC	15	0.66	8.6	0.62
R-26+DMPC	8	0.35	3.1	0.53
R-26+DLPC	13	0.43	0.7	0.6
WT+DLPC	36 2.6	0.45 0.15	62 1.1	0.57 0.43

[a, c] Rate constant of the slower kinetic components observed in the recovery kinetics at 22 and 8 °C, respectively;

[b, d] Relative amplitudes of the slower kinetic components at 22 and 8 °C, respectively;

Table C2. Fitting parameters of the kinetic traces recorded in proteoliposomes and presented in Figure 5.7

sample	$k_{(22\ ^\circ C)}$[a] (s^{-1}) $\times 10^3$	$A_{(22\ ^\circ C)}$[b]	$k_{(8\ ^\circ C)}$[c] (s^{-1}) $\times 10^3$	$A_{(8\ ^\circ C)}$[d]
R-26-DLPC	41 1	0.5 0.5	**0.13** 28	0.93 0.07
R-26-DOPC	7.8 0.41	0.5 0.5	**2.5** 0.4	0.62 0.38
R-26-DLPC*	ND	ND	**23** 0.93	0.68 0.32
WT-DLPC	12 **0.47**	0.2 0.8	4.1 **0.15**	0.42 0.58

[a, c] Rate constant of the observed kinetic components at 22 and 8 °C, respectively;

[b, d] Relative amplitudes of the observed kinetic components at 22 and 8 °C, respectively;

* Rapid cooling (4 °C/min);

ND, not determined.